

Chemical Vapor Deposition of Organosilicon and Sacrificial Polymer Thin Films

by

Thomas Bryan Casserly

B.S. in Chemical Engineering
Texas A&M University, 1999

Submitted to the Department of Chemical Engineering
in Partial Fulfillment of the Requirements for the Degree of

DOCTOR OF PHILOSOPHY IN CHEMICAL ENGINEERING
AT THE
MASSACHUSETTS INSTITUTE OF TECHNOLOGY

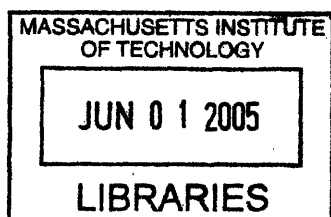
June 2005

© 2005 Massachusetts Institute of Technology. All rights reserved.

Signature of Author
Department of Chemical Engineering
May 13, 2005

Certified by
Karen K. Gleason
Professor of Chemical Engineering
Thesis Supervisor

Accepted by
Daniel Blankschtein
Professor of Chemical Engineering
Chairman, Committee for Graduate Students



ARCHIVES

Chemical Vapor Deposition of Organosilicon and Sacrificial Polymer Thin Films

By

Thomas Bryan Casserly

Submitted to the Department of Chemical Engineering
on May 13, 2005 in Partial Fulfillment of the
Requirements for the Degree of
Doctor of Philosophy in Chemical Engineering

ABSTRACT

Chemical vapor deposition (CVD) produced films for a wide array of applications from a variety of organosilicon and organic precursors. The structure and properties of thin films were controlled by varying processing conditions such as the method and power of precursor activation, pressure, flow rates, and substrate temperature. Systematic variance of deposition conditions allows for the design of materials for a specific application, highlighting the versatility of CVD processes. Spectroscopic tools including Fourier transform infrared spectroscopy, variable angle spectroscopic ellipsometry, X-ray photoelectron spectroscopy, Raman spectroscopy, and nuclear magnetic resonance (NMR) spectroscopy were utilized to characterize film structure and understand the relationship between the structure and properties of materials. Computational quantum mechanics is a power tool applied to explain observed phenomena such as unreferenced chemical shifts in the ^{29}Si NMR of organosilicon thin films, and to examine the thermochemistry of a family of methyl- and methoxymethylsilanes enabling the prediction of initial reactions occurring in the CVD process.

Thesis Supervisor: Karen K. Gleason
Title: Professor of Chemical Engineering

To Mom and Dad

&

To my girls, Holly and Catherine

ACKNOWLEDGEMENTS

While many applaud the accomplishment that is the conclusion of my graduate career at MIT, the praise is most often misplaced. I accomplish nothing on my own merit but what is made possible by Christ. I owe a great deal of thanks to countless individuals for their thoughts, prayers, support, friendship, generosity and advice which carried me to this end.

To my advisor, Karen, for always pushing the right buttons leading me and guiding me and fostering my maturation as a writer and scientist, I am eternally grateful. You expect the best of me and your encouragement even in the face of my greatest challenges provided the drive to succeed for you, myself and everyone counting on me and supporting me.

To my thesis committee members, Professors Herb Sawin and Bernhardt Trout, who generously gave of their time, talent and expertise while always encouraging me to pursue and develop new ideas.

On this journey, I have been blessed to work with some truly exceptional individuals. Many thanks to the members of the Gleason group, past and present, I am proud to have shared time with each of you. Ken, your knowledge, kindness, generosity and heart are without rival. Dan, your inspired leadership of "team low-k" even in the face your own self deprecating humorous pessimism rang true to the great teacher and researcher that you are. April, your smile and grace made the long hours in lab and interminable conference sessions enjoyable. Kelvin, I am honored to have worked with such a brilliant and generous researcher and you will always be "the man."

To all the individuals who played alongside me on the intramural fields, I will always look back fondly on the memories made and championships won. I am especially grateful to the fourteen other members of the victorious CHEME Octathon team that won in my final year after four runner up finishes. I must also thank all the department degenerates whose money I have taken and who more often have taken my money at the table. You gentlemen of the fields and tables provided many a night of camaraderie that will surely be missed. To Paul, who I shared not only the field and the table with but also the first year offices, thanks for your humor, generosity and lasting friendship and for helping Holly with her accent.

To my sisters, Colleen and Amanda, who will never let my head get too big and have been a constant well of support, prayers, and entertainment, I thank you and love you and families dearly.

To my loving, caring, supportive parents, who have always believed in me and instilled in me the desire to always learn something new and make new discoveries, you have given me the greatest gift, a perfect example of a loving family. You have taught me to love selflessly, give freely, and dream beyond my imagination. No words can ever express the depth of my gratitude and love.

Finally to my bride, Holly, there are not words in any language that can describe how I feel about you. You have given so freely of yourself, supported our family, met my every need, showed me how it was done by beating me to graduation with your commencement at Harvard, and provided the motivation to finally graduate. There is no way that I would have made it to this point without you. To my baby Catherine, you are my pride and joy and I love you with all of my heart. Without your smile or Daddy playtime or especially your naps with Daddy, the final push to graduation would have been unbearable. Thank you all.

LIST OF ACRONYMS, ABBREVIATIONS, AND SYMBOLS

$\angle XYZ$	Bond angle between atoms listed
$\langle r \rangle$	Average Connectivity Number
1MS	Methylsilane
2MO ₂ MS	Dimethoxydimethylsilane
2MS	Dimethylsilane
3MOMS	Trimethoxymethylsilane
3MS	Trimethylsilane
4MOS	Tetramethoxysilane
4MS	Tetramethylsilane
AFM	Atomic Force Microscopy
ASM	Asymmetric stretching mode
BDE	Bond dissociation energies
C	Capacitance
CMP	Chemical Mechanical Polishing
CP	Cross-polarization
CSGT	Continuous Set of Gauge Transformations
CVD	Chemical Vapor Deposition
CW	Continuous Wave
D	Di-oxygen substituted (CH ₃) ₂ SiO ₂
D ₁	Dimethylsilanone
D ₂	Tetramethylcyclodisiloxane
D ₃	Hexamethylcyclotrisiloxane
D ₄	Octamethylcyclotetrasiloxane
DFT	Density functional theory
E	Total Energy
FM	Mass Flow
FTIR	Fourier Transform Infrared Spectroscopy
G ₂	Gaussian 2 theory for calculating heats of formation
GIAO	Gauge-Independent Atomic Orbital
HFCVD	Hot filament Chemical Vapor Deposition
IGAIM	Individual Gauges for Atoms In Molecules
ILD	Interlayer dielectric
IMD	Inter-metal dielectric
ITS	Interferometry for Thermal Stability
k	Dielectric Constant
L	Length
M	Mono-oxygen substituted (CH ₃) ₃ SiO
M, MW	Molecular Weight
MAS	Magic angle spinning
Me	Methyl (CH ₃)
MMA	Methylmethacrylate
MO ₃ MS	Methoxytrimethylsilane
MSQ	Methylsilsesquioxane

n	Index of Refraction
n_{633}	Index of refraction at 633 nm
NMR	Nuclear magnetic resonance
NSF	National Science Foundation
oR_n	Organically substituted n unit siloxane ring bound to film structure
OSG	Organosilicate Glass
P	Pitch
P	Pressure
PDMS	Polydimethylsiloxane
PECVD	Plasma-Enhanced Chemical Vapor Deposition
PMMA	Polymethylmethacrylate
PNB	Polynorbornene
PP	Pulsed plasma
PPECVD	Pulsed Plasma-Enhanced Chemical Vapor Deposition
ppm	Parts per million
PTFE	Polytetrafluoroethylene
Q	Quad-oxygen substituted SiO_4
r	Deposition Rate
R	Gas Constant
R	Resistance
RF	Radio Frequency
sccm	Standard Cubic Centimeters per Minute
SIA	Semiconductor Industry Association
SiCOH	Organosiloxane / Carbon Doped Oxide
SRC	Semiconductor Research Corporation
SSM	Symmetric stretching mode
T	Temperature
T	Tri-oxygen substituted $(CH_3)SiO_3$
T_f	Filament Temperature
T_i	Thickness of layer i
TMS	Tetramethylsilane
VASE	Variable Angle Spectroscopic Ellipsometry
XPS	X-Ray photoelectron spectroscopy
ZPE	Zero-point energy
γ	Vibrational rocking mode
δ	Vibrational bending mode
ΔG°_{rxn}	Standard Gibbs Free Energy of Reaction
$\Delta H^{\circ}_{f \text{ or } rxn}$	Standard Enthalpy of Formation or Reaction
ϵ_0	Vacuum Permittivity
ν	Vibrational stretching mode
ρ	Metal resistivity
ΣD_0	Sum of the atomization energies
σ_{iso}	Isotropic shielding constants

TABLE OF CONTENTS

ABSTRACT	2
DEDICATION	3
ACKNOWLEDGEMENTS.....	4
LIST OF ACRONYMS, ABBREVIATIONS, AND SYMBOLS	5
LIST OF FIGURES	11
LIST OF TABLES	14

CHAPTER ONE

INTRODUCTION	16
1.1 MOTIVATION.....	17
1.2 LOW-K MATERIAL OPTIONS AND APPROACHES	19
1.3 CHEMICAL VAPOR DEPOSITION.....	23
1.4 COMPUTATIONAL QUANTUM MECHANICS.....	25
1.5 THESIS FRAMEWORK.....	26
REFERENCES.....	28

CHAPTER TWO

HOT-FILAMENT CHEMICAL VAPOR DEPOSITION OF ORGANOSILICON THIN FILMS FROM HEXAMETHYLCYCLOTRISILOXANE AND OCTAMETHYLCYCLOTETRASIOLOXANE	29
ABSTRACT	30
2.1 INTRODUCTION	31
2.2 EXPERIMENTAL.....	32
2.3 RESULTS AND DISCUSSION.....	34
2.3.1 <i>Deposition Rate</i>	34
2.3.2 <i>Fourier Transform Infra-Red (FTIR) Spectroscopy</i>	36

2.3.3	<i>Raman Spectroscopy</i>	41
2.3.4	<i>Nuclear Magnetic Resonance (NMR) Spectroscopy</i>	47
2.3.5	<i>X-Ray Photoelectron Spectroscopy (XPS)</i>	51
2.3.6	<i>Atomic Force Microscopy (AFM)</i>	52
2.3.7	<i>Chemical Reactions</i>	53
2.3.8	<i>Film Structure</i>	59
2.4	CONCLUSIONS	61
	REFERENCES.....	62

CHAPTER THREE

	DENSITY FUNCTIONAL THEORY CALCULATION OF ²⁹SI NMR CHEMICAL SHIFTS OF ORGANOSILOXANES	64
	ABSTRACT	65
3.1	INTRODUCTION	66
3.2	METHODOLOGY AND EXPERIMENTS	69
3.3	RESULTS AND DISCUSSION.....	72
3.4	CONCLUSIONS	81
	REFERENCES.....	83

CHAPTER FOUR

	ENTHALPIES OF FORMATION AND REACTION FOR PRIMARY REACTIONS OF METHYL- AND METHOXYMETHYLSILANES FROM DENSITY FUNCTIONAL THEORY	85
	ABSTRACT	86
4.1	INTRODUCTION	87
4.2	COMPUTATIONAL METHOD.....	89
4.3	RESULTS AND DISCUSSION.....	92
4.3.1	<i>Enthalpies of Formation</i>	92
4.3.2	<i>Reaction Enthalpies and Bond Dissociation Energies</i>	97
4.4	CONCLUSIONS	105

REFERENCES.....	107
-----------------	-----

CHAPTER FIVE

CHEMICAL VAPOR DEPOSITION OF ORGANOSILICON THIN FILMS FROM METHOXYMETHYLSILANES 109

ABSTRACT	110
5.1 INTRODUCTION	111
5.2 RESULTS AND DISCUSSION.....	112
5.2.1. <i>Fourier Transform Infrared (FTIR) Spectroscopy</i>	112
5.2.2. <i>Optical and Electrical Characterization</i>	122
5.2.3. <i>Interpreting the results in light of DFT simulations</i>	124
5.3 CONCLUSIONS	126
5.4 EXPERIMENTAL.....	127
REFERENCES.....	130

CHAPTER SIX

EFFECT OF SUBSTRATE TEMPERATURE ON THE PLASMA POLYMERIZATION OF POLY(METHYL MEHTACRYLATE) 131

ABSTRACT	132
6.1 INTRODUCTION	133
6.2 RESULTS AND DISCUSSION.....	134
6.2.1 <i>Fourier Transform Infrared (FTIR) Spectroscopy to determine optimal W/FM</i>	134
6.2.2 <i>Thermal properties/degradation of PMMA</i>	137
6.2.3 <i>X-Ray Photoelectron Spectroscopy (XPS)</i>	142
6.2.4 <i>Raman Spectroscopy</i>	146
6.2.5 <i>Deposition Kinetics</i>	151
6.3 CONCLUSIONS	152
6.4 EXPERIMENTAL.....	153
REFERENCES.....	156

CHAPTER SEVEN

CONCLUSIONS AND FUTURE DIRECTIONS	158
7.1 CONCLUSIONS	159
7.1.1 <i>CVD Materials</i>	159
7.1.2 <i>Computational Quantum Mechanics</i>	161
7.2 FUTURE DIRECTIONS.....	162

LIST OF FIGURES

CHAPTER ONE

FIGURE 1-1.	PROGRESSION OF THE SIA TECHNOLOGY ROADMAP FOR DIELECTRICS.....	18
FIGURE 1-2.	PROCESS FLOW FOR SIMPLE AIR GAP FABRICATION.....	21
FIGURE 1-3.	SCHEMATIC OF A TYPICAL PECVD VACUUM REACTOR.	25

CHAPTER TWO

FIGURE 2-1.	ARRHENIUS PLOT OF D ₃ AND D ₄ FILMS PRODUCED BY HFCVD. MEASURED DEPOSITION RATES, R (LEFT AXIS), ARE DENOTED BY SOLID MARKERS, AND THICKNESS-BASED DEPOSITION YIELDS, R/FM (RIGHT AXIS), ARE DENOTED BY EMPTY MARKERS. STRAIGHT LINES WERE FITTED TO THE DEPOSITION YIELD DATA BY REGRESSION.	35
FIGURE 2-2.	FTIR SPECTRA OF A. D ₃ PECVD FILM DEPOSITED UNDER CONTINUOUS-WAVE EXCITATION AND B. D ₃ HFCVD FILM DEPOSITED AT 1000°C.	37
FIGURE 2-3.	FTIR SPECTRA OF D ₃ HFCVD FILMS DEPOSITED AT FILAMENT TEMPERATURES OF A. 860°C, B. 1000°C, AND C. 1100°C.....	38
FIGURE 2-4.	FTIR SPECTRA OF D ₄ HFCVD FILMS DEPOSITED AT FILAMENT TEMPERATURES OF A. 800°C, B. 900°C, AND C. 1000°C.	39
FIGURE 2-5.	MICRO-RAMAN SPECTRA OF A. D ₃ , B. D ₄ , C. PDMS, D. D ₄ HFCVD FILM DEPOSITED AT A FILAMENT TEMPERATURE OF 1000°C, AND E. D ₃ HFCVD FILM DEPOSITED AT A FILAMENT TEMPERATURE OF 1100°C.....	42
FIGURE 2-6.	MICRO-RAMAN SPECTRA OF D ₃ HFCVD FILMS DEPOSITED AT FILAMENT TEMPERATURES OF 860°C, 1000°C, AND 1100°C.	46
FIGURE 2-7.	MICRO-RAMAN SPECTRA OF D ₄ HFCVD FILMS DEPOSITED AT FILAMENT TEMPERATURES OF 800°C, 900°C, AND 1000°C.	46
FIGURE 2-8.	²⁹ SI SOLID-STATE CP-MAS NMR SPECTRA OF D ₃ HFCVD FILM DEPOSITED AT FILAMENT TEMPERATURES OF 860°C, 1000°C, AND 1100°C.....	48
FIGURE 2-9.	²⁹ SI SOLID-STATE CP-MAS NMR SPECTRA OF D ₄ HFCVD FILM DEPOSITED AT FILAMENT TEMPERATURES OF 800°C, 900°C, AND 1000°C.....	49
FIGURE 2-10.	ATOMIC FORCE MICROGRAPH OF D ₄ HFCVD FILM DEPOSITED AT A FILAMENT TEMPERATURE OF 900°C. RMS ROUGHNESS OVER IMAGE AREA IS 1.1 NM. RMS ROUGHNESS OF BARE SILICON IS 0.53 NM.....	53

FIGURE 2-11. REACTION PATHWAYS FOR THE PRODUCTION OF POLYMERIZATION PRECURSOR SPECIES IN D ₃ AND D ₄ HFCVD.	54
--	----

CHAPTER THREE

FIGURE 3-1. NON-BRANCHING GROUPS, M (+6 PPM) & D (-22PPM) AND BRANCHING GROUPS, T (-68 PPM) & Q (-105 PPM) COMMONLY FOUND IN OSG THIN FILMS WITH ²⁹ SI CHEMICAL SHIFTS IN ().	68
FIGURE 3-2. LABELED ²⁹ SI NMR SPECTRA OF HFCVD FILM FROM D ₃ WITH A FILAMENT TEMPERATURE OF 1150°C.	68
FIGURE 3-3. OSG GROUPS SIMULATED: A. SiH ₃ CAPPED D, B. D GROUPS WITH M ^H ENDGROUPS, C. TWO D ₃ [*] RINGS BONDED VIA Si-Si, D. D ₃ [*] PENDANT TO LINEAR CHAIN OF 3 D UNITS VIA Si-Si, E. D ₃ [*] PENDANT TO LINEAR CHAIN OF 3 D UNITS VIA Si-O, AND F. D ₃ [*] TERMINAL TO LINEAR CHAIN OF TWO D UNITS VIA Si-O. (D ₃ [*] ≡ METHYL ABSTRACTED D ₃)	72
FIGURE 3-4. ²⁹ SI NMR OF HFCVD FILMS FROM D ₃ WITH FILAMENT TEMPERATURES OF 860°C, 1000°C, & 1100°C. ¹¹	78
FIGURE 3-5. ²⁹ SI NMR OF HFCVD FILMS FROM D ₄ WITH FILAMENT TEMPERATURES OF 800°C, 900°C, & 1000°C. ¹¹	79
FIGURE 3-6. ²⁹ SI NMR SPECTRA OF 1150°C D ₃ FILM FIT TO RESOLVE CHEMICAL SHIFTS AT -8.5 PPM, -14.5 PPM AND -19.1 PPM.....	80

CHAPTER FOUR

FIGURE 4-1. FAMILY PLOT FOR METHOXYMETHYLSILANES – A. (CH ₃) _N Si(OCH ₃) _{4-N} , B. (CH ₃) _N SiOH(OCH ₃) _{3-N} , C. (CH ₃) _N SiH(OCH ₃) _{3-N} , D. (CH ₃) _N SiH ₂ (OCH ₃) _{2-N} , E. (CH ₃) _N SiO·(OCH ₃) _{3-N} , AND F. (CH ₃) _N Si·(OCH ₃) _{3-N}	96
FIGURE 4-2. FAMILY PLOT FOR METHYLSILANES – A. (CH ₃) _N SiH _{4-N} , B. (CH ₃) _N Si·H _{3-N} , C. (CH ₃) _N Si·H _{2-N} (¹ A ₁), AND D. (CH ₃) _N Si·H _{2-N} (³ B ₁).....	97
FIGURE 4-3. BDES FOR METHYLSILANES AND METHYLSILYL RADICALS AS A FUNCTION OF METHYL SUBSTITUTION (N).	99
FIGURE 4-4. BDES FOR THE Si-C, Si-O, AND O-C BONDS FOR METHOXYMETHYLSILANES AS A FUNCTION OF INCREASING METHYL CONTENT (N).....	100

CHAPTER FIVE

FIGURE 5-1.	FTIR SPECTRA OF PECVD THIN FILMS DEPOSITED FROM MO_3MS , $2\text{MO}_2\text{MS}$, AND 3MOMS WITH INSET FOCUSED ON M, D, T REGION FROM $1300\text{--}1240\text{ cm}^{-1}$	113
FIGURE 5-2.	FTIR SPECTRA OF PECVD THIN FILMS FROM $2\text{MO}_2\text{MS}$, $2\text{MO}_2\text{MS} + \text{H}_2$, AND $2\text{MO}_2\text{MS} + \text{O}_2$ WITH AN ADDITIONAL (---) SPECTRUM OF THE $2\text{MO}_2\text{MS} + \text{O}_2$ FILM AFTER ANNEAL.....	117
FIGURE 5-3.	FTIR SPECTRA OF PECVD FILMS DEPOSITED FROM 3MOMS AND HYDROGEN WITH $3\text{MOMS}:\text{H}_2$ GAS FLOW RATIOS OF 1:1.5, 1:4 AND 1:8.....	120
FIGURE 5-4.	FTIR SPECTRA OF FILMS DEPOSITED FROM 3MOMS , $3\text{MOMS} + \text{H}_2$, AND $3\text{MOMS} + \text{O}_2$ AT PLASMA POWERS OF 20W (BLACK LINES), 40W (MEDIUM GRAY LINES), AND 100W (LIGHT GRAY LINES).	122
FIGURE 5-5.	DIELECTRIC CONSTANT OF PECVD FILMS FROM METHOXYMETHYLSILANES, WITH HYDROGEN, AND WITH OXYGEN FOR THE AS DEPOSITED SAMPLES AND AFTER ANNEALING AS A FUNCTION OF THE INDEX OF REFRACTION AT A WAVELENGTH OF 633 NM.	123

CHAPTER SIX

FIGURE 6-1.	FTIR SPECTRA OF PECVD THIN FILMS FROM MMA WITH W/FM OF (A) 168.3, (B) 84.2, (C) 67.3, AND (D) 4.8 J/G ALONG WITH A (E) PMMA STANDARD.....	135
FIGURE 6-2.	ONSET OF THERMAL DECOMPOSITION AS A FUNCTION OF SUBSTRATE TEMPERATURE FOR BOTH CW AND PP CVD PMMA FILMS.	140
FIGURE 6-3.	PERCENT RESIDUE REMAINING AFTER ANNEAL AS A FUNCTION OF SUBSTRATE TEMPERATURE FOR BOTH CW AND PP CVD PMMA FILMS.	141
FIGURE 6-4.	FIT XPS SPECTRA, C 1S AND O 1S FOR THE PMMA STANDARD AND THE PECVD FILM CW1.	143
FIGURE 6-5.	PMMA WITH LABELED CARBON (1-4) AND OXYGEN (1^*-2^*) MOIETIES.....	144
FIGURE 6-6.	RAMAN SPECTRA OF FILMS PP4, CW4, PP1, CW1, AND A PMMA STANDARD (STD.).	149
FIGURE 6-7.	DETAIL OF THE RAMAN SPECTRA OF FILMS PP4, CW4, PP1, CW1, AND A PMMA STANDARD AT THE METHOXY AND SKELETAL STRETCHING REGION.	150
FIGURE 6-8.	ARRHENIUS PLOT OF DEPOSITION RATE AS A FUNCTION OF SUBSTRATE TEMPERATURE AT CONSTANT W/FM = 4.8 J/G SHOWING RELATIVE APPARENT ENERGIES 3:1 FOR CW:PP.....	152

LIST OF TABLES

CHAPTER TWO

TABLE 2-1.	FTIR ASSIGNMENTS FROM THE LITERATURE.	37
TABLE 2-2.	RAMAN ASSIGNMENTS FROM THE LITERATURE.....	43
TABLE 2-3.	RAMAN SILOXANE SYMMETRIC STRETCHING MODE (SSM) ASSIGNMENTS	45
TABLE 2-4.	²⁹ Si NMR STRUCTURES AND CHEMICAL SHIFTS COMMONLY OBSERVED IN OSG CVD FILMS.....	48
TABLE 2-5.	XPS ELEMENTAL RATIOS FOR HFCVD FILMS FROM D ₃ AND D ₄	51

CHAPTER THREE

TABLE 3-1.	SUMMARY OF CALCULATED ²⁹ Si NMR CHEMICAL SHIFTS OF KNOWN MOIETIES USING VARIOUS METHODS AT THE B ₃ LYP/6-311++G(D,P) LEVEL. (TMS σ_{iso} GIAO: 339.2 PPM, IGAIM: 338.0 PPM, CSGT: 338.0 PPM).....	73
TABLE 3-2.	SUMMARY OF CALCULATED ²⁹ Si NMR CHEMICAL SHIFTS OF UNKNOWN MOIETIES USING VARIOUS METHODS AT THE B ₃ LYP/6-311++G(D,P) LEVEL. (TMS σ_{iso} GIAO: 339.2 PPM, IGAIM: 338.0 PPM, CSGT: 338.0 PPM).....	75

CHAPTER FOUR

TABLE 4-1.	TOTAL ENERGIES AND UN-SCALED ZERO-POINT ENERGIES, IN HARTREE, WITH THERMAL CORRECTIONS TO ENTHALPY, SUM OF ATOMIZATION ENERGIES AND ENTHALPIES OF FORMATION (BOTH THEORY AND EXPERIMENTAL WITH DEVIATIONS), IN KCAL/MOL.	94
TABLE 4-2.	BOND DISSOCIATION ENERGIES FOR METHYLSILANES AND METHYLSILYL RADICALS.	98
TABLE 4-3.	BOND DISSOCIATION ENERGIES FOR METHOXYMETHYLSILANES.....	100
TABLE 4-4.	GIBBS FREE ENERGY OF REACTION AND ENTHALPY OF REACTION AT 298 K AND 1 ATM FOR A SERIES OF REACTIONS OF METHYLSILANES WITH OXYGEN AND METHOXYMETHYLSILANES WITH OXYGEN AND WITH HYDROGEN.	103

CHAPTER FIVE

TABLE 5-1.	FTIR PEAK ASSIGNMENTS FOR OSG THIN FILMS FROM THE LITERATURE. ^{9, 15-19} ..	115
------------	--	-----

CHAPTER SIX

TABLE 6-1.	FTIR ASSIGNMENTS FOR PMMA FROM THE LITERATURE ²⁰	137
TABLE 6-2.	SUMMARY OF ONSET OF THERMAL DECOMPOSITION AND % RESIDUE FOR PECVD FILMS DEPOSITED AT VARIOUS SUBSTRATE TEMPERATURES WITH A CONSTANT W/FM OF 4.8 J/G.....	138
TABLE 6-3.	COMPARISON OF XPS SPECTRA FITS FROM FIGURE 6-4 WITH REFERENCE DATA.	144
TABLE 6-4.	ELEMENTAL ANALYSIS AND C/O RATIO FROM XPS SCANS ALONG WITH CALCULATED UPPER AND LOWER BOUNDS FOR FUNCTIONAL GROUP LOSS.	146
TABLE 6-5.	RAMAN ASSIGNMENTS FROM THE LITERATURE. ^{10, 40}	148

CHAPTER ONE

INTRODUCTION

1.1 MOTIVATION

As the semiconductor industry continues to decrease device feature size, processor clock speeds are increasingly limited by the resistance-capacitance (RC) delay of interconnect structures.¹ Advances in lithography have enabled semiconductor manufacturers to decrease device size allowing for shorter, thinner, and more densely packed metal interconnects. For instances in which each level of a dielectric, metal, dielectric stack are of equal thickness, the RC delay can be expressed as:¹

$$RC = 2\rho\kappa\epsilon_0 \left(\frac{4L^2}{P^2} + \frac{L^2}{T^2} \right) \quad (1-1)$$

where

ρ is the metal resistivity

κ is the dielectric constant of the material between the metal lines

ϵ_0 is the permittivity of space

L is the line length

P is the metal pitch

T is the thickness of the metal line

As is evident in Equation 1-1, as the wire density increases, indicated by a decrease in pitch (P), RC delay increases. There are two approaches to this problem from a materials standpoint. Semiconductor companies have implemented the use of copper in place of aluminum at the 0.13 micron process node to take advantage its lower resistivity.¹ The other is to lower the dielectric constant of the insulating film. The introduction of copper is a logical first step to reduce the RC delay; however, the

RC delay will continue to increase for future process nodes if the dielectric constant remains unchanged. Reducing the dielectric constant not only reduces the RC delay, but has the added benefit of reducing power consumption and line-to-line crosstalk noise as well. Therefore, there is a need for and a large field of research dedicated to developing low-k materials for future process nodes.

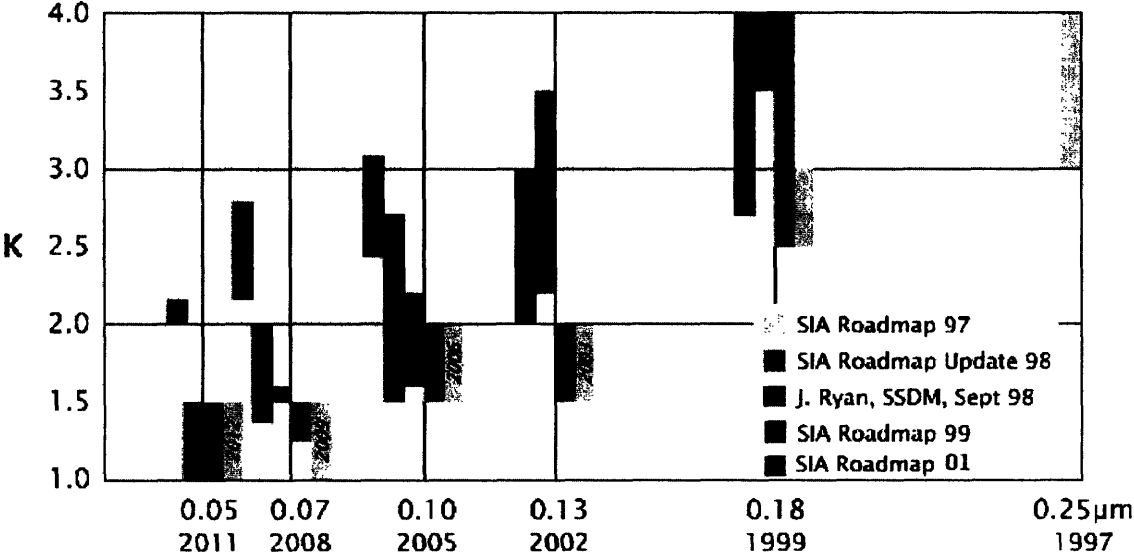


Figure 1-1. Progression of the SIA Technology Roadmap for Dielectrics.

The Semiconductor Industry Association (SIA) technology roadmap for dielectrics outlines the dielectric constant requirements for the next ten years and is updated regularly. From Figure 1-1 it can be seen that the implementation of low-k materials has been repeatedly pushed back. The most recent roadmap pushed integration of low-k films back even further, calling for a dielectric constant below 3.0 for the first time in 2007. This is due to the inability of the industry to develop and integrate a single choice for the next generation low-k material. Silicon dioxide (SiO₂) is an excellent dielectric material due to its excellent mechanical and thermal properties and has been the industry standard from the beginning. However, SiO₂

has a dielectric constant of approximately 4.0, which is too high for future devices. The current industry standard for low-k dielectrics is a fluorine-doped oxide (SiOF, $3.3 < \kappa < 3.7$). Companies and researchers have developed a variety of CVD organosilicate glasses (OSG, $2.7 < \kappa < 3.3$) for use as the next low-k material such as Black Diamond™ from AMD, Flowfill™ from Trikon, and CORAL™ from Novellus.² Companies have also developed spin-on OSGs, such as Dow's SILK™ and AlliedSignal's Accuspin 418™. Each of these products still face many challenges before wide spread implementation. Further down the dielectric roadmap fluorocarbons ($2.0 < \kappa < 2.7$) and other polymers have been proposed. While these materials all have dielectric constants lower than that of SiO₂, they also create many challenges for integration due to issues concerning thermal and dimensional stability, chemical and mechanical polishing (CMP) stability, as well as the complexity of integrating an entirely new material into the fabrication process.³

1.2 LOW-K MATERIAL OPTIONS AND APPROACHES

Dielectric requirements for the sub-0.1 micron process node indicate a dielectric constant less than 2.0 (see Figure 1-1). Air has the lowest dielectric constant of ~1.0. Incorporating void space in the form of pores into current low-k films will enable a reduction of the dielectric constant below 2.0. Creating a porous low-k material typically utilizes a porogen, which is removed following deposition by a thermal annealing or UV radiation step. Kohl *et al.*⁴ demonstrated this idea by spin coating a 80/20 mixture of a commercially available spin-on dielectric composed of methyl silsesquioxane (MSQ, $k = 2.7$) and a sacrificial polymer,

substituted polynorbornene (PNB) containing cross-linking groups. After spin coating and soft bake below the decomposition temperature of PNB, the MSQ/PNB film was heated to 425°C thermally decomposing the PNB leaving a porous MSQ film with a measured dielectric constant of 2.3. While porous films have the desired effect of reducing the dielectric constant of the remaining material, the mechanical and heat transfer properties of the film are adversely affected. The mechanical strength of porous films scales with porosity, p , by $(1-p)^3$ while the thermal conductivity scales by $(1-p)^{1.5}$.⁵

Most porous films lack the mechanical strength required for integration into current semiconductor manufacturing. Due to poor mechanical strength porous films may collapse or otherwise fail during various fabrication steps and affect the surrounding structures decreasing yield and increasing cost. Due to the uncertainty involved in using porous films, some researchers have investigated the possibility of using air as a dielectric.^{3, 6, 7} While air does not have the thermal conductivity or mechanical strength of other dielectrics, it does have the lowest possible dielectric constant, 1.0, and is the only choice for the ultimate low-k material. By using air as a dielectric, concerns about inhomogeneous pore structure causing device failure are eliminated. While the mechanical and thermal conductivity of air leaves much to be desired, the sacrificial material chosen can be a robust material providing mechanical strength and dimensional stability during critical fabrication steps eliminating risks and uncertainties associated with porous low-k materials.

The first logical step of integration of air as a dielectric is in the form of air gaps. Air gaps can be created in one of two ways. The first is to deposit a non-conformal dielectric layer on top of a patterned surface.^{8, 9} This technique has many

challenges. This process can only be used with metals that can be etched (which excludes copper interconnects) or requires removal of the inter-metal dielectric (IMD) via a challenging etch step. Another challenge is reproducibility of air gaps across structures of varying dimensions and non-ideal air gap geometries which often require multiple steps to ensure the dielectric overcoat does not fail. An alternative process is to deposit and pattern sacrificial layer, followed by metal deposition and etch back. The stack is then capped with a dielectric overcoat. Finally, the sacrificial layer is removed by a thermal annealing step. In a process using a sacrificial layer it is important to remove all of the sacrificial material. Any remaining residue will raise the dielectric constant and may have negative interactions with the final device. It is therefore very important to understand the decomposition mechanism, diffusion of the sacrificial material through the overlying inter-layer dielectric (ILD), and the completeness of removal.

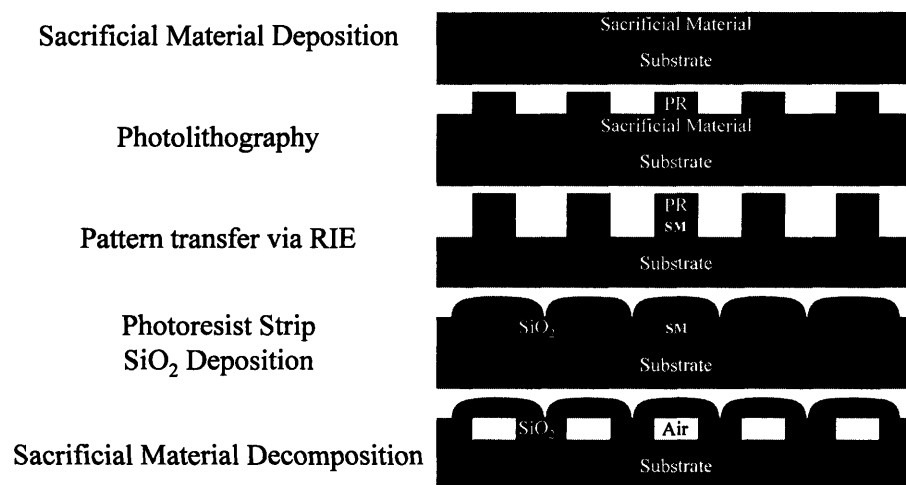


Figure 1-2. Process flow for simple air gap fabrication.

Fabrication techniques for closed cavity void space using sacrificial materials have been proposed by Anand *et al.*⁶ and Kohl *et al.*^{3,7} The methods effectively differ only in choice of sacrificial material. A process flow cartoon follows in Figure 1-2.

The process of Anand *et al.* utilized magnetron sputtered amorphous carbon as a sacrificial material. The carbon was patterned to create trenches for metal deposition. Tungsten was deposited via blanket-CVD over a barrier layer of titanium nitride followed by an etchback. Silicon dioxide was then sputter-deposited capping the carbon and tungsten. The stack was then placed in an oxygen ambient furnace at 450°C for 2 hr which ashed the amorphous carbon leaving behind air gap structures. The effective dielectric constant of the air gaps was measured to be 1.01. While successful in creating air gap structures, the high-temperature annealing step in an oxygen environment would cause copper oxidation increasing the interconnect resistivity.

Kohl *et al.*^{3,7} propose a similar process using spin-on deposited functionalized polynorbornene (PNB) as the sacrificial material. The PNB polymer used was heated at a rate of 3°C/min under constant nitrogen purge. TGA shows decomposition occurring between 370°C and 425°C. This process included etching holes in the overcoat material to prevent overcoat damage during SL removal, and approximately 3% of the polymer remained as residue negatively impacting the dielectric properties of the air gap structure. For both process, the elevated temperatures for extended annealing times may cause undesired changes in dopant profiles. The use of a CVD sacrificial material is preferred over a spin-coated material because the latter produces more waste, increases worker solvent exposure, and may dissolve previous layers when attempting to build multilevel structures. While these approaches pose integration issues, they do demonstrate the feasibility of fabricating air gap structures via the use of a sacrificial material and the ability to lower the dielectric constant by incorporating air gaps.

The key to successful air gap fabrication is the sacrificial material. The ideal sacrificial material should be safe and easy to deposit, be thermally and dimensionally stable below its decomposition temperature able to withstand patterning, metal deposition and etchback, and decompose efficiently and completely in the absence of oxygen without affecting the overlying dielectric or metal lines. Facile and repeatable synthesis is a requirement of any material introduced into semiconductor manufacturing. It is necessary for device fabrication that a sacrificial material be dimensionally stable during patterning and the subsequent deposition of metal and overlying dielectric materials which may include wet and/or plasma chemistries. Industry experts expect level-1 dielectric materials (and thus a sacrificial material) will face eight or more thermal cycles during production.² Any instability during these steps will cause device failure. During decomposition of the sacrificial material gas molecules formed must diffuse through the overlying dielectric without altering its chemical or mechanical properties. Any interactions of the decomposition species with the metal or overlying dielectric will alter their material properties and affect device performance. For this same reason, it is necessary for the sacrificial material to decompose in the absence of oxygen.

1.3 CHEMICAL VAPOR DEPOSITION

There are two techniques for the deposition of low dielectric constant films, chemical vapor deposition (CVD) and spin-on. In a spin-on process, the low-k material dissolved in a solvent is poured onto a wafer which is spun at a high rate to remove excess material and create a thin coating. The solvent is removed during a

soft bake or curing step which is followed by a hard bake during which the low-k material is cross-linked and solidified. This process increases risk to workers due to solvent exposure and generates large quantities of waste. On a per wafer basis for a base case comparing spin-on and CVD organosilicon low-k dielectric films, chemical consumption was 350% higher for the spin-on deposition method.¹⁰ In a CVD process, the precursor gas is activated by thermal or plasma excitation and reacts to grow film on the surface of the wafer. While development of porous films by CVD has proved to be difficult, CVD is an entirely solventless process with minimal worker exposure to any potentially harmful materials. Also, CVD is used for current dielectric deposition meaning the changes in manufacturing process flow would be evolutionary.

Organosilicon (OSG) films have been proposed for use as a low-k material ($2.7 < k < 3.3$) to replace current inter-layer dielectrics (ILDs). Hot filament chemical vapor deposition (HFCVD) is one method to deposit organosilicon films.¹¹ HFCVD utilizes a resistively heated wire to thermally activate gases fed into the CVD reactor. Thin films are deposited on a silicon wafer placed on a cooled substrate beneath the filament array. Another CVD method more familiar to the semiconductor industry is plasma enhanced CVD (PECVD) which utilizes a low-density plasma generated by radio frequency excitation of the precursor gas. The plasmas are composed of ions, radicals, and excited neutrals from the gas that react on a temperature-controlled substrate to deposit a thin film.¹² A typical PECVD reactor is depicted in Figure 1-3.

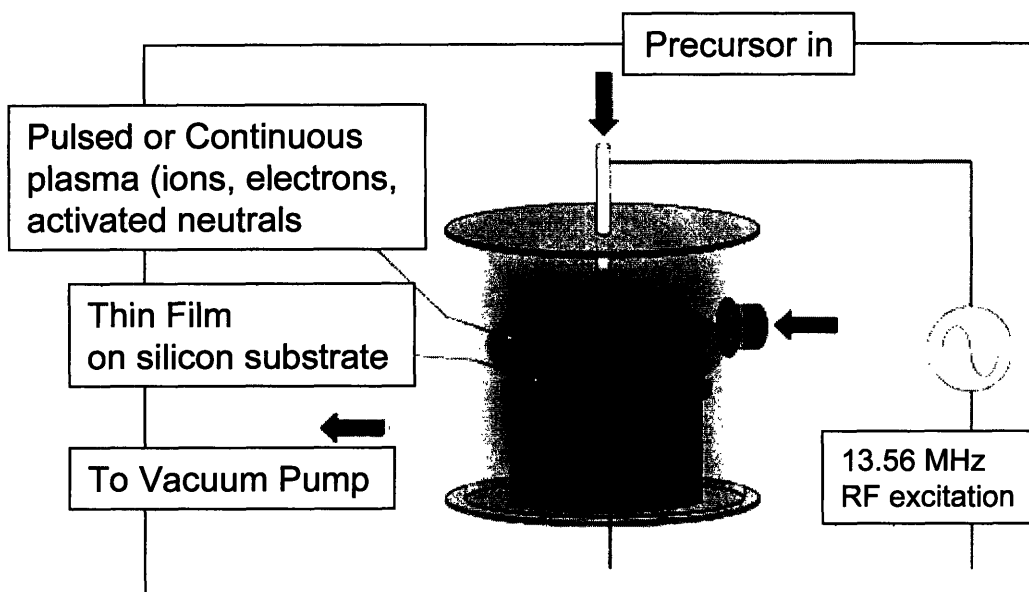


Figure 1-3. Schematic of a typical PECVD vacuum reactor.

There are many candidates for the next generation low-k inter-layer dielectric (ILD). Many of these materials, whether deposited by spin-on or CVD, contain the same atoms; silicon, carbon, oxygen, and hydrogen (Si:O:C:H). These materials, commonly referred to as organosilicate glasses (OSGs), are typically carbon-doped oxides or siloxanes deposited by CVD or plasma-enhanced CVD.¹³⁻¹⁵ Research in this field has primarily focused on the use of plasma-enhanced chemical vapor deposition (PECVD) for producing organosilicon films with desirable properties (see Wróbel and Wertheimer¹⁶ for an extensive review).

1.4 COMPUTATIONAL QUANTUM MECHANICS

Recent advances in computing power have increased the application for computation quantum mechanics. Ab initio molecular simulations can be used to calculate molecular geometries and energies, vibrational frequencies, electron densities, examine reaction pathways, and calculate properties such as shielding

tensors. Utilizing commercially available packages such as GAUSSIAN,¹⁷ the thermochemistry and kinetics of many systems has been examined.

1.5 THESIS FRAMEWORK

This thesis examines the chemistry involved in the deposition of thin OSG and sacrificial polymer thin films by hot filament and plasma enhanced CVD as well as the structure property relationship of the resulting films. This thesis utilizes computational quantum mechanics to explain observed phenomena in some cases and predict CVD chemistry in others. Always, the focus is the development and analysis of new materials created using CVD.

CHAPTER TWO reports the HFCVD deposition and structure determination of OSG thin films from hexamethylcyclotrisiloxane and octamethylcyclotetrasiloxane. The impact of filament temperature was evaluated on the structure and properties of the films.

CHAPTER THREE reports the use of density functional theory to predict ²⁹Si nuclear magnetic resonance chemical shifts of Organosilicon material. Quantum mechanics was utilized to identify previously unreported chemical shifts in the OSG literature and provide detailed insight into the deposition chemistry of OSG thin films from cyclic siloxane precursors.

CHAPTER FOUR reports the heats of formation and reaction for a family of methyl- and methoxymethylsilanes. Density functional theory was utilized to calculate the thermochemistry of OSG precursor fragmentation patterns, bond

dissociation energies, and elementary reactions with oxygen and hydrogen. The finding resulted in the design of an experimental CVD study.

CHAPTER FIVE reports the PECVD deposition and characterization of OSG thin films from methoxytrimethylsilane, dimethoxydimethylsilane, and trimethoxymethylsilane. The relationship between the optical and electric properties of the films with the deposition chemistry and resulting film structure are examined. Low-k OSG thin films are deposited using selective reducing chemistry.

CHAPTER SIX reports the PECVD deposition of polymethylmethacrylate and examines the impact of plasma power and substrate temperature on the structure and thermal properties of the polymer film. Polymethylmethacrylate has a wide range of applications including use as a porogen for creating porous OSGs or as sacrificial material for air gap fabrication. The thermal properties of the PECVD polymethylmethacrylate can be systematically varied to fit the needs of the desired application.

CHAPTER SEVEN presents concluding thoughts concerning the five technical chapters and comments on the extendibility of this work for future applications.

REFERENCES

1. G. A. Sai-Halasz, *Proc. IEEE*, **83**, 20 (1995).
2. L. Peters, in *Semiconductor International*, Vol. 25, 2002, 55.
3. P. A. Kohl, Q. Zhao, K. Patel, D. Schmidt, S. A. Bidstrup-Allen, R. Shick, and S. Jayaraman, *Electrochem. Solid-State Lett.*, **1**, 49 (1998).
4. A. T. Kohl, R. Mimna, R. Shick, L. Rhodes, Z. L. Wang, and P. A. Kohl, *Electrochemical and Solid-State Letters*, **2**, 77 (1999).
5. M. Morgen, E. T. Ryan, C. H. Jie-Jue Hua, T. Cho, and P. S. Ho, *Annual Review of Material Science*, **30**, 645 (2000).
6. M. B. Anand, M. Yamada, and H. Shibata, *IEEE Trans. Electron Devices*, **44**, 1965 (1997).
7. D. Bhusari, H. A. Reed, M. Wedlake, A. M. Padovani, S. A. Bidstrup-Allen, and P. A. Kohl, *Journal of Microelectromechanical systems*, **10**, 400 (2001).
8. B. P. Shieh, The Center for Integrated Systems, Stanford University, Stanford CA, 2002.
9. V. Arnal, J. Torres, P. Gayet, R. Gonella, P. Spinelli, M. Guillermet, J.-P. Reynard, and C. Vérove, in *UTC 2001*, STMICROELECTRONICS (2001).
10. N. H. Hendricks, in *NSF/SRC ERC for Environmentally Benign Semiconductor Manufacturing Retreat 2000*, (2000).
11. M. C. Kwan and K. K. Gleason, *Chemical Vapor Deposition*, **3**, 299 (1997).
12. R. D'Agostino, *Plasma deposition, treatment, and etching of polymers*, p. xiii, Academic Press, Boston, (1990).
13. L. Peters, in *Semiconductor International*, Vol. 23, 2000, 108.
14. M. J. Loboda, *Microelectronic Engineering*, **50**, 15 (2000).
15. A. Grill and V. Patel, *Journal of Applied Physics*, **85**, 3314 (1999).
16. A. M. Wróbel and M. R. Wertheimer, in *Plasma deposition, treatment and etching of polymers*, R. d'Agostino, Editor, p. 163, Academic Press, Boston (1990).
17. M. J. Frisch, G. W. Trucks, H. B. Schlegel, G. E. Scuseria, M. A. Robb, J. R. Cheeseman, V. G. Zakrzewski, J. J. A. Montgomery, R. E. Stratmann, J. C. Burant, S. Dapprich, J. M. Millam, A. D. Daniels, K. N. Kudin, M. C. Strain, O. Farkas, J. Tomasi, V. Barone, M. Cossi, R. Cammi, B. Mennucci, C. Pomelli, C. Adamo, S. Clifford, J. Ochterski, G. A. Petersson, P. Y. Ayala, Q. Cui, K. Morokuma, D. K. Malick, A. D. Rabuck, K. Raghavachari, J. B. Foresman, J. Cioslowski, J. V. Ortiz, A. G. Baboul, B. B. Stefanov, G. Liu, A. Liashenko, P. Piskorz, I. Komaromi, R. Gomperts, R. L. Martin, D. J. Fox, T. Keith, M. A. Al-Laham, C. Y. Peng, A. Nanayakkara, C. Gonzalez, M. Challacombe, P. M. W. Gill, B. G. Johnson, W. Chen, M. W. Wong, J. L. Andres, M. Head-Gordon, E. S. Replogle, and J. A. Pople, Gaussian, Inc., Pittsburg PA, 1998.

CHAPTER TWO

HOT-FILAMENT CHEMICAL VAPOR DEPOSITION OF ORGANOSILICON THIN FILMS FROM HEXAMETHYLCYCLOTRISILOXANE AND OCTAMETHYLCYCLOTETRASILOXANE

H. G. Pryce Lewis, T. B. Casserly, and K. K. Gleason, *J. Electrochem. Soc.*, **148**, F212 (2001).

ABSTRACT

A non-plasma technique, hot-filament chemical vapor deposition (HFCVD), is an alternative method to produce organosilicon films of novel structure. Films are deposited onto room temperature substrates from the precursors hexamethylcyclotrisiloxane (D3) and octamethylcyclotetrasiloxane (D4) at high rates (>1 micron/min). Filament temperature can be used to control film structure, and the limited reaction pathways available via thermal decomposition make it possible to elucidate the chemistry of the growth process. During film growth, there appears to be competition between reaction pathways for the incorporation of cyclic and linear siloxane structures. For both D3 and D4 HFCVD films, Infrared, Raman, and Nuclear Magnetic Resonance spectroscopies indicate the incorporation of ring structures consisting of three siloxane units. The concentration of these structures increases as filament temperature is raised, and is especially pronounced for films deposited from D3. In comparison, films grown from D4 show a greater degree of incorporation of linear, unstrained structures over the range of filament temperatures studied. In contrast to plasma-deposited organosilicon films, crosslinking in HFCVD films occurs predominantly via silicon-silicon bonding and not from siloxane bonds with tertiary or quaternary silicon atoms.

Acknowledgments: We gratefully acknowledge the support of the NIH under contract NO1-NS-9-2323, and the NSF/SRC Engineering Research Center for Environmentally Benign Semiconductor Manufacturing in funding this work. This work also made use of the MRSEC Shared Facilities supported by the National Science Foundation under Award Number DMR-9400334 and NSF Laser Facility grant #9708265-CHE.

2.1 INTRODUCTION

Organosilicon thin films produced by chemical vapor deposition (CVD) have attracted considerable interest in a wide variety of applications, ranging from biocompatible coatings for medical implants to permselective membranes.¹⁻⁹ In particular, organosilicon films are presently under consideration as low dielectric constant, or low-k, interlayer dielectric (ILD) candidates for future semiconductor processing. These materials, termed organosilicate glasses (OSGs), are typically carbon-doped oxides or siloxanes deposited by CVD or plasma-enhanced CVD.¹⁰⁻¹² Research in this field has primarily focused on the use of plasma-enhanced chemical vapor deposition (PECVD) for producing organosilicon films with desirable properties (see Wróbel and Wertheimer¹ for an extensive review).

A plasma-based deposition technique, however, has inherent deficiencies. Plasma polymers tend to show high dielectric loss as compared to conventional polymers, as well as an aging effect upon exposure to the atmosphere. It has been proposed that exposure of the growing film to UV irradiation and ion bombardment during the deposition process can result in the formation of trapped free radicals, or dangling bonds, in the film.¹³ These defect sites are then subject to oxidation upon exposure to the atmosphere. The effect of ion bombardment is also to increase the crosslink density in plasma films, which often results in brittle, inflexible films. Pulsed-PECVD is a technique that can be used to minimize plasma exposure during film growth. In this method, plasma excitation is modulated to alter the dynamics of competing deposition pathways, allowing for greater compositional control and lower crosslink density in the resulting films.¹³⁻¹⁷ Using pulsed-PECVD with the

precursor hexamethylcyclotrisiloxane (D3), we have demonstrated flexible, conformal coatings on nonplanar substrates suitable for implantation.³

Hot-filament chemical vapor deposition (HFCVD, also known as pyrolytic CVD) does not suffer from the UV irradiation and ion bombardment associated with plasma exposure. In addition, HFCVD allows for more control over precursor fragmentation pathways than PECVD. Thermal activation is limited to the gas phase and independent control of the substrate temperature can be exercised. Indeed, HFCVD using hexafluoropropylene oxide as the precursor gas has been shown to produce fluorocarbon films with low dangling bond density and having a chemical structure which is spectroscopically similar to polytetrafluoroethylene (PTFE).^{17, 18}

In this study, we consider the structure of films produced by HFCVD using the precursors hexamethylcyclotrisiloxane, $[(\text{CH}_3)_2\text{SiO}]_3$, and octamethylcyclotetrasiloxane, $[(\text{CH}_3)_2\text{SiO}]_4$, commonly known as D3 and D4. Previously, we demonstrated that polymeric thin films could be deposited from D4 by HFCVD at rates of up to 2500 nm/min depending on filament temperature.¹⁹ In this work, we show that filament temperature (T_f) has a strong influence on composition for both D3 and D4 HFCVD films, and postulate a structure for these novel films.

2.2 EXPERIMENTAL

Films were deposited on silicon wafer substrates in a custom built vacuum chamber, which has been described previously.¹⁸ Thermal excitation was accomplished by resistively heating tantalum wire (diameter 0.5 mm) strung on a

filament holder. Springs on the holder maintained wire tension to compensate for thermal expansion and prevent drooping. The filament wire was mounted in a parallel array designed to minimize thermal gradients between individual wires and offer uniform heating over an area the size of a wafer. The filament holder straddled a cooled stage on which a silicon wafer substrate was placed. A filament to substrate standoff of 1.3 cm was used. Pure precursor was vaporized in a heated vessel and delivered through a needle valve to maintain flow rates of approximately 14 sccm for D3 and 11 sccm for D4. Pressure in the reactor was maintained at 300 mtorr by a butterfly valve. No diluent gas was used.

Filament temperature was measured using a 2.2 μm infrared pyrometer. For oxidized tantalum, a spectral emissivity of 0.20 was estimated from direct contact thermocouple measurements. Due to the difficulties of direct measurement at high temperatures, reported temperatures are probably accurate to $\pm 50^\circ\text{C}$. However, temperatures were consistent from run to run and there was little variation in power requirements for heating the wire. Substrate temperature was maintained below 60°C by backside water cooling. Films were deposited on 100 mm diameter p-type (100) silicon wafers at filament temperatures ranging from 800°C to 1200°C . Deposition rates were monitored *in situ* using interferometry and checked using profilometry at the center of each wafer after deposition.

For film characterization, infrared spectroscopy was performed using a Nicolet Magna 860 FTIR spectrometer operating in transmission mode. All spectra were normalized to a standard thickness of 150 nm and baseline corrected for purposes of comparison. Resonant Raman spectra were obtained using a Kaiser Optical Systems Hololab 5000R Modular Research Micro-Raman Spectrograph,

with 785 nm laser line excitation and 15 mW power at the sampling stage under 50x magnification. High resolution solid-state NMR spectra were acquired on a homebuilt NMR spectrometer²⁰ equipped with a 6.338 T Oxford superconducting magnet and a 3.2 mm Chemagnetics probe with spinning capabilities up to 25 kHz. Magic angle spinning (MAS) and cross-polarization (CP) from the proton spin bath were used to resolve isotropic chemical shifts and reduce acquisition time. Approximately 10 mg of film was scraped off the wafer and packed into a zirconia rotor, which was spun at 7 kHz. 14,512 acquisitions were performed for signal averaging. A ¹H-²⁹Si CP time of 5 ms was chosen to maximize the overall signal intensity. Experiments confirmed that the contact time between the silicon and proton spin baths was sufficient to provide uniform ²⁹Si polarization. Indeed, a direct comparison of NMR spectra acquired with direct- and cross-polarization confirmed that CP spectra were quantitative. All NMR spectra were referenced to tetramethylsilane (TMS) and are plotted in ppm. X-Ray Photoelectron Spectroscopy (XPS) was performed on a Kratos AXIS ULTRA spectrometer using a monochromatized aluminum K- α source. Atomic force microscopy (AFM) was performed on a Digital Instruments Dimension 3000. Images were taken under tapping mode with a standard etched silicon tip.

2.3 RESULTS AND DISCUSSION

2.3.1 DEPOSITION RATE

The measured deposition rate, r , and the thickness-based deposition yield, r/FM (where F is the volumetric flow rate, and M is the molecular weight of the

precursor), are plotted in Arrhenius form in Figure 2-1. The deposition yield expresses the deposition rate per unit mass of the precursor compound, and allows the relative reactivities of D3 and D4 to be compared directly.²¹ As shown in Figure 2-1, the deposition yield appears to follow an Arrhenius-type relationship as a function of filament temperature. The highest deposition rate observed was 1574 nm/min, for D4 at a filament temperature of 1050°C. No film deposition was detected at filament temperatures below 800°C with either precursor. At the higher filament temperatures, run times were limited to 1.5 minutes to produce thin films appropriate for subsequent characterization. These temperatures are consistent with other studies of the vacuum pyrolysis of D4.²² Regression of the data in Figure 2-1 yielded apparent activation energies of 218 ± 35 kJ/mol for D3, and 301 ± 102 kJ/mol for D4 (at a 90% confidence level).

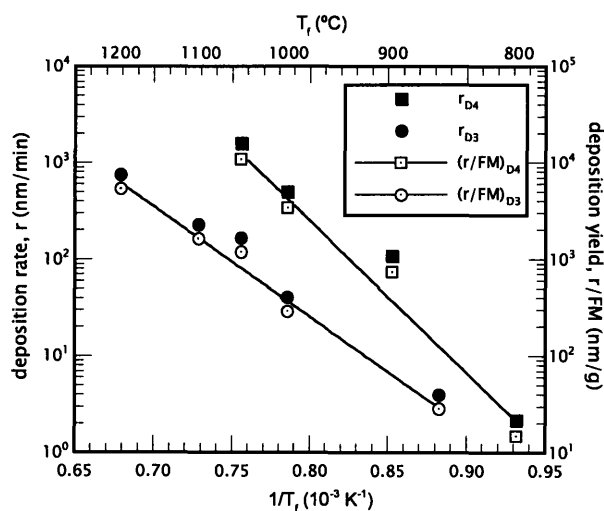


Figure 2-1. Arrhenius plot of D3 and D4 films produced by HFCVD. Measured deposition rates, r (left axis), are denoted by solid markers, and thickness-based deposition yields, r/FM (right axis), are denoted by empty markers. Straight lines were fitted to the deposition yield data by regression.

2.3.2 FOURIER TRANSFORM INFRA-RED (FTIR) SPECTROSCOPY

A comparison of the FTIR spectra of D3 films deposited using HFCVD and continuous-wave excitation PECVD is shown in Figures 2-2a and 2-2b. The spectrum for the CW PECVD film (Figure 2-2a) was taken from previous work by our group.³ Assignments have been made from the literature and are shown in Table 2-1. Comparison of these spectra indicates that the HFCVD film differs structurally from the PECVD film. Only sp^3 -carbon bonding is observed in the HFCVD film, and no crosslinking of Type II, i.e. via carbon-crosslinks, is evident.³ Carbon is thus preserved primarily as methyl, giving rise to the distinct pair of symmetric and asymmetric CH stretches²³⁻²⁵ at 2907 and 2964 cm^{-1} . The asymmetric stretching mode (ASM) of the siloxane group (SiOSi) shows two distinct bands for the HFCVD film, a characteristic observed in the IR signatures of polydimethylsiloxanes with chain lengths of more than two siloxane units or ring sizes of larger than eight units.^{26, 27} Below 1000 cm^{-1} , absorption bands associated with $SiMe_2$ rocking and stretching are observed at 878 and 805 cm^{-1} , and those associated with $SiMe_3$ rocking near 840 cm^{-1} . Qualitatively, the PEVD film appears to have a higher $SiMe_3/SiMe_2$ ratio, suggesting that the HFCVD film may be less branched than its PECVD analog.³

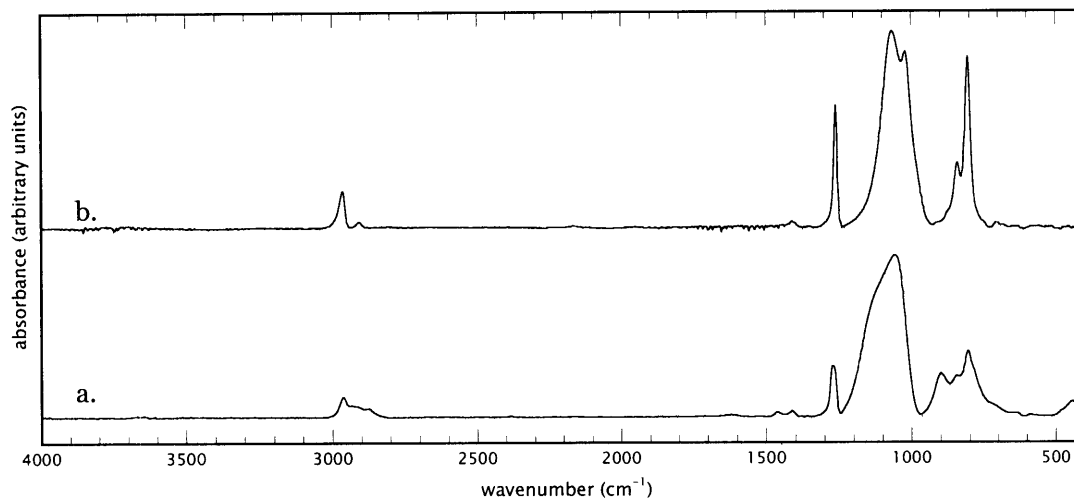


Figure 2-2. FTIR spectra of a. D3 PECVD film deposited under continuous-wave excitation and b. D3 HFCVD film deposited at 1000°C.

Table 2-1. FTIR assignments from the literature.

Wavenumber (cm ⁻¹)	Mode ^a	Comment	Reference
2963 – 2965	$\nu^{\text{A}}_{\text{CH}}$	in sp ³ CH ₃	24, 25, 31, 36
2935	$\nu^{\text{A}}_{\text{CH}}$	in sp ³ CH ₂	24, 25
2907	$\nu^{\text{S}}_{\text{CH}}$	in sp ³ CH ₃	24, 25, 31, 36
2878	$\nu^{\text{S}}_{\text{CH}}$	in sp ³ CH ₂	24, 25
1463	$\delta^{\text{A}}_{\text{CH}_2}$		24, 25
1412	$\delta^{\text{A}}_{\text{CH}_3}$	in SiMe _x	24, 25, 27, 31, 36
1262	$\delta^{\text{S}}_{\text{CH}_3}$	in SiMe _x	25, 27, 30, 31, 36
1020 – 1075	$\nu^{\text{A}}_{\text{SiOSi}}$		24, 25, 27, 31, 36
878	$\gamma^{\text{S}}_{\text{CH}_3}$	in SiMe ₂	25, 27, 30, 36
804 – 806	$\nu^{\text{A}}_{\text{Si-C}}, \gamma^{\text{A}}_{\text{CH}_3}$	in SiMe ₂	25, 27, 30, 31, 36
839 – 845	$\gamma^{\text{A}}_{\text{CH}_3}$	in SiMe ₃	25, 27, 30, 36

^a ν , δ , and γ denote stretching, bending and rocking modes respectively, A and S denote asymmetric and symmetric vibrations.

FTIR spectra of films deposited at filament temperatures of 860°C, 1000°C, and 1200°C using D3, and 800°C, 900°C, and 1000°C using D4, are also shown (Figures 2-3 and 2-4, respectively). The region around the ASM has been expanded for detail. Strong absorptions associated with SiMe₂ (805 cm⁻¹), methyl in SiMe_x

(1412 cm^{-1}), and the ASM (1020-1075 cm^{-1}) are apparent. The band at about 880 cm^{-1} observed in the low filament temperature D4 film is usually associated with the symmetric CH_3 rocking mode in SiMe_2 . The disappearance of this band at higher filament temperatures may be due to the conformational constraints present in a more highly networked structure. Similar effects in this infrared region have been observed in temperature-dependent spectroscopy studies of other organosilicon compounds.^{28, 29}

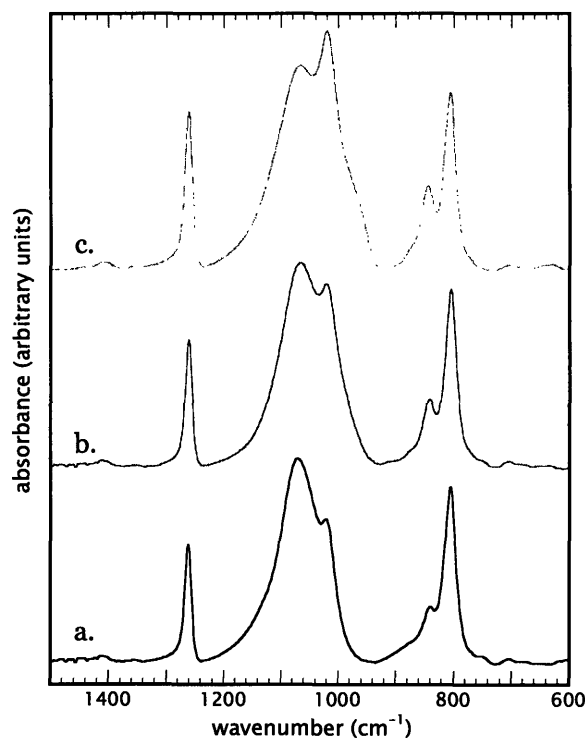


Figure 2-3. FTIR spectra of D3 HFCVD films deposited at filament temperatures of a. 860°C, b. 1000°C, and c. 1100°C

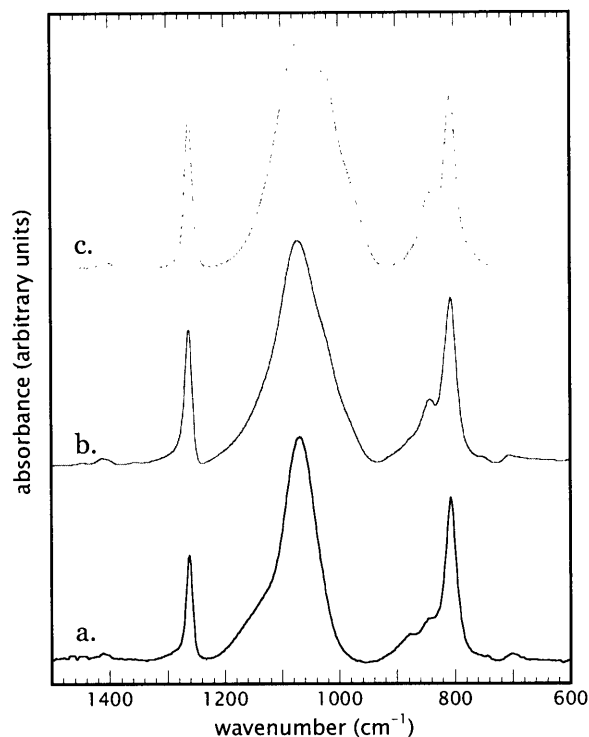


Figure 2-4. FTIR spectra of D4 HFCVD films deposited at filament temperatures of a. 800°C, b. 900°C, and c. 1000°C.

Conventionally^{25, 27, 30}, the band around 845 cm⁻¹ is assigned to an asymmetric CH₃-rocking mode in SiMe₃, with an accompanying symmetric CH₃-rocking mode at 760 cm⁻¹. The SiMe₃ group is a chain or branch termination group that is associated with an M group in siloxanes³, where M is the trimethylsiloxane unit (CH₃)₃SiO-. The relative intensities of the SiMe₂ and SiMe₃ bands depends on the length of chains in open-chain regions of the film structure, and the strength of the SiMe₃ band is an indication that chains are either short or highly branched.^{26, 31} The SiMe₃/SiMe₂ ratio also increased only slightly as filament temperature was increased, suggesting that the chain length and branching was similar for both sets of films. Other data obtained for these films, particularly from NMR analysis, show only small quantities of M groups in the films, with the highest concentrations appearing in low filament-

temperature D3 and high filament-temperature D4 films. This implies that short chain segments or branches of similar length are present in low concentrations in almost all the films produced.

Significant changes in the relative intensities of the bands of the ASM band are observed for both D3 and D4 films. The spectra of the D3 film shows a doublet for all three filament temperatures, with the shoulder on the doublet switching from the low- to high-wavenumber side at higher filament temperatures (compare Figures 2-3a and 2-3c). By contrast, the spectra of the D4 film deposited at a filament temperature of 800°C (Figure 2-4a) showed only a singlet, and the IR spectra resembled that of the precursor D4.^{26, 27} Unlike D4, however, which is a liquid at room temperature, the film was solid and contiguous and came off the wafer in flakes when scraped with a razor. The D4 film deposited at higher filament temperature showed behavior similar to that of the D3 film. As filament temperature was increased, the low-wavenumber peak of the ASM doublet increased in intensity, exceeding that of the high-wavenumber peak above 1050°C (spectra not shown), as in the case of the D3 film.

The ASM doublet of the film deposited from D3 at a filament temperature of 1100°C (Figure 2-3c) resembles that observed in FTIR analyses of other organosilicon PECVD films.^{3, 25, 32} Typically for these films, the low-wavenumber band was more intense than the high-wavenumber band. This ASM signature is also observed in spin-on methyl silsesquioxane (MSQ) films.³³ For bulk polydimethylsiloxane (PDMS), the intensities of these bands are approximately equal at room temperature.³⁴ To our knowledge, no IR spectra with an ASM doublet similar to that observed in Figures 2-3a, 2-3b and 2-4c have been reported for

organosilicon films deposited by CVD from comparable precursors. The configuration of the ASM doublet is likely to be conformational in origin. For PDMS, the splitting of the doublet has been attributed to coupling between adjacent chain segments.³¹ In other work using Raman spectroscopy, the splitting of the symmetric SiOSi stretching mode has been correlated to the crystalline state of PDMS.³⁵

The intensity ratio of the two bands of the ASM doublet has been correlated with the length of chains or size of rings in the polymethylsiloxane network.²⁵⁻²⁷ In particular, for a series of linear and cyclic polymethylsiloxanes of increasing chain length or ring size, a doublet was observed in FTIR spectra only when chain lengths exceeded two siloxane units and ring size exceeded five siloxane units. The ASM singlet for D3 was offset at 1,020 cm^{-1} compared to larger ring structure. The band at 1,020 cm^{-1} may thus be associated with an increasing proportion of six-membered D3-like rings in the film structure. This is in the same region as the low-wavenumber band of the ASM doublet in PDMS, however, making it difficult to differentiate between the presence of chains and bound D3 rings using IR analysis.³¹

2.3.3 RAMAN SPECTROSCOPY

Though some work has been done in characterizing pure organosilicon compounds using Raman spectroscopy, little has been reported on the use of Raman for characterizing more complex organosilicon materials, such as those produced by CVD. Figure 2-5 compares the Raman spectra of the pure compounds D3, D4, and PDMS with that of HFCVD films grown from D3 and D4 using high filament temperatures. Assignments in Table 2-2 have been made based on the literature.^{28, 31, 36, 37} The symmetric siloxane stretching mode (SSM), which is weak in FTIR spectra,

is strong in the Raman spectra. The position of the symmetric siloxane Raman band is shifted to higher wavenumbers for D₃ due to ring strain, and bands associated with ring deformation can be observed for both D₃ and D₄.³¹ Raman spectroscopy is thus a sensitive probe for observing ring structure. Indeed, Raman spectroscopy is capable of identifying siloxane ring “defects” in SiO₂ films produced by sol-gel³⁸⁻⁴¹ and CVD processes.⁴² Raman spectra for these materials exhibit specific bands corresponding to ring structures comprised of different numbers of silicon atoms. In particular, Raman bands at 605 cm⁻¹ and 495 cm⁻¹ in silica have been attributed to rings with three and four siloxane units, termed R₃ and R₄ respectively.^{38, 39, 41, 42}

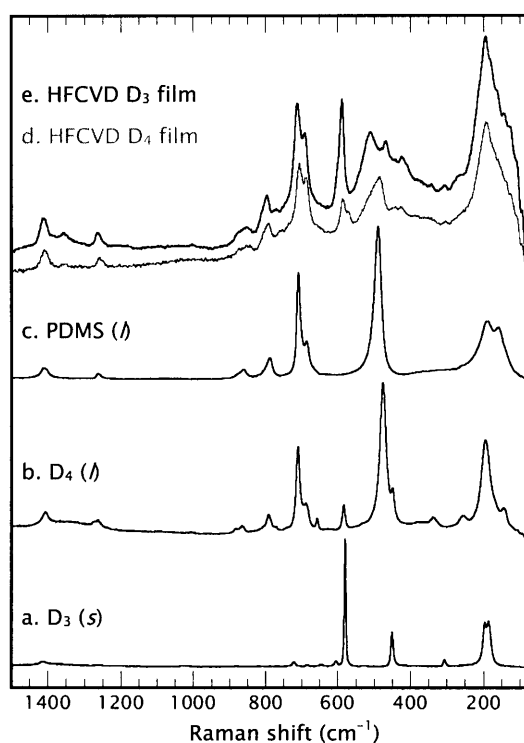


Figure 2-5. Micro-Raman spectra of a. D₃, b. D₄, c. PDMS, d. D₄ HFCVD film deposited at a filament temperature of 1000°C, and e. D₃ HFCVD film deposited at a filament temperature of 1100°C.

Table 2-2. Raman assignments from the literature.

Raman shift (cm ⁻¹)	Mode ^a	Comment	Reference
1410	$\delta^A_{CH_3}$		23, 28, 36
1260 – 1265	$\delta^S_{CH_3}$		23, 28, 36
795	ν^A_{SiC}	In SiC ₂	23, 28, 36, 37
707 – 712	ν^S_{SiC}	In SiC ₂	23, 28, 36, 37
690	$\gamma^A_{CH_3}$		23, 28, 37
581	ν^S_{SiOSi}	In D3	31, 37, 72
489	ν^S_{SiOSi}	In PDMS	23, 36
476	ν^S_{SiOSi} and/or ring deformation	In D4	23, 37
450	Ring deformation	In D3 and D4	23, 37
424 – 426	Possible Si-Si stretch		44
190 – 194	δ^S_{SiC}	in SiC ₂	31, 37
160	δ^S_{SiC} and twist	In PDMS	31
145	δ^S_{SiC}	In D4	31

^a ν , δ and γ , denote stretching, bending and rocking modes respectively, A and S denote asymmetric and symmetric vibrations.

As observed in Figure 2-5, the Raman shift region of the HFCVD films from 400 cm⁻¹ to 600 cm⁻¹ differs from that of the pure compounds. Both HFCVD films show a band in the range 586 – 590 cm⁻¹ which is not observed in PDMS or other linear siloxane compounds.³¹ This is close to the band assigned to the siloxane symmetric stretching mode (SSM) at 581 cm⁻¹ in pure D3. During an experiment in which polarization of the Raman beam was changed from the parallel to the perpendicular mode, the band in the HFCVD film was also found to be polarized, which is consistent with results observed for the SSM in D3.^{31, 37} This band may thus be evidence of a bound D3-like ring structure in the film. The 5 – 10 cm⁻¹ shift from the position of this band in D3 may be conformational in origin and a result of the strain of being locked into a semi-networked structure. Such shifts are possible, and Table 2-3 shows Raman assignments for the SSM mode in different chemical

environments. In the highly networked environment of vitreous and chemical vapor-deposited silica, the characteristic vibrational mode of the six-membered planar ring of siloxane units, R_3 , has been observed at shifts as high as 608 cm^{-1} .^{38, 40, 43} By contrast, the SSM mode is typically observed from $581\text{-}587\text{ cm}^{-1}$ for unconstrained D_3 . The band around 590 cm^{-1} for the HFCVD films falls between these extremes, and is thus assigned to an oR_3 group. The term oR_n is derived from the R_n unit observed in silica, and is intended to represent an organically substituted ring consisting of n siloxane units, which is bound into the film structure. By analogy, there may also be rings consisting of four siloxane units bound into the film structure (oR_4). Table 2-3 shows that the band at 485 cm^{-1} observed primarily for the D_4 HFCVD films falls between the SSM bands for D in PDMS, R_4 in silica, and unperturbed D_4 . This suggests that the band is associated with oR_4 groups and/or unstrained siloxane units in the film. The unstrained siloxane units may be present in linear structures or in ring structures larger than four units, and are designated as lD . The predominance of these groups in the D_4 films, particularly at low filament temperature, suggest that they are unique to the pyrolysis chemistry of D_4 and may be the four siloxane-unit ring analog, oR_4 .

Table 2-3. Raman siloxane symmetric stretching mode (SSM) assignments

Symbol	Raman shift (cm ⁻¹)	Comment	Reference
R ₃	600-608	In vitreous and/or CVD silica.	38-42
<i>o</i> R ₃	586-590	In D ₃ and D ₄ HFCVD films.	
D ₃	581-587	In D ₃ .	31, 37, 72
D	489-497	In PDMS.	23, 36
R ₄	490-495	In vitreous and/or CVD silica.	38-42
<i>o</i> R ₄ and/or <i>l</i> D	485	In D ₃ and D ₄ HFCVD films.	
D ₄	475-480	In D ₄ .	23, 28, 36, 37

The Raman spectra of the HFCVD films also show a low-intensity band at 425 cm⁻¹ not observed in any of the pure compounds. No assignment could be found for this band in the literature, but it is in the region associated with a silicon-silicon stretching mode.⁴⁴ The Si-Si stretch gives a strong Raman band at 400 – 405 cm⁻¹ for hexamethyldisilane, and is highly sensitive to silicon substituents. For polar substituents, shifts can be large. For example, the Si-Si stretching mode for FMe₂SiSiMe₂F has been reported at 433 cm⁻¹, a shift of 30 cm⁻¹ from the unsubstituted disilane.⁴⁵ Hence, this band is tentatively assigned to a Si-Si bond in the film structure.

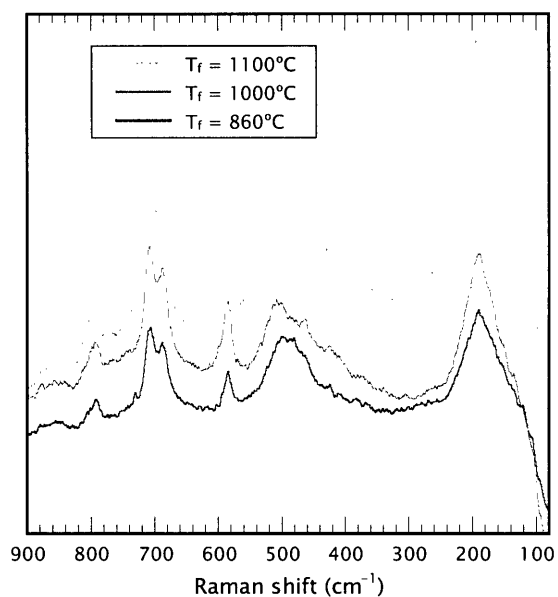


Figure 2-6. Micro-Raman spectra of D3 HFCVD films deposited at filament temperatures of 860°C, 1000°C, and 1100°C.

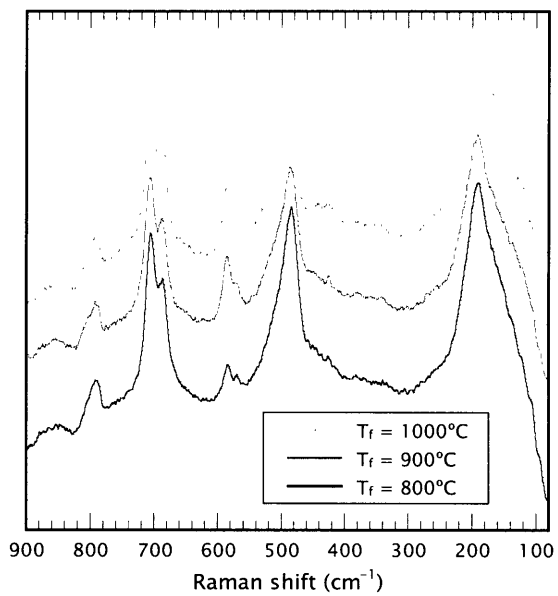


Figure 2-7. Micro-Raman spectra of D4 HFCVD films deposited at filament temperatures of 800°C, 900°C, and 1000°C.

Figure 2-6 and 2-7 show the effect of filament temperature as probed by Raman spectroscopy. The spectra of the films deposited from D3 (Figure 2-6) show an increasing intensity of the bands from oR_3 units and Si-Si bonds as filament temperature is increased, and the D3 film deposited at 1100°C shows significant ring incorporation. FTIR spectra for these films show a similar increase in intensity in the low-wavenumber band of the ASM doublet (see Figure 2-3), suggesting that this band at 1020 cm^{-1} is indeed associated with three siloxane-unit ring structures. By contrast, the spectra of the films deposited from D4 (Figure 2-7) show a strong band at 485 cm^{-1} , assigned to the presence of oR_4 and/or unstrained D units. A slight increase in oR_3 incorporation is observed as T_f increases, but this band does not dominate as it does in the spectra of the D3 films (Figure 2-6). Hence, the D3 and D4 films differ structurally at high filament temperatures, despite the similarities in structures suggested by FTIR.

2.3.4 NUCLEAR MAGNETIC RESONANCE (NMR) SPECTROSCOPY

The ^{29}Si CP-MAS NMR spectra obtained for the D3 and D4 HFCVD films are shown in Figures 2-8 and 2-9. Typical chemical shifts reported in the literature for organosilicon CVD films are included in Table 2-4.^{20, 32, 46-49} As suggested by the data in this table, films deposited by other CVD methods commonly show a wide variety of bonding environments, including the presence of M, D, T, and Q groups as well as their hydrogenated analogs.^{32, 49, 50} By contrast, only two primary peaks were observed in these HFCVD films.

Table 2-4. ^{29}Si NMR structures and chemical shifts commonly observed in OSG CVD films.

Symbol	Structure	Chemical Shift, δ (ppm)	Reference
M	$(\text{SiO})\text{Si}^*(\text{CH}_3)_3$	+6	32, 49, 52, 73
M ^H	$(\text{SiO})\text{Si}^*(\text{H})(\text{CH}_3)_2$	-6	47, 49, 52
D	$(\text{SiO})_2\text{Si}^*(\text{CH}_3)_2$	-10 in D3 -20 in D4 -22 in PDMS	32, 46, 48, 49, 52
D ^H	$(\text{SiO})_2\text{Si}^*(\text{H})(\text{CH}_3)$	-34 to -37	46, 47, 49, 52, 74
T	$(\text{SiO})_3\text{Si}^*(\text{CH}_3)$	-67	32, 46, 49, 52
T ^H	$(\text{SiO})_3\text{Si}^*(\text{H})$	-84	20, 47
Q	$(\text{SiO})_4\text{Si}^*$	-105 to -110	32, 46, 48, 49, 52

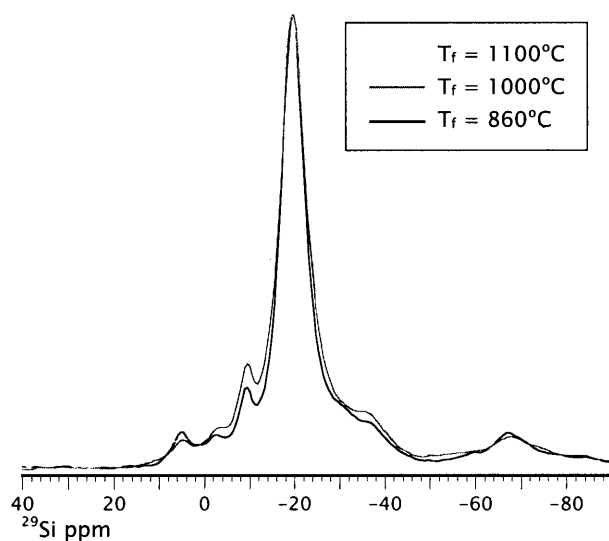


Figure 2-8. ^{29}Si Solid-State CP-MAS NMR spectra of D3 HFCVD film deposited at filament temperatures of 860°C, 1000°C, and 1100°C.

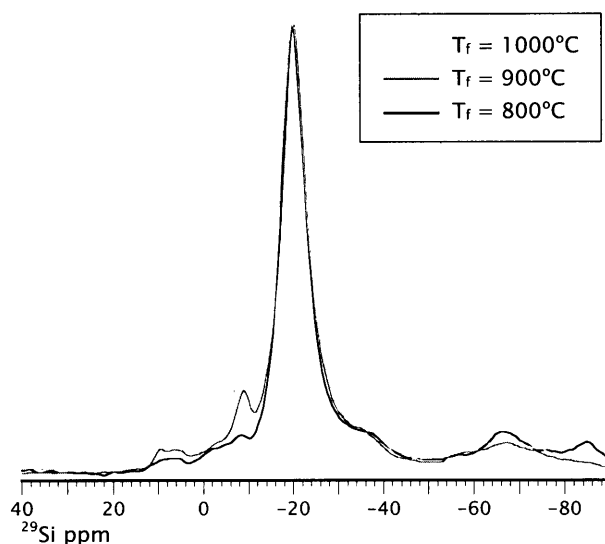


Figure 2-9. ^{29}Si Solid-State CP-MAS NMR spectra of D4 HFCVD film deposited at filament temperatures of 800°C, 900°C, and 1000°C.

The major peak at -19 ppm is assigned to the D unit, $(\text{SiO})_2\text{Si}^*(\text{CH}_3)_2$.^{32, 46, 48,}
⁴⁹ The chemical shift for this moiety depends on the conformation of the siloxane chain, typically varying from -22 ppm for PDMS to -10 ppm for D3 (due to ring strain). The lack of a doublet for this resonance analogous to that observed in FTIR is probably due to the longer time scales used for signal averaging in NMR. The closest assignment for the peak at -9 ppm suggested by the literature was for M^{H} $[(\text{SiO})\text{Si}^*(\text{H})(\text{CH}_3)_2]$, which is typically reported at -6 ppm.^{47, 49} However, there is little evidence of Si-H bonding (usually observed near 2140 cm^{-1}) in FTIR spectra of the HFCVD films. Since the Si-H stretching vibration has high oscillator strength⁵¹, even low concentrations of this moiety should yield a visible peak in the FTIR spectra. Furthermore, CP contact time experiments produced no change in the relative intensities of the major peaks at -9 ppm and -19 ppm. It is anticipated that silicon directly bonded to hydrogen would increase cross-polarization rate. Thus, the peak at -9 ppm is not indicative of an M^{H} structure. As suggested by the Raman

spectroscopy, this peak is assigned rather to the presence of oR_3 ring structures in the film. This assignment is close to the reported shift of -10 ppm for the D unit in the strained molecule D3.^{46, 48, 52} The major peak at -19 ppm is then associated with oR_4 and/or unstrained siloxane units. The shift of $+3$ ppm from an unstrained D group suggests that this unit may be primarily present in the form of a ring structure rather than a linear chain.⁴⁸

For both the D3 and D4 films, the peak at -9 ppm increases in intensity as filament temperature increases (see Figures 2-8 and 2-9). While this peak is present in the spectra of the D3 films over the whole range of filament temperatures, it is of very low intensity in the spectra of the D4 film deposited at a filament temperature of 800°C . This is consistent with Raman data, which shows very little oR_3 in this film. The M peak at $5-6$ ppm is also more intense in the D3 film deposited at filament temperature of 860°C than in its 1100°C counterpart. Since M is more likely to be associated with linear structures in the film, a lower M content at high filament temperatures is consistent with the higher content of ring structures suggested by Raman spectroscopy. The NMR spectra of both D3 and D4 films show a low and constant concentration of T groups, and almost no Q group. T and Q groups are conventional crosslinking and/or branching groups in organosilicon materials, and are observed in significant concentrations in the films produced using PECVD.^{3, 32, 49, 50} The absence of these groups suggests that crosslinking in the film must be associated with some other bonding structure. Based upon the evidence of Si-Si bonding observed in Raman spectroscopy, it is postulated that crosslinking in these films occurs preferentially via this bonding.

2.3.5 X-RAY PHOTOELECTRON SPECTROSCOPY (XPS)

Elemental ratios obtained using XPS analysis are reported in Table 2-5. The highest O:Si ratio is 1.23 for the D4 film deposited at a filament temperature of 800°C. The higher O:Si ratio for the this film is consistent with ²⁹Si NMR data indicating a greater concentration of T groups.

Table 2-5. XPS elemental ratios for HFCVD films from D3 and D4.

Precursor	T _f (°C)	O/Si	C/Si
D3	860	1.19	1.63
	1000	1.14	1.42
	1100	1.12	1.38
D4	800	1.23	1.86
	900	1.10	1.44
	1000	1.12	1.34

A C:Si ratio of less than 2.0 indicates that all films are deficient in carbon as compared to the precursor molecules. C1s high-resolution scans confirm that carbon is present exclusively as methyl. The methyl content appears to depend on filament temperature, with a significant loss of methyl at high filament temperatures for both D3 and D4 films. In all but one film, Si2p high-resolution scans showed no evidence of silicon oxidation states other than 2+, confirming that very little T and Q is present in the films. For the D3 film deposited at a filament temperature of 1100°C, the Si2p and C1s high-resolution scans show slight shouldering on the main peaks. One source for this shouldering may be the slight increase in T group concentration observed in ²⁹Si NMR (Figure 2-8). However, this is inconsistent with the low O/Si ratio reported for this film, and similar shouldering is not observed in the D4 film deposited at filament temperature of 800°C which shows a greater O/Si ratio. More

likely, the shouldering is a shift associated with Si-Si bonding that becomes visible when the concentration of this moiety is high. The origin of the shouldering in the C1s scan is uncertain but is unlikely to originate from carbonyl or methylene moieties in the films, as these would be visible using other spectroscopic techniques (e.g. FTIR).

2.3.6 ATOMIC FORCE MICROSCOPY (AFM)

AFM indicated that the films were very smooth. A typical micrograph is shown in Figure 2-10, in this case for a D4 film deposited at a filament temperature of 900°C. RMS roughnesses for all films were of the order of 1.0 nm. The RMS roughness of the silicon substrate was 0.53 nm.⁵³ This in contrast to fluorocarbon films deposited using HFVCD, which often show greater roughness and characteristic morphology.⁵⁴ This morphology is possible due to the lack of ion and electron bombardment which tends to cause densification and damage to the growing film during PECVD. The smoothness of our films deposited using a similar HFCVD process suggests that there is efficient packing on the molecular level in the organosilicon films.

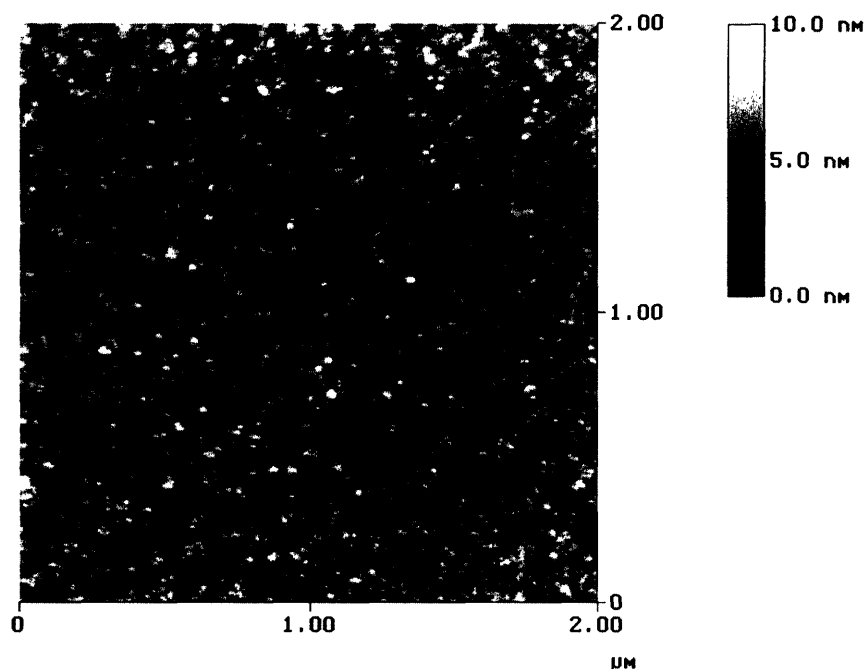


Figure 2-10. Atomic force micrograph of D4 HFCVD film deposited at a filament temperature of 900°C. RMS roughness over image area is 1.1 nm. RMS roughness of bare silicon is 0.53 nm.

2.3.7 CHEMICAL REACTIONS

Possible pathways for the production of film growth species under thermal excitation are shown in Scheme 1. Reactions 1 through 3 describe respectively the molecular rearrangement of D4 to produce D3 and the intermediate species dimethylsilanone (D₁, Me₂Si=O), methyl abstraction from the ring to produce a radical ring species, and ring-opening to produce a linear diradical group. Reactions 4 through 6 are analogous pathways for D3.

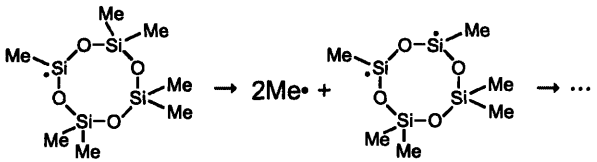
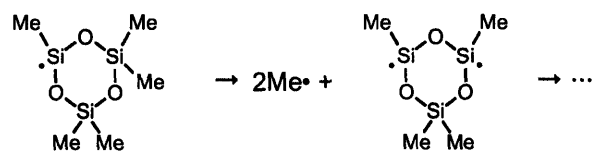
Reaction	Description
(1) $D_4 \leftrightarrow D_3 + Me_2Si=O$	<i>Intramolecular Rearrangement</i>
(2) $D_4 \rightarrow Me\cdot + $ 	<i>Methyl Abstraction</i>
(3) $D_4 \leftrightarrow \cdot O(Me_2SiO)_3Me_2Si\cdot$ or $\cdot O(Me_2SiO)_3Me_2Si^+$	<i>Ring Opening</i>
(4) $D_3 \leftrightarrow D_2 + Me_2Si=O$	<i>Intramolecular Rearrangement</i>
(5) $D_3 \rightarrow Me\cdot + $ 	<i>Methyl Abstraction</i>
(6) $D_3 \leftrightarrow \cdot O(Me_2SiO)_2Me_2Si\cdot$ or $\cdot O(Me_2SiO)_2Me_2Si^+$	<i>Ring Opening</i>

Figure 2-11. Reaction pathways for the production of polymerization precursor species in D3 and D4 HFCVD.

Previous studies have investigated the gas-phase pyrolysis of D3 and D4 over a temperature range from 400 to 1100°C and a pressure range from 10⁻⁴ to 1.0 Torr.^{22, 55-58} For the pyrolysis of D4, the only products observed were D3 and D₅, with the rate of formation of D₅ decreasing rapidly above 2% decomposition until D3 was the only product at high conversions.^{57, 58} The formation of the intermediate D₁ was postulated to explain the observed results, and the presence of D₅ explained by recombination of D₁ with D4. Other authors have postulated the existence of D₁^{56, 59, 60}, and evidence for its existence has been collected in matrix IR studies of the vacuum pyrolysis of D4²². In the latter study, temperatures from 900°C to 1,050°C were used, closer to those used in our work, and significant conversion of D4 to D3 was also noted at these higher temperatures. D₁ may result from the intramolecular

rearrangement of D₄ at high temperatures, and similar thermal rearrangements have been observed in other dimethylsiloxanes. It has been suggested that these involve the formation of a bicyclic transition state, accounting for the predominant cleavage of the Si-O bond over the weaker Si-C bond.^{22, 56, 60-64}

D₁ may be a growth precursor for the organosilicon films, with a polymerization mechanism analogous to that postulated for the diradical difluorocarbene (CF₂) during HFCVD of fluorocarbon films.⁶⁵ Indeed, heterogeneous loss of D₁ has been postulated to account for discrepancies in the mass balance in previous pyrolysis studies of D₄.⁵⁸ For the early stages of this pyrolysis (<4% decomposition), an activation energy of 301±6.3 kJ/mol was reported for reaction 1.⁵⁸ This is close to the apparent activation energy of 301±102 kJ/mol estimated from the kinetic data in Figure 2-1 for D₄, and suggests that reaction 1 may be the predominant pathway for the pyrolysis of D₄ at low filament temperatures. It is illuminating to apply the reported rate law to our CVD system. At low filament temperatures (e.g., 800°C), where the conversion of D₄ is likely to be less than 4% and 569°C may be representative of the gas phase temperatures some distance from the filament, the conversion of D₄ using this rate law is calculated to be 0.3%. Assuming a film density²⁵ of 1.3 g/cm³, the production of D₁ could yield film growth at a rate of 10.8 nm/min on a 4-inch wafer. By comparison, the measured deposition rate at 800°C was 2.2 nm/min. At higher filament temperatures (above 1,000°C), the conversion of D₄ exceeds 4% and the rate law no longer applies. Hence, film growth by D₁ generated via reaction 1 is possible, and could lead to a linear siloxane backbone structure. This may explain the higher C/Si ratio in XPS and the lack of

ASM doublet structure in FTIR for the D₄ film deposited at a filament temperature of 800°C.

In contrast to D₄, the pyrolysis of D₃ is not expected to yield significant quantities of D₁. The D₂ ring is highly unstable^{60, 66} and the elimination of D₁ from D₃ as shown in reaction 4 is known to be highly endothermic.^{58, 62} The lack of this pathway for producing growth species may explain the lower deposition yields observed for D₃, despite the molecule's planar strained conformation and typically high reactivity in heterolytic reactions. Instead, the rupture of the silicon-methyl bond via reaction 5 is likely to predominate. In preliminary studies, Davidson *et al.*⁵⁸ reported on the kinetics of this reaction for the loss of one methyl group between 578°C and 662°C. Calculations at 662°C analogous to those performed for reaction 1 showed that a loss of one methyl group from D₃ via reaction 5 could account for a conversion of 0.6% of the precursor, and could yield film growth at a rate of 76.2 nm/min. If only one methyl group were lost per D₃ molecule, the oR₃ ring structure could be incorporated into the film as a terminal group. Additional methyl abstraction processes may also occur after the initial loss, resulting in incorporation of the oR₃ structure as a polymeric (loss of two methyl groups) or networked unit (loss of three methyl groups). Incorporation requires bonding of the oR₃ group to another oR₃ group and/or a D₁ unit, and, in the absence of free oxygen, involves a silicon-silicon bond. This may be the origin of the assigned silicon-silicon group observed in Raman spectroscopy. By similar reasoning, methyl abstraction from D₄, as shown in reaction 2, and subsequent incorporation of the oR₄ group is possible. However, no kinetic data has been found for reaction 2.

Ring-opening is also possible for both D3 and D4, as illustrated in reactions 3 and 6. However, direct homolytic cleavage of the Si-O bond in cyclosiloxanes to produce diradicals of the form $\cdot\text{SiMe}_2(\text{OSiMe}_2)_n\text{O}\cdot$ is unlikely.^{60, 62} Free radical polymerization of diradical species produced by reactions 3 and 6 is thus improbable. Ionic polymerization also seems unlikely in an HFCVD environment, where ions are expected to be short-lived. Such pathways are more likely in a plasma environment, where ionic species formed from the ring-opening of cyclic dimethylsiloxanes have been postulated to explain growth mechanisms in organosilicon PECVD from similar precursors^{1, 67-69} Furthermore, if the ring-opening reaction were the primary contributor to the production of film growth species, it is anticipated that greater ring strain in D3 would be reflected in higher growth yields for that precursor. Instead, Figure 2-1 shows that deposition yields for D4 are consistently higher than for D3. For comparison, ring strains of 10.5 kJ/mol for D3 and 1.00 kJ/mol for D4 have been reported.⁶⁶ Hence, polymerization of linear species produced via reactions 3 and 6 does not appear to be a dominant mode of film growth.

Growth of the D3 and D4 HFCVD films is thus believed to occur mainly through the combination of growth precursors generated via reactions 1, 2, and 5. For D4, there is competition between the generation of D₁ via reaction 1 and the generation of *o*R₄ groups from methyl abstraction in reaction 2. Since reaction 1 produces D3, there is an additional pathway for the incorporation of *o*R₃ groups generated via reaction 5. At low filament temperatures, reaction 1 may dominate, resulting in film growth primarily from D₁ species. At higher filament temperatures, however, evidence of *o*R₃ incorporation suggests that reaction 5 starts to compete.

For D₃, reaction 5 is the predominant source of potential growth precursors in the form of *oR*₃ structures. However, it does not appear to be the only source, as all films from D₃ show some evidence of incorporation of *oR*₄ and/or *ID* units in the film structure. Pyrolysis studies of D₃ have shown evidence of appreciable concentrations of D₄ in the pyrolyzate, and it was found that the concentration of D₄ in the pyrolyzate decreased as pyrolysis temperature increased.^{55, 56} At low filament temperatures, where D₄ concentrations are higher, there is probably a significant contribution of reaction 1 to the chemistry. At higher temperatures, where D₃ concentrations are high, reaction 1 is probably less favorable and D₄ reacts preferentially via the methyl abstraction process in reaction 2. This may explain the shift observed in the Raman band assigned to *oR*₄ and/or *ID* as filament temperature increases (Figure 2-6). For the 860°C film, this band is centered close to 495 cm⁻¹, but shifts to about 505 cm⁻¹ for filament temperatures above 1000°C. There also appears to be a new band that appears near 465 cm⁻¹ above this temperature. Most likely, the band centered around 495 cm⁻¹ is indicative of a linear siloxane unit derived from the polymerization of D₁. The two bands that appear at higher temperature are indicative of an *oR*₄ unit (at 505 cm⁻¹) and a larger structure such as *oR*₅ (at 465 cm⁻¹). The five-membered siloxane ring, *oR*₅, could originate from D₅ via methyl abstraction processes analogous to those in reactions 2 and 5.

It is thus postulated that growth of the D₃ HFCVD film occurs in two distinct regimes: at low filament temperatures, there is growth primarily from linear polymeric units (*ID*) and by the incorporation of rings consisting of three siloxane units (*oR*₃); at high filament temperatures, there is growth primarily from three- and higher-membered siloxane rings (*oR*₃, *oR*₄, *oR*₅, and higher). This growth model is

consistent with previous studies of D₃ pyrolysis, in which it was observed that as temperature increased, the composition of the pyrolyzate changed from a linear polymeric mixture of molecular weight 1810 to a mixture of cyclic components consisting mainly of D₃, D₄, and D₅.⁵⁵

2.3.8 FILM STRUCTURE

The physical properties of the D₃ and D₄ HFCVD films show evidence of crosslinking. In particular, as-deposited films are found to be insoluble in common solvents, and form visible flakes when scraped off the wafer. In contrast, a polymethylsiloxane polymer with a composition of 30% T and 70% D groups – corresponding to C:Si = 1.70 – is a liquid at ambient conditions, and more crosslinked polymethylsiloxanes remain resinous up to a composition of about 90% T and 10% D groups – corresponding to C:Si = 1.10.⁶⁶ The HFCVD films show higher C:Si values between 1.90 and 1.30, but are coherent, hard, and show no evidence of tackiness. Qualitatively, films deposited at higher filament temperatures are observed to be harder than those deposited at lower filament temperatures, suggesting higher crosslink densities. However, the concentration of T and Q groups observed in NMR even at high filament temperatures is not sufficient to explain the lack of resinous character in the films. Some other type of crosslinking group must be present.

Spectroscopic evidence suggests that this networking occurs via silicon-silicon bonding which may originate during film growth from ring structures that have lost methyl groups, as illustrated in reactions 2 and 5 in Scheme 1. These reactions produce cyclic structural units capable of silicon-silicon bonding. Ring structures are

then “tiled” into the film structure and observed as the moieties oR_3 and oR_4 . Analogous silicon-silicon bonding of cyclic structures has been observed in radiation-induced crosslinking of D4,⁷⁰ and occurrences of Si-Si bonding have also been reported for other organosilicon materials, including siloxane polymers and hexamethyldisiloxane.⁷¹ Raman data confirm that, for both D3 and D4 films, there is a simultaneous increase in intensity for bands assigned to oR_3 and silicon-silicon bonding as filament temperature is raised. Reactions 2 and 5 thus appear to be the dominant pathway for silicon-silicon bonding.

Increased crosslink density by silicon-silicon bonding is expected to occur at the expense of methyl groups. This is confirmed by XPS data from Table 2-5, which show a decrease in methyl content as filament temperature is increased, with little corresponding change in oxygen content. From the data, it is possible to speculate on the average number of silicon-silicon bonds per structural unit. To form part of a polymeric chain, at least two methyl abstraction events are required per structural unit. For the case where only three-membered siloxane rings are incorporated, data from Table 2-5 correspond to an average loss of 2.0 methyl groups per ring. For the case where only four-membered rings are incorporated, these data correspond to an average loss of 2.6 methyl groups per ring. A loss of at least three methyl groups per ring is necessary to produce a networked structure. The data are thus consistent with incorporation of both oR_3 and oR_4 units in HFCVD films.

2.4 CONCLUSIONS

Hot-filament CVD is a technique that is capable of producing smooth organosilicon thin films of unique structure at high deposition rates. Filament temperature can be used for controlling the film structure. During the growth process, there appears to be competition between pathways for the incorporation of three-membered and higher-order siloxane ring structures, and pathways for the incorporation of linear structures in the films. For both D3 and D4, there is greater incorporation of ring structures consisting of three siloxane units (oR_3) as filament temperature is increased. The incorporation of these structures is more pronounced for films grown from D3. The D3 films also show evidence of higher-order ring structures such as oR_4 and oR_5 at high filament temperatures. By contrast, D4 films show a greater degree of incorporation of linear, unstrained structures (ID) over the range of filament temperatures studied. Ring structures are generated from methyl abstraction processes, and are incorporated into the structure via silicon-silicon bonds. In contrast to organosilicon films produced by plasma processing, crosslinking via silicon-silicon bonding appears to predominate over that from siloxane bonds containing tertiary or quaternary silicon atoms.

REFERENCES

1. A. M. Wróbel and M. R. Wertheimer, in *Plasma Deposition, Treatment, and Etching of Polymers*, R. d'Agostino, Editor, p. 163, Academic Press, San Diego, CA (1990).
2. F. F. Shi, *Surf. Coat. Tech.*, **82**, 1 (1996).
3. H. G. Pryce Lewis, D. J. Edell, and K. K. Gleason, *Chem. Mater.*, **12**, 3488 (2000).
4. A. S. Chawla, *Biomaterials*, **2**, 83 (1981).
5. Z. Ogumi, Y. Uchimoto, and Z. Takehara, *J. Electrochem. Soc.*, **136**, 625 (1989).
6. M. Kusabiraki, *J. Appl. Polym. Sci., Appl. Polym. Symp.*, **46**, 473 (1990).
7. P. K. Tien, G. Smolinsky, and R. J. Martin, *Appl. Opt.*, **11**, 637 (1972).
8. Y. Ishikawa, S. Sasakawa, M. Takase, Y. Iriyama, and Y. Osada, *Makromol. Chem., Rapid Commun.*, **6**, 495 (1985).
9. H. Matsuyama, A. Kariya, and M. Teramoto, *J. Appl. Polym. Sci.*, **51**, 689 (1994).
10. L. Peters, *Semicond. Int.*, **23**, 108 (2000).
11. M. J. Loboda, *Microelect. Eng.*, **50**, 15 (2000).
12. A. Grill and V. Patel, *J. Appl. Phys.*, **85**, 3314 (1999).
13. H. Yasuda and T. Hsu, *J. Polym. Sci., Polym. Chem. Ed.*, **15**, 81 (1977).
14. C. R. Savage, R. B. Timmons, and J. W. Lin, in *Adv. Chem. Ser.*, 236, p. 745, American Chemical Society, Washington, DC (1993).
15. N. M. Mackie, N. F. Dalleska, D. G. Castner, and E. R. Fisher, *Chem. Mater.*, **9**, 349 (1997).
16. C. B. Labelle, S. M. Karecki, L. R. Reif, and K. K. Gleason, *J. Vac. Sci. Technol. A*, **17**, 3419 (1999).
17. K. K. S. Lau and K. K. Gleason, *J. Fluorine Chem.*, **104**, 119 (2000).
18. S. J. Limb, K. K. S. Lau, D. J. Edell, E. F. Gleason, and K. K. Gleason, *Plasmas Polym.*, **4**, 21 (1999).
19. M. C. Kwan and K. K. Gleason, *Chem. Vap. Dep.*, **3**, 299 (1997).
20. W. K. Chang, M. Y. Liao, and K. K. Gleason, *J. Phys. Chem.*, **100**, 19653 (1996).
21. A. M. Wróbel, S. Wickramanayaka, Y. Nakanishi, Y. Fukuda, and Y. Hatanaka, *Chem. Mater.*, **7**, 1403 (1995).
22. V. N. Khabashesku, Z. A. Kerzina, A. K. Maltsev, and O. M. Nefedov, *J. Organomet. Chem.*, **364**, 301 (1989).
23. A. L. Smith, *Spectrochim. Acta.*, **16**, 87 (1960).
24. K. M. McNamara, B. E. Williams, K. K. Gleason, and B. E. Scruggs, *J. Appl. Phys.*, **76**, 2466 (1994).
25. C. Rau and W. Kulisch, *Thin Solid Films*, **249**, 28 (1994).
26. N. Wright and M. J. Hunter, *J. Am. Chem. Soc.*, **69**, 803 (1947).
27. R. E. Richards and H. W. Thompson, *J. Chem. Soc.*, 124 (1949).
28. T. Alvik and J. Dale, *Acta Chem. Scand.*, **25**, 2142 (1971).
29. G. G. Kirei and M. P. Lisitsa, *Opt. Spectrosc.*, **12**, 403 (1962).
30. L. J. Bellamy, *The Infra-red Spectra of Complex Molecules*, 2nd ed., p. 334, John Wiley & Sons, Inc., New York, (1958).
31. A. L. Smith and D. R. Anderson, *Appl. Spectrosc.*, **38**, 822 (1984).
32. I. Tajima and M. Yamamoto, *J. Polym. Sci., A, Polym. Chem.*, **25**, 1737 (1987).
33. A. T. Kohl, R. Mimna, R. Shick, L. Rhodes, Z. L. Wang, and P. A. Kohl, *Electrochem. Solid-State Lett.*, **2**, 77 (1999).
34. M. C. Kwan, Ph.D. Thesis, Massachusetts Institute of Technology, Cambridge, MA (1997).
35. M. Soutzidou, A. Panas, and K. Viras, *J. Polym. Sci., B, Polym. Phys.*, **36**, 2805 (1998).
36. H. Kriegsmann, in *Advances in Molecular Spectroscopy; Proceedings*, A. Mangini, Editor, **3**, p. 1000, Pergamon Press, New York (1962).
37. G. Fogarasi, H. Hacker, V. Hoffmann, and S. Dobos, *Spectrochim. Acta.*, **30A**, 629 (1974).
38. F. L. Galeener, *J. Non-Cryst. Solids*, **49**, 53 (1982).
39. C. A. M. Mulder, R. K. Janssen, P. Bachmann, and D. Leers, *J. Non-Cryst. Solids*, **72**, 243 (1985).
40. C. J. Brinker, D. R. Tallant, E. P. Roth, and C. S. Ashley, *J. Non-Cryst. Solids*, **82**, 117 (1986).

41. B. Humbert, A. Burneau, J. P. Gallas, and J. C. Lavalley, *J. Non-Cryst. Solids*, **143**, 75 (1992).
42. T. Nakano, N. Mura, and A. Tsuzumitani, *Jpn. J. Appl. Phys.*, **34**, L1064 (1995).
43. C. A. M. Mulder and A. A. J. M. Damen, *J. Non-Cryst. Solids*, **93**, 387 (1987).
44. U. G. Stolberg and H. P. Fritz, *Z. Anorg. Allg. Chemie.*, **330**, 1 (1964).
45. M. Hayashi, *J. Chem. Soc. Japan*, **78**, 1472 (1957).
46. R. K. Harris, J. D. Kennedy, and W. McFarlane, in *NMR and the Periodic Table*, R. K. Harris and B. E. Mann, Editors, p. 309, Academic Press, New York (1978).
47. E. A. Williams, in *Annual Reports on NMR spectroscopy*, G. A. Webb, Editor, p. 235, Academic Press, London (1983).
48. D. J. Burton, R. K. Harris, K. Dodgson, C. J. Pellow, and J. A. Semlyen, *Polym. Commun.*, **24**, 278 (1983).
49. R. A. Assink, A. K. Hays, R. W. Bild, and B. L. Hawkins, *J. Vac. Sci. Technol. A*, **3**, 2629 (1985).
50. S. Roualdes, N. Hovnanian, A. van der Lee, J. Sanchez, and J. Durand, *J. Phys. IV France*, **9**, 1147 (1999).
51. D. R. Anderson, in *Analysis of Silicones*, A. L. Smith, Editor, 41, p. 407, Wiley, New York (1974).
52. H. Marsmann, in *NMR: Oxygen-17 and Silicon-29*, P. Diehl, E. Fluck, and R. Kosfeld, Editors, 17, p. 65, Springer-Verlag, New York (1981).
53. C. B. Labelle and K. K. Gleason, *J. Appl. Polym. Sci.*, **74**, 2439 (1999).
54. K. K. S. Lau, J. A. Caulfield, and K. K. Gleason, *Chem. Mater.*, **12**, 3032 (2000).
55. M. Sobolevskii, I. Skorokhodov, V. Ditsent, L. Sobolevskaya, and G. Moiseyeva, *Vysokomol. Soedin., Ser. A*, **12**, 2714 (1970).
56. L. E. Gusel'nikov, N. S. Nametkin, T. K. Islamov, A. A. Sobtsov, and V. M. Vdovin, *Izvest. Akad. Nauk SSSR, Ser. Khimi.*, **20**, 84 (1971).
57. I. M. T. Davidson and J. F. Thompson, *Chem. Comm.*, 251 (1971).
58. I. M. T. Davidson and J. F. Thompson, *J. Chem. Soc., Faraday Trans. 1*, **71**, 2260 (1975).
59. G. Raabe and J. Michl, *Chem. Rev.*, **85**, 419 (1985).
60. M. G. Voronkov, *J. Organomet. Chem.*, **557**, 143 (1998).
61. T. Howard Thomas and T. C. Kendrick, *J. Polym. Sci., A-2, Polym. Phys.*, **7**, 537 (1969).
62. L. E. Gusel'nikov and N. S. Nametkin, *Chem. Rev.*, **79**, 529 (1979).
63. N. Grassie and I. G. MacFarlane, *Eur. Polym. J.*, **14**, 875 (1978).
64. D. J. Bannister and J. A. Semlyen, *Polym.*, **22**, 377 (1981).
65. K. K. S. Lau, K. K. Gleason, and B. L. Trout, *J. Chem. Phys.*, **113**, 4103 (2000).
66. W. Noll, *Chemistry and Technology of Silicones*, 2nd ed., Academic Press, New York, (1968).
67. A. M. Wróbel, M. Kryszewski, and M. Gazicki, *J. Macromol. Sci. - Chem.*, **A20**, 583 (1983).
68. P. Favia, R. d'Agostino, and F. Fracassi, *Pure Appl. Chem.*, **66**, 1373 (1994).
69. G. Smolinsky and M. J. Vasile, *Int. J. Mass Spectrom. Ion Phys.*, **12**, 147 (1973).
70. S. W. Kantor and R. C. Osthoff, U.S. Patent No. 2,793,222 (1957).
71. R. A. Shaw, in *International Symposium on Organosilicon Chemistry*, p. 297, Butterworths, London (1966).
72. D. M. Adams and W. S. Fernando, *J. Chem. Soc., Dalton Trans.*, **4**, 410 (1973).
73. R. K. Harris and B. J. Kimber, *J. Organomet. Chem.*, **70**, 43 (1974).
74. H.-G. Horn and H. C. Marsmann, *Makromol. Chem.*, **162**, 255 (1972).

CHAPTER THREE

DENSITY FUNCTIONAL THEORY CALCULATION OF ^{29}Si NMR CHEMICAL SHIFTS OF ORGANOSILOXANES

T. B. Casserly, and K. K. Gleason, *J. Phys. Chem. B*, accepted (2005).

ABSTRACT

Density functional theory at the B3LYP/6-311++G(*d,p*) level is applied to calculate the ^{29}Si NMR chemical shifts of a variety of organosiloxane moieties including monomers or precursors for polymerization and representative segments of organosiloxane polymers or thin films. The calculated shifts of two linear dimethylsiloxane compounds, hexamethylcyclotrisiloxane (D3), and octamethylcyclotetrasiloxane (D4) compare well with their known values having an average error of 3.4 ppm. The same method is applied to structures believed to occur in organosilicate glass (OSG) thin films deposited using hot filament chemical vapor deposition (HFCVD) from D3 and D4. The chemical shift at -15 ppm is identified as a cross-linking Si-Si bond between two strained D groups and has not previously been reported. Retention of the strained ringed structure in HFCVD films deposited from D3 is confirmed. The rings are bonded to the matrix through either Si-O or Si-Si bonds, with the later only becoming prevalent when higher filament temperatures were employed. The strained ring structure is also observed in films deposited from a precursor with a larger unstrained ring structure, D4. These observations suggest that the known gas phase conversion pathways of D4 to D3 and dimethylsilanone as well as the methyl abstraction reaction from D3 are operative in the HFCVD reaction chemistry.

ACKNOWLEDGEMENTS: The authors thank Novellus and the Semiconductor Research Corporation for fellowship funding and the NSF/SRC Engineering Research Center for Environmental Benign Semiconductor Manufacturing for funding support. Special thanks to Professor Bernhardt Trout and his research group at MIT for sharing their GAUSSIAN expertise.

3.1 INTRODUCTION

Cyclic siloxanes have long been used in the synthesis of a variety of siloxane polymers.¹⁻⁶ Recently, methylated cyclic siloxanes have gained a great deal of importance as precursors for making low dielectric constant organosilicate glass (OSG) thin films via chemical vapor deposition (CVD).⁷⁻¹³ Understanding the structure of these films is critical to understanding how to improve physical properties such as thermal stability, modulus, hardness, or dielectric constant.

Structural characterization of these OSG films via ²⁹Si nuclear magnetic resonance (NMR) provides detailed resolution of the chemical bonding structure.^{11, 13-17} Characterizing the intricate film structure of materials created using CVD is often difficult because of the complex nature of the CVD process. As opposed to the ordered liquid phase chemistry capable of producing nearly flawless linear polymers, plasma enhanced CVD has incredibly complex chemistry as a result of the destructive plasma excitation of precursor gases. Even the more controllable chemistries and methods of excitation can create a material containing a never before reported bonding environment. Because there is a paucity of good model compounds for such new and complex bonding environments, many times the NMR spectra of CVD thin films contain unknown or unreferenced ²⁹Si chemical shifts.

Often times, speculation based on incomplete evidence is the only means to provide an explanation for the unidentified NMR peak. With the advancement of ab initio quantum mechanics and density functional theory (DFT) computing methods as well as the rapid increase in computing power, this speculation can often be tested.^{18, 19} Chemical shifts predicted using DFT calculations have shown good

agreement with experiment.²⁰⁻²⁴ These methods have been tested for calculating the ²⁹Si NMR chemical shifts of silanes²¹, silane derivatives²², silane and silanol impurities in silica clusters²⁴, and SiO₂ polymorphs.²³ Additionally, DFT methods have been used to predict polymer chemical shifts using an oligomeric approach.²⁰

Previous work by Gleason, *et al.* presents the results of a hot-wire or hot filament CVD process using hexamethylcyclotrisiloxane (D₃) and octamethylcyclotetrasiloxane (D₄) to create low dielectric constant polymeric OSG thin films.¹¹ Hot-filament (HF) CVD utilizes a resistively heated wire, or filament, to provide the thermal energy required to excite the precursor gases which react to deposit a film on a cooled silicon substrate.^{7, 11, 25-27} Even utilizing HFCVD for finer control over the chemistry in the deposition process, OSGs often contain complex bonding networks that do not have good model compounds for NMR reference.

There are four common bonding environments in OSG thin films.²⁸ Figure 3-1 presents the four groups resulting from fully methylated OSG precursors. Precursors with different groups bonded to the silicon will have analogous structures. An M unit is a chain terminator containing three methyl groups (mono oxygen). A D unit is a linear unit bonded to two methyl groups and two oxygen atoms (di oxygen). The T unit is a branching group forming network bonds and has one methyl group and three oxygen atoms (tri oxygen). Finally, a Q group is silicon bonded to four oxygen atoms (quad oxygen) as in pure silicon dioxide. The NMR assignments are as follows: M (+6 ppm), D (-22 ppm), T (-68 ppm), and Q (-105 ppm) relative to TMS.^{14, 29} In the case where one of the methyl groups of an M or D group is replaced by a hydrogen atom, the groups are referred to as M^H (-6 ppm) and D^H (-34 ppm) respectively.^{14, 29}

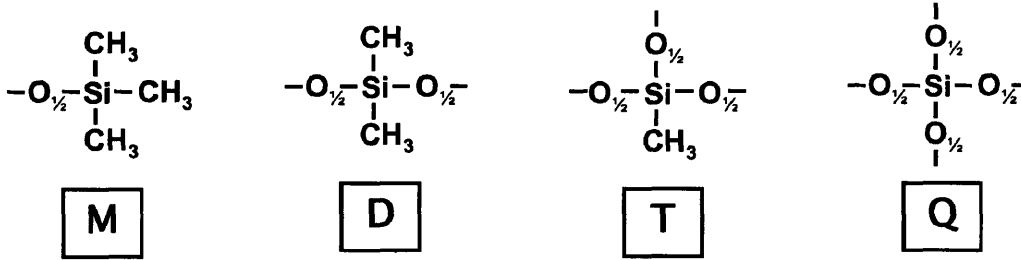


Figure 3-1. Non-branching groups, M (+6 ppm) & D (-22ppm) and branching groups, T (-68 ppm) & Q (-105 ppm) commonly found in OSG thin films with ^{29}Si chemical shifts in ().

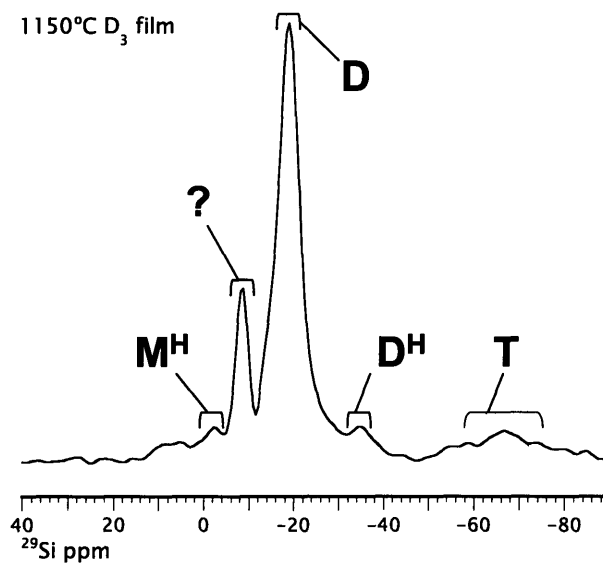


Figure 3-2. Labeled ^{29}Si NMR spectra of HFCVD film from D_3 with a filament temperature of 1150°C.

As shown in Figure 3-2, the ^{29}Si NMR spectra of films deposited via HFCVD from hexamethylcyclotrisiloxane (D_3) displays a predominance of D units, with significantly lower incorporation of M^{H} , D^{H} and T units. Additionally, the second most intense peak in Figure 3-2 appears at a chemical shift of -9 ppm which was previously unreported in the literature of OSG thin films.¹¹

In this paper, the accuracy of various ab initio quantum mechanics methods for predicting NMR chemical shifts will be evaluated for known shifts of OSG film bonding environments. Additionally, model compounds representing complex portions of the OSG film matrix, some containing more than 60 atoms and over 270 electrons, will be used to aid the assignments of unknown bonding environments evident in ^{29}Si NMR spectra of OSG thin films. Finally, the insights provided by the new assignments concerning OSG film structure and deposition chemistry will be discussed.

3.2 METHODOLOGY AND EXPERIMENTS

Structures of interest were built using GAUSSVIEW, and all calculations were performed using the program GAUSSIAN98³⁰ on a variety of computers with a minimum of dual 1.0 GHz Intel Pentium IIITM processors and 512MB of RAM. Geometries were initially optimized using the Hartree-Fock (HF) method with a 6-31G(*d*) basis set and further refined using the density functional theory B3LYP method with the expanded 6-311++G(*d,p*) basis set. The B3LYP method³¹ utilizes a three hybrid functional combining the HF and Slater exchange, the 1988 Becke density gradient correction to exchange,³² the LYP functional of Lee, Yang, and Parr^{31, 33} for both local and non-local correlation, and the 1980 VWN functional III of Vosko, Wilk, and Nusair for local correlation.³⁴ The B3LYP hybrid functional has proven to provide accurate geometries while not as computationally expensive as higher order methods such as Møller-Plesset perturbation theory and the complete basis set theory.^{35, 36}

NMR shielding tensors were then calculated for the optimized geometries at the B3LYP/6-311++G(d,p) level. Both sets of polarization and diffuse functions and were utilized to increase the accuracy of the electron density of the structures in order to properly simulate the shielding of the molecules. The B3LYP method was found to provide excellent agreement with experimental results for silanes.²¹ GAUSSIAN98 provides four methods for computing NMR shielding tensors, the Continuous Set of Gauge Transformations (CSGT) method³⁷⁻³⁹, the Gauge-Independent Atomic Orbital (GIAO) method⁴⁰⁻⁴⁴, the Individual Gauges for Atoms In Molecules (IGAIM) method^{37, 38}, and the Single Gauge Origin method which is a known bad method for large systems.³⁰ The NMR shielding tensors were calculated using all available methods.

Of interest in this work are the ²⁹Si NMR shielding constants of a variety of siloxane molecules and structures including the standard reference compound for ²⁹Si NMR, tetramethylsilane (TMS). The isotropic shielding constants for each compound of interest are calculated using DFT methods previously described and compared to the isotropic shielding constant for the reference TMS calculated at the same level. The chemical shift on the relative Delta, δ , scale is calculated as follows where δ is the chemical shift measured in ppm and σ_{iso}^{TMS} and σ_{iso}^* represent the isotropic shielding constants of the reference (TMS) and atom of interest (*) respectively, which sets the chemical shift of TMS equal to zero.

$$\sigma_{iso}^{TMS} - \sigma_{iso}^* = \delta^*$$

This sets this chemical shift of TMS equal to zero. Molecules simulated in addition to the reference TMS include the cyclic siloxanes tetramethylcyclodisiloxane

(D2), hexamethylcyclotrisiloxane (D3), and octamethylcyclotetrasiloxane (D4). Additionally, structures containing moieties believed to exist in OSG thin films are also modeled and are shown in Figure 3-3. Two approximations of the linear D group found in polydimethylsiloxane (PDMS) are simulated, one consisting of a D group capped by SiH₃ groups (Group A), the other consisting of two linear D groups with M^H end groups (Group B). Some unique OSG network forming structures were simulated as well including two methyl abstracted D₃ rings bonded together via a Si-Si bond (Group C), a methyl abstracted D₃ bonded to a linear chain of three D units via a Si-Si bond (Group D), a methyl abstracted D₃ bonded pendant to a linear chain of three D units via a Si-O bond (Group E), and a methyl abstracted D₃ bonded terminal to linear chain of two D units via a Si-O bond (Group F).

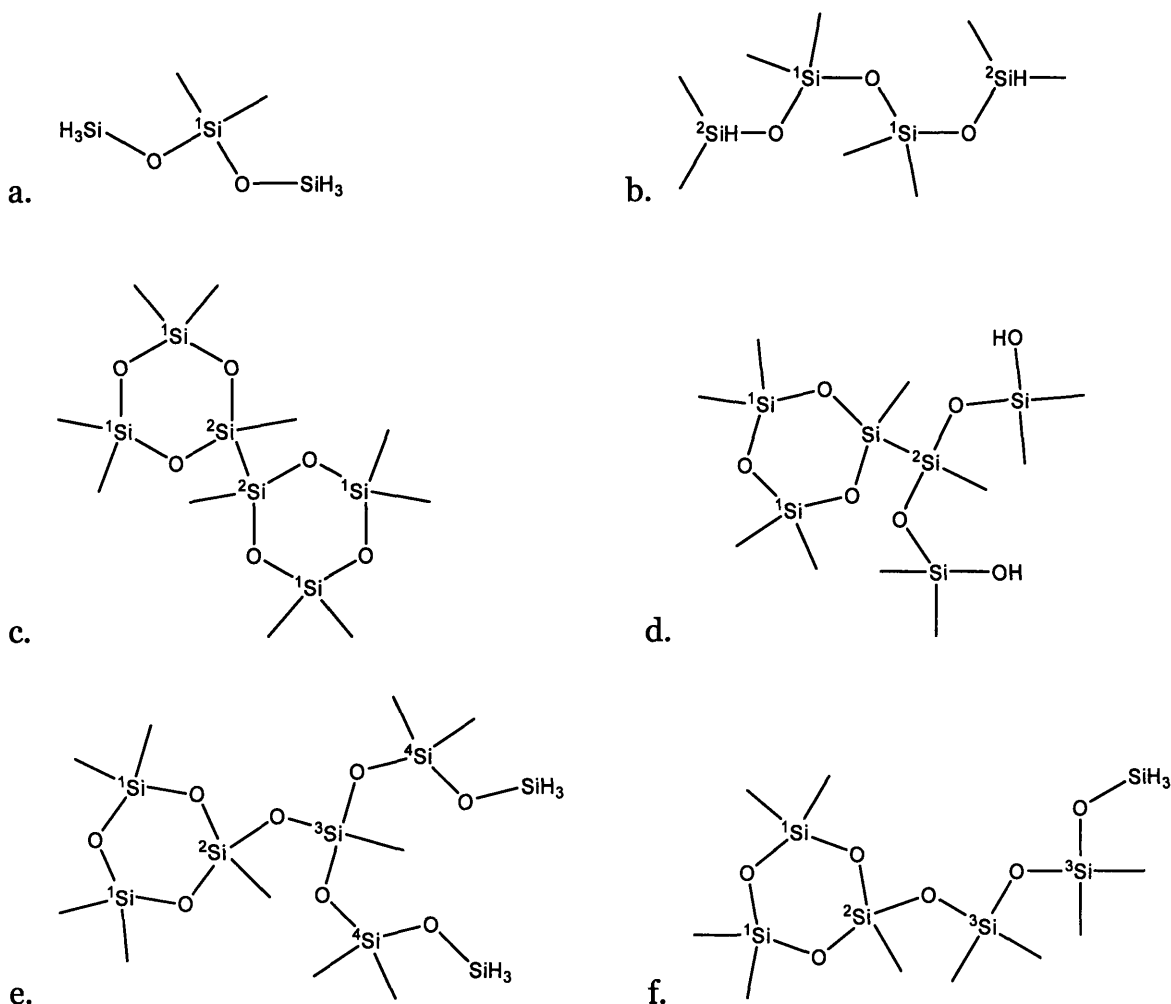


Figure 3-3. OSG groups simulated: a. SiH₃ capped D, b. D groups with M^H endgroups, c. Two D₃^{*} rings bonded via Si-Si, d. D₃^{*} pendant to linear chain of 3 D units via Si-Si, e. D₃^{*} pendant to linear chain of 3 D units via Si-O, and f. D₃^{*} terminal to linear chain of two D units via Si-O. (D₃^{*} ≡ methyl abstracted D₃)

3.3 RESULTS AND DISCUSSION

Computed chemical shifts relative to tetramethylsilane (TMS) calculated via the GIAO, IGAIM, and CSGT methods are reported in Table 3-1 along with available literature values. The average error for each method is reported and compares favorably with the work of others. Reported errors for DFT calculations are typically on the order of 2-12 ppm^{21, 22, 24} with errors larger than 25 ppm for silicon at the

center of a single shell and as small as ± 1 ppm for a silicon at the center of the large 3 shell approach of Xue, *et al.* for silicon polymorphs.²³

Table 3-1. Summary of calculated ²⁹Si NMR chemical shifts of known moieties using various methods at the B3LYP/6-311++G(d,p) level. (TMS σ_{iso} GIAO: 339.2 ppm, IGAIM: 338.0 ppm, CSGT: 338.0 ppm)

Group	Structure	Literature		GIAO	IGAIM	CSGT
		δ ppm	notes	δ ppm	δ ppm	δ ppm
D3	(SiO) ₂ Si*(CH ₃) ₂ [D]	-8.9, -9.9	14, 29	-4.8	-8.8	-8.8
D4	(SiO) ₂ Si*(CH ₃) ₂ [D]	-19.5, -20.2	14, 29	-24.0	-27.4	-27.4
Group A (chain)	(SiO) ₂ Si(CH ₃) ₂ [D]	-22.4, -23.5	14, 29	-17.7	-21.7	-21.7
Group B (chain)	(SiO) ₂ Si(CH ₃) ₂ [D]	-22.4, -23.5	14, 29	-23.9	-27.3	-27.3
	(CH ₃) ₂ (H)Si ² (OSi) [M ^H]	-6.5	14, 29	-7.3	-10.5	-10.5

$$|\Delta|_{\text{av}}^{\text{a}} = 3.14 \quad |\Delta|_{\text{av}}^{\text{b}} = 3.55 \quad |\Delta|_{\text{av}}^{\text{c}} = 3.55$$

$|\Delta|_{\text{av}}^{\text{a}}$ \equiv Average difference between the DFT calculated shift and average literature values for ^a GIAO, ^b IGAIM, & ^c CSGT methods.

All four compounds in Table 3-1 have reported values of experimentally determined ²⁹Si NMR shifts. The first two are cyclic molecules comprised only of D units. The last two are linear structures, Group A (Figure 3-3a) and Group B (Figure 3-3b). The chemical shifts calculated by all three methods agree well with literature data for the strained D moiety in D3. The six-member D3 ring is a planar ring that does not allow for the typical $160 \pm 15^\circ$ \angle OSiO bond angle creating 2.5 kcal/mol of ring strain.^{45, 46} The calculated \angle OSiO bond and is only 134.1° with a \angle SiOSi bond angle of only 105.9° as opposed to the typical tetrahedral 109.5° which leads to deshielding of the silicon and causes the shift downfield from an unstrained D group. By comparison, D4 has a ring strain of only 0.24 kcal/mol and rings containing eight or more siloxane units are thought to have no ring strain.^{45, 46} Bond angles for D4

were calculated to be 160.55° and 109.46° for the $\angle\text{OSiO}$ and $\angle\text{SiOSi}$ bonds respectively. The difference in chemical shift of the D unit in D3 versus D4 is a result of this large difference in ring strain and the $\angle\text{SiOSi}$ and $\angle\text{OSiO}$ bond angles. The increased strain in D3 reduces shielding and pushes the experimentally observed chemical shift of the D unit in D3 downfield. The DFT calculations also predict this effect; however, the absolute magnitude of the agreement between calculation and experiment for D4 is not as good as in the case of D3 molecule. The D3 molecule is planar and the silicon atoms are surrounded by a cloud of methyl groups making interactions of the silicon atoms with other molecules difficult. However, D4 is a larger and slightly puckered ring allowing for interactions of the silicon atoms with other molecules. These calculations were performed on single molecules while the reference chemical shifts were obtained by solution NMR. The difference between the calculated and experimental chemical shifts for D4 can be attributed to molecular interactions that are not accounted for in the simulation. This error could likely be reduced by taking an approach similar to the three shell approach of Xue, *et al.*²³, but not without a very large computational cost.

The difference between the unstrained D group in Group A and Group B is a result of the conformation of the optimized geometry. The short unstrained D group represented in Group A allows the oxygen to remain in the gauche position placing a methyl group in the trans position, while the lowest energy confirmation for Group B places an oxygen atom in the trans position (as in PDMS⁴⁷) providing greater shielding (corresponding to the shift upfield).⁴⁸ The calculated shifts for both linear D groups and the M^{H} moiety show good agreement with the literature values. The relative agreement of the IGAIM and CSGT methods and GIAO method with

literature values for known molecules indicates the validity of DFT as a predictive methodology for ^{29}Si NMR shifts for organosiloxanes.

Table 3-2. Summary of calculated ^{29}Si NMR chemical shifts of unknown moieties using various methods at the B3LYP/6-311++G(d,p) level. (TMS σ_{iso} GIAO: 339.2 ppm, IGAIM: 338.0 ppm, CSGT: 338.0 ppm)

Group	Structure	GIAO δ ppm	IGAIM δ ppm	CSGT δ ppm
D2	$(\text{SiO})_2\text{Si}^+(\text{CH}_3)_2$ [D]	34.3	32.2	32.2
Group C (2 D3 rings)	$(\text{SiO})_2\text{Si}^+(\text{CH}_3)_2$ [D in strained ring]	-4.2	-8.5	-8.5
	$\text{CH}_3(\text{SiO}_2)\text{Si}^2\text{Si}^2(\text{SiO}_2)\text{CH}_3$	-12.4	-15.9	-15.9
Group D (D3 pendant to linear chain via Si-Si)	$(\text{SiO})_2\text{Si}^+(\text{CH}_3)_2$ [D in strained ring]	-2.0	-5.8	-5.8
	(Si of strained ring) $\text{Si}^2(\text{SiO}_2)\text{CH}_3$	-25.0	-29.6	-29.6
Group E (D3 pendant to linear chain via T)	$(\text{SiO})_2\text{Si}^+(\text{CH}_3)_2$ [D in strained ring]	-3.8	-7.6	-7.6
	$(\text{SiO})_3\text{Si}^2(\text{CH}_3)$ [T in strained ring]	-63.5	-64.5	-64.5
	$(\text{SiO})_3\text{Si}^3(\text{CH}_3)$ [T in chain]	-75.0	-76.0	-76.0
	$(\text{SiO})_2\text{Si}^4(\text{CH}_3)_2$ [D in chain]	-17.5	-20.7	-20.7
Group F (D3 termination of linear chain via T)	$(\text{SiO})_2\text{Si}^+(\text{CH}_3)_2$ [D in strained ring]	-4.7	-7.9	-7.9
	$(\text{SiO})_3\text{Si}^2(\text{CH}_3)$ [T in strained ring]	-63.7	-65.1	-65.1
	$(\text{SiO})_2\text{Si}^3(\text{CH}_3)_2$ [D in chain]	-21.6	-24.9	-24.9

Reported in Table 3-2 are the chemical shifts of five moieties which are not represented by precise model compounds in the experimental ^{29}Si NMR literature. The first structure is a cyclic dimer of D units while the structures of the final four molecules are shown in Figure 3-3c, 3-3d, 3-3e, and 3-3f, and will be referred to as Groups C, D, E, and F, respectively. The later structures represent different means for incorporation of a 6-membered D3-like ring into the film structure through either Si-Si or Si-O bonds. Due to the molecular instability of D2, a measured chemical shift for the very strained D moiety in D2 has not been reported in the literature. The calculated shift of approximately +32 ppm is consistent with the

trend of decreased shielding with increased ring strain and decreased $\angle\text{OSiO}$ (88.7° calc.) and $\angle\text{SiOSi}$ (91.3° calc.) bond angles as evident when comparing the shift of D₃ to D₄. Group C revealed a new shift for a Si-Si bond between two strained D groups occurring at approximately -15 ppm while the shift for the strained D group in the six-member rings remains constant. If the D₃-like ring is bonded to an unstrained silicon via a Si-Si bond as in Group D, the chemical shift of the unstrained silicon is approximately -30 ppm. The shift upfield for this Si-Si bond as compared to the Si-Si bond in Group C is expected due to less strain on the silicon. The calculated shift of strained D in Group D is approximately -6 ppm is likely a result of interactions with the hydroxyl end groups of the linear PDMS chain. The calculated shifts for Groups E & F agree very well with the shifts expected from the literature. The downfield shift of the strained D group in Groups E & F as compared to D₃ is due to the oxygen of the T group which further strains the ring opposite the T group reducing the $\angle\text{OSiO}$ bond angles an additional 0.3-4 degrees. The calculated chemical shifts for the linear D moieties of both Groups E & F agree well with the literature value for linear D groups reported in Table 3-1. The chemical shifts of the T groups in Groups E & F agree well with the observed spectra presented in Figure 3-2. The shifts of the T groups within a strained ring agree well with the reported literature value of -65 ppm for a simple T group surrounded by M groups, $\text{CH}_3\text{Si}^*[\text{OSi}(\text{CH}_3)_3]_3$, and is shifted slightly downfield compared to a generic T group, $\text{CH}_3\text{Si}(\text{O}-)_3$, with a reported shift of -68 ppm.²⁹ These strained T groups are shifted approximately 10 ppm downfield from the calculated shift of the T group bonded to unstrained D groups in Group E. This shift is of the same magnitude of the shift between strained and unstrained D groups and is a result of the strain on the silicon

atom and the resulting decreased $\angle\text{OSiO}$ bond angles as two of the three oxygen atoms in the strained T groups are incorporated into a D₃-like ring.

All strained D moieties of six-member rings fall in the range of -2.0 to -8.8 ppm while linear D moieties fall in range between -17.5 and -27.3 ppm for the compounds simulated in Tables 1 and 2. The chemical shift for Si-Si bonds associated with strained rings appears at -15 ppm. These assignments will be applied to evaluate previously published NMR spectra of HFCVD OSG thin films.

A series of films deposited via hot filament CVD from D₃ and D₄ precursors were examined in a previous work.¹¹ The ²⁹Si NMR spectra of OSG of these films contain a number of shifts previously assigned through reference to the literature. The peaks at -6 ppm, -20 ppm, and -67 ppm were assigned to the shifts corresponding to M^H, D, and T groups respectively. Additionally, the spectra of these films contained a shift at -9 ppm which could not be definitively assigned. The calculated shifts confirm the previous assignments accounting for the M^H group at -6 ppm (Group B), the unstrained D at -20 ppm (Groups A-B, E-F), and the T group at -67 ppm (Groups E-F) while suggesting that the shift at -9 ppm corresponds to a strained D group (Groups C-F) resulting from the incorporation of planar six-member D₃-like rings into the film structure. For films deposited from D₃, this is possible through a methyl abstraction reaction of the D₃ precursor creating a radical able to bond to an existing radical site on the film. For films deposited from D₄, D₃ must first be produced via the intra-molecular conversion of D₄ to dimethylsilanone and D₃ which can undergo a subsequent methyl abstraction reaction. The intramolecular reaction has an activation energy of 300.9 ± 6.1 kcal/mol which is less than the 383 ± 39 kcal/mol required for methyl abstraction from a D₃

molecule.^{49, 50} Bands corresponding to ring deformation for both D₃ and D₄ can be observed and differentiated using Raman spectroscopy.⁵¹ Raman spectra of HFCVD OSG thin films from both D₃ and D₄ contain the clear signature of a six-member D₃-like ring, providing further evidence of ring incorporation.¹¹ The degree of ring incorporation increases with increasing filament temperature for films from each series as shown in the ²⁹Si NMR spectra in Figures 3-4 & 3-5. The D₃-like rings can be bonded to the film via Si-Si bonds as in Groups C & D or through T groups as in Groups E & F.

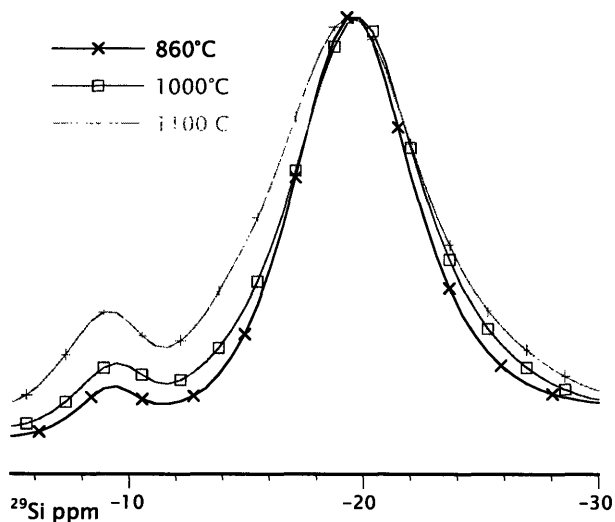


Figure 3-4. ²⁹Si NMR of HFCVD films from D₃ with filament temperatures of 860°C, 1000°C, & 1100°C. ¹¹

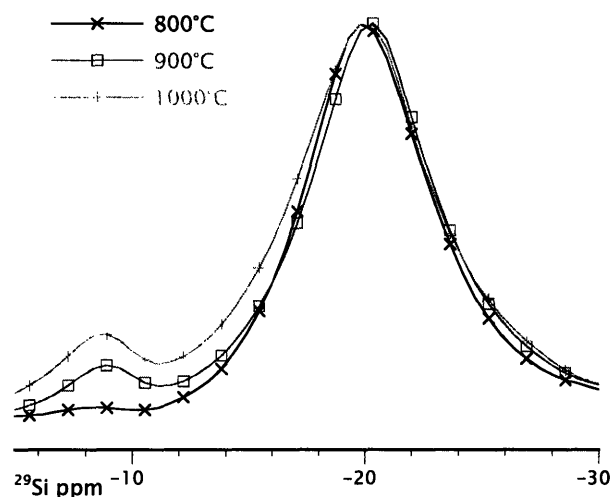


Figure 3-5. ^{29}Si NMR of HFCVD films from D4 with filament temperatures of 800°C, 900°C, & 1000°C. ¹¹

Closer inspection of the ^{29}Si NMR spectra of these films shown in Figures 3-4 & 3-5 between -5 and -30 ppm provides insight into the bonding environment of six-member D₃-like rings included in the film. Least-squares fitting of the spectra to resolve individual peaks can determine the contributions of each type of bonding environment. While the majority of the films show only a small degree of degree of Si-Si bonding, the film deposited from D₃ with a filament temperature of 1150°C contains a significant amount of Si-Si bonding indicating the presence of D₃ rings tiled to each other through Si-Si bonds. From the calculated spectra of Group C, we expect a peak at -8 ppm for the strained D and -15 ppm for the Si-Si bond in addition to the backbone of linear D present in the film and occurring at -21 ppm as calculated in Group B. Figure 3-6 shows the fit spectra. The peaks in are centered at -8.5 ppm, -14.5 ppm, and -19.1 ppm corresponding to the strained D in D₃, cross-linking of strained D groups via a Si-Si bond, and linear D respectively. The integrated area of

the peak at -8.5 ppm must be at least two times as large as the peak at -14.5 ppm to correctly account for the number of bonds. The integrated area of the strained D peak is approximately 3.1 times the area of the peak corresponding to the Si-Si bond, indicating that while a large number of the D₃-like rings are bonded to the film through Si-Si bonds, there is evidence to support D₃ ring incorporation through a Si-O bond in a T group either pendant or terminal to a PDMS-like chain of linear D groups as well as represented by Groups E & F.

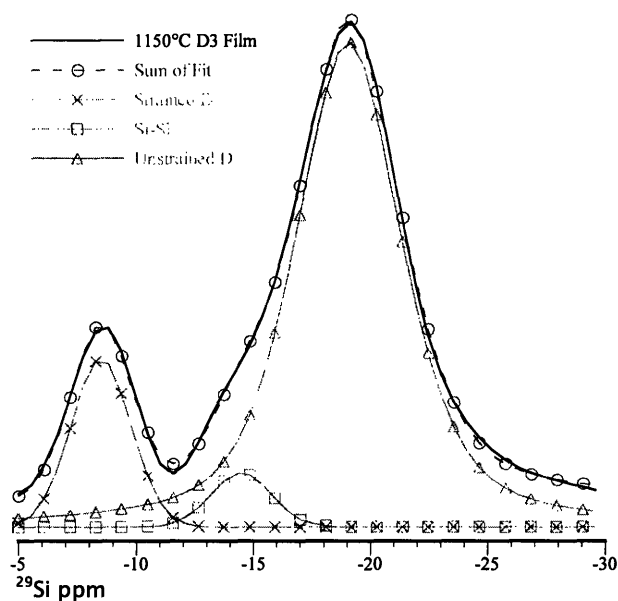


Figure 3-6. ²⁹Si NMR spectra of 1150°C D₃ film fit to resolve chemical shifts at -8.5 ppm, -14.5 ppm and -19.1 ppm.

Least squares fitting of the spectra from the remaining deposition conditions indicates an increased concentration of methyl abstracted D₃ molecules as a function of temperature. This is evidenced by the increasing presence of the strained D moiety and by the increasing presence of strained Si-Si bond relative to that of the strained D moiety. This relative increase as a function of increasing temperature indicates that at elevated temperatures the methyl abstracted D₃

molecules can react with each other to create a structure similar to Group C. The evidence of Si-Si bonds between strained D groups as would occur if many methyl abstracted D₃ rings were “tiled” together is only convincing at very high filament temperatures, >1100°C. This coupled with the fact that there is no spectroscopic evidence of a D₃-like ring bonded via a Si-Si bond pendant to a linear chain as in Group D, indicates that the majority of six-member D₃-like rings are bonded to the structure of the film through T groups either pendant or terminal to linear chains as in Groups E & F respectively.

3.4 CONCLUSIONS

Using density functional theory at the B₃LYP/6-311++G(*d,p*) level and three methods of calculating NMR shielding tensors (GIAO, IGAIM, and CGST) the known chemical shifts of OSG compounds were calculated to within an accuracy of 0.1-7.4 ppm with an average error of approximately 3.5 ppm. This compares favorably with results of similar work which yielded errors on order of 6-10 ppm²², errors of 0.2-11 ppm with relative error of 10% on shifting of neighbors²⁴ and errors as large as 26 ppm for the one shell and as small as ± 1 ppm for the large 3 shell approach used by Xue, *et al.*²³ Molecules containing over 60 atoms and more than 270 electrons were successfully modeled, providing reasonable models for portions of the OSG matrix. The same methods were used to calculate the chemical shifts for previously unassigned bonding environments.

The chemical shift reported at -15 ppm and assigned to the cross-linking Si-Si bond between two strained D groups has not previously been reported in the

literature to the knowledge of the authors and leads to a greater understanding of the structure of thin films deposited from cyclic siloxanes. Retention of the strained ringed structure in HFCVD films deposited from the D₃ precursor is confirmed. The rings are bonded to the matrix through either Si-O or Si-Si bonds, with the later only becoming prevalent when higher filament temperatures were employed. The strained ring structure is also observed in films deposited from a precursor with a larger unstrained ring structure, D₄. These observations suggest that the known gas phase conversion pathways of D₄ to D₃ and dimethylsilanone as well as the methyl abstraction reaction from D₃^{11, 49, 50} are operative in the HFCVD reaction chemistry.

REFERENCES

1. S. Boileau, *Makromolekulare Chemie-Macromolecular Symposia*, **73**, 177 (1993).
2. J. Chojnowski and J. Kurjata, *Macromolecules*, **27**, 2302 (1994).
3. K. Kazmierski, M. Cypryk, and J. Chojnowski, *Macromolecular Symposia*, **132**, 405 (1998).
4. G. P. Cai and W. P. Weber, *Macromolecules*, **33**, 6310 (2000).
5. J. Chojnowski, M. Cypryk, W. Fortuniak, K. Rozga-Wijas, and M. Scibiorek, *Polymer*, **43**, 1993 (2002).
6. J. Chojnowski, M. Cypryk, W. Fortuniak, M. Scibiorek, and K. Rozga-Wijas, *Macromolecules*, **36**, 3890 (2003).
7. M. C. Kwan and K. K. Gleason, *Chemical Vapor Deposition*, **3**, 299 (1997).
8. D. D. Burke and K. K. Gleason, *Journal of the Electrochemical Society*, **151**, F105 (2004).
9. A. Grill, *Journal of Applied Physics*, **93**, 1785 (2003).
10. A. Grill and D. A. Neumayer, *Journal of Applied Physics*, **94**, 6697 (2003).
11. H. G. Pryce Lewis, T. B. Casserly, and K. K. Gleason, *Journal of the Electrochemical Society*, **148**, F212 (2001).
12. H. G. Pryce Lewis, D. J. Edell, and K. K. Gleason, *Chemistry of Materials*, **12**, 3488 (2000).
13. I. Tajima and M. Yamamoto, *Journal of Polymer Science: Part A: Polymer Chemistry*, **25**, 1737 (1987).
14. R. A. Assink, A. K. Hays, R. W. Bild, and B. L. Hawkins, *Journal of Vacuum Science and Technology A*, **3**, 2629 (1985).
15. P.-Y. Mabboux and K. K. Gleason, submitted to *Journal of The Electrochemical Society* (2004).
16. I. Tajima and M. Yamamoto, *Journal of Polymer Science: Polymer Chemistry Edition*, **23**, 615 (1985).
17. Q. G. Wu and K. K. Gleason, *Plasmas and Polymers*, **8**, 31 (2003).
18. M. Buhl, M. Kaupp, O. L. Malkina, and V. G. Malkin, *Journal of Computational Chemistry*, **20**, 91 (1999).
19. I. Alkorta and J. Elguero, *International Journal of Molecular Sciences*, **4**, 64 (2003).
20. P. S. Asirvatham, V. Subramanian, R. Balakrishnan, and T. Ramasami, *Macromolecules*, **36**, 921 (2003).
21. T. Heine, A. Goursot, G. Seifert, and J. Webert, *Journal of Physical Chemistry A*, **105**, 620 (2001).
22. C. Corminboeuf, T. Heine, and J. Weber, *Chemical Physics Letters*, **357**, 1 (2002).
23. X. Y. Xue and M. Kanzaki, *Solid State Nuclear Magnetic Resonance*, **16**, 245 (2000).
24. J. Casanovas, F. Illas, and G. Pacchioni, *Chemical Physics Letters*, **326**, 523 (2000).
25. J. A. Caulfield, K. K. S. Lau, and K. K. Gleason, *Chemistry of Materials* (2000).
26. S. K. Murthy and K. K. Gleason, *Macromolecules*, **35**, 1967 (2002).
27. H. G. Pryce Lewis, J. A. Caulfield, and K. K. Gleason, *Langmuir*, **17**, 7652 (2001).
28. A. M. Wróbel and M. R. Wertheimer, in *Plasma deposition, treatment and etching of polymers*, R. d'Agostino, Editor, p. 163, Academic Press, Boston (1990).
29. H. Marsmann, in *NMR: Oxygen-17 and Silicon-29*, P. Diehl, E. Fluck, and R. Kosfeld, Editors, 17, p. 65, Springer-Verlag, New York (1981).
30. M. J. Frisch, G. W. Trucks, H. B. Schlegel, G. E. Scuseria, M. A. Robb, J. R. Cheeseman, V. G. Zakrzewski, J. A. Montgomery, R. E. Stratmann, J. C. Burant, S. Dapprich, J. M. Millam, A. D. Daniels, K. N. Kudin, M. C. Strain, O. Farkas, J. Tomasi, V. Barone, M. Cossi, R. Cammi, B. Mennucci, C. Pomelli, C. Adamo, S. Clifford, J. Ochterski, G. A. Petersson, P. Y. Ayala, Q. Cui, K. Morokuma, D. K. Malick, A. D. Rabuck, K. Raghavachari, J. B. Foresman, J. Cioslowski, J. V. Ortiz, B. B. Stefanov, G. Liu, A. Liashenko, P. Piskorz, I. Komaromi, R. Gomperts, R. L. Martin, D. J. Fox, T. A. Keith, M. A. Al-Laham, C. Y. Peng, A. Nanayakkara, C. Gonzalez, M. Challacombe, P. M. W. Gill, B. G. Johnson, W. Chen, M. W. Wong, J. L. Andres, M. Head-Gordon, E. S. Replogle, and J. A. Pople, Gaussian Inc., Pittsburgh, PA, 1998.
31. B. Miehl, A. Savin, H. Stoll, and H. Preuss, *Chemical Physics Letters*, **157**, 200 (1989).
32. A. D. Becke, *Physical Review A*, **38**, 3098 (1988).

33. C. T. Lee, W. T. Yang, and R. G. Parr, *Physical Review B*, **37**, 785 (1988).
34. S. H. Vosko, L. Wilk, and M. Nusair, *Canadian Journal of Physics*, **58**, 1200 (1980).
35. L. A. Curtiss, K. Raghavachari, P. C. Redfern, and J. A. Pople, *Chemical Physics Letters*, **270**, 419 (1997).
36. K. K. S. Lau, K. K. Gleason, and B. L. Trout, *Journal of Chemical Physics*, **113**, 4103 (2000).
37. T. A. Keith and R. F. W. Bader, *Chemical Physics Letters*, **194**, 1 (1992).
38. T. A. Keith and R. F. W. Bader, *Chemical Physics Letters*, **210**, 223 (1993).
39. J. R. Cheeseman, G. W. Trucks, T. A. Keith, and M. J. Frisch, *Journal of Chemical Physics*, **104**, 5497 (1996).
40. F. London, *J. Phys. Radium, Paris* **8**, 397 (1937).
41. R. McWeeny, *Physical Review*, **126**, 1028 (1962).
42. R. Ditchfield, *Molecular Physics*, **27**, 789 (1974).
43. J. L. Dodds, R. McWeeny, and A. J. Sadlej, *Molecular Physics*, **41**, 1419 (1980).
44. K. Wolinski, J. F. Hinton, and P. Pulay, *Journal of the American Chemical Society*, **112**, 8251 (1990).
45. D. W. Scott, *Journal of the American Chemical Society*, **68**, 2294 (1946).
46. M. G. Voronkov, *Zhurnal Obshchei Khimii*, **66**, 167 (1996).
47. V. Crescenzi and P. J. Flory, *Journal of the American Chemical Society*, **86**, 141 (1964).
48. D. J. Burton, R. K. Harris, K. Dodgson, C. J. Pellow, and J. A. Semlyen, *Polymer Communications*, **24**, 278 (1983).
49. I. M. T. Davidson and J. F. Thompson, *Chemical Communications*, 251 (1971).
50. I. M. T. Davidson and J. F. Thompson, *Journal of the Chemical Society, Faraday Transactions 1*, **71**, 2260 (1975).
51. A. L. Smith and D. R. Anderson, *Applied Spectroscopy*, **38**, 822 (1984).

CHAPTER FOUR

ENTHALPIES OF FORMATION AND REACTION FOR PRIMARY REACTIONS OF METHYL- AND METHOXYMETHYLSILANES FROM DENSITY FUNCTIONAL THEORY

T. B. Casserly, and K. K. Gleason, *J. Electrochem. Soc.*, submitted (2005).

ABSTRACT

The enthalpies of formation and enthalpies of reaction at 298 K for a set of Si:C:O:H species derived from methylsilanes and methoxymethylsilanes were computed using the B3LYP density functional theory. Total energies were calculated at the B3LYP/6-311+G(3df,2p)//B3LYP/6-311+G(d) level. Zero point energies and thermal corrections were calculated using B3LYP/6-311+G(d)//B3LYP/6-311+G(d) vibrational energies scaled by a factor of 0.96. The average absolute deviation of enthalpies of formation and reaction were 3.89 and 1.86 kcal/mol, respectively. Bond strengths and reactions with O atom and H atom are examined in the context of understanding the initial reactions in chemical vapor deposition. The Si–H bond was calculated to be 8.4 kcal/mol stronger than the Si–C bond in methylsilanes and to increase by 0.6 kcal/mol with increased methylation; however, the thermochemistry of methylsilane reactions with O atom favors scission of the Si–H bond to produce hydroxyl and methylsilyl radicals. Thermodynamic control over the reaction pathways of methoxymethylsilanes is possible only when considering the reaction with H atom for which methoxymethylsilanol formation is favored. This illuminates a conceivable strategy to control the Si–O–Si bonding network while retaining methyl functionality in a CVD thin film by controlling the ratio of methoxy functionality and free hydrogen in the reactor. Density functional theory is a useful tool in understanding and subsequently controlling the initial chemistry in the CVD process.

ACKNOWLEDGEMENTS: The authors thank Novellus and the Semiconductor Research Corporation for fellowship funding and Tokyo Electron Limited and the NSF/SRC Engineering Research Center for Environmental Benign Semiconductor Manufacturing for funding support. Special thanks to Dr. Kenneth K.S. Lau and Professor Bernhardt L. Trout and his research group at MIT for sharing their GAUSSIAN expertise.

4.1 INTRODUCTION

Methylsilanes are common precursors used in plasma enhanced chemical vapor deposition (CVD) to create low dielectric constant thin films with applications semiconductor devices.^{1, 2} Finding a low dielectric constant material to replace silicon dioxide has been an active area of research for a long time.²⁻⁸ The main challenge in perfecting this class of materials referred to as organosilicate glasses (OSGs) has been to decrease the dielectric constant with the addition of alkyl functionality while maintaining the structural strength of the Si–O network. Molecular simulation of possible OSG precursors is important to allow for intelligent precursor selection for robust OSG thin film deposition via CVD. Ab initio quantum mechanics have been useful in understanding the kinetics of oxygen atoms with silane,⁹ methyl-¹⁰ dimethyl- and trimethylsilane,¹¹ predicting the thermochemistry of gas phase difluorocarbene reactions,¹² and predicting ²⁹Si NMR chemical shifts of OSGs.¹³ In this paper, the initial fragmentation patterns of potential OSG precursors are examined using density functional theory.

Density functional theory (DFT) is used to determine the molecular structure and enthalpies of formation for a family of methyl- and methoxymethylsilanes and their radical fragments. The bond dissociation energies (BDEs) and enthalpies of reaction for reactions such as methyl abstraction and silanol formation are examined. This method is used to reveal potential fragmentation and reaction patterns for a first screening of CVD precursors. The well designed computational experiment is extremely valuable due to its potential to save monetary, personnel, chemical and time resources required for laboratory experimentation.

The simulations allow for a calculation of reaction enthalpies which can be used to select appropriate precursors for OSG precursors. A series containing over 120 reactions was studied leading to the design of a laboratory experiment focusing on the reaction of trimethoxymethylsilane and hydrogen atom. The results of the simulations allowed for the intelligent design of laboratory experiments and the elimination of entire series of possibilities.

DFT is a theoretical method for predicting molecular geometries, vibrational frequencies, transition states, and as an extension bond energies, heats of formation and energetics of reactions. Of particular merit is the B3LYP hybrid functional which produced the best agreement, among many DFT methods, with the experimental enthalpies of formation contained in the enlarged G2 test set.¹⁴ The B3LYP method¹⁵ utilizes a three hybrid functional combining the HF and Slater exchange, the 1988 Becke density gradient correction to exchange,¹⁶ the LYP functional of Lee, Yang, and Parr^{15, 17} for both local and non-local correlation, and the 1980 VWN functional III of Vosko, Wilk, and Nusair for local correlation.¹⁸

The B3LYP hybrid functional has proven to provide accurate geometries while not as computationally expensive as higher order methods such as Møller-Plesset perturbation theory, the complete basis set theory, or the composite Gaussian-2 (G2) theory.^{12, 14} Considering the silane derivatives in the G2 test set, G2 theory gives errors of 2.9, 0.5, 1.2, 2.2, and 0.4 kcal/mol for $\text{Si}\cdot\text{H}_2$ (1A_1), $\text{Si}\cdot\text{H}_2$ (3B_1), $\cdot\text{SiH}_3$, SiH_4 , and CH_3SiH_3 , respectively, while B3LYP theory gives errors of 2.1, 2.3, 3.2, 1.9 and -1.0 kcal/mol.¹⁴ While G2 theory performs better, the considerable computational expense is not warranted considering the marginal improvement.

This work makes use of energies calculated from B3LYP/6-311+G(3df,2p)//B3LYP/6-311+(d), and scaled zero-point and thermal corrections utilizing scaled vibrational frequencies from B3LYP/6-311+(d)//B3LYP/6-311+(d) calculations. A factor of 0.96 was used to scale both zero-point energies and vibrational frequencies as it has produced the best agreement with experiments in several studies.^{12, 19-22} The recommended factor of 1.0015 was used to scale entropies for the calculation of Gibbs free energies.²¹ The focus of this work is to determine the thermochemistry of the methyl- and methoxymethylsilane systems; however, these results are interpreted as they correspond to the CVD of thin films from these precursors. By increasing understanding of the bond strengths and primary reactions of these precursors with oxygen atom and hydrogen atom, intelligent selection of CVD precursors is possible.

4.2 COMPUTATIONAL METHOD

Structures of interest were built using GAUSSVIEW, and all calculations were performed using the program GAUSSIAN98²³ on a variety of computers with a minimum of dual 1.0 GHz Intel Pentium IIITM processors and 512MB of RAM. Geometries were initially optimized using the Hartree-Fock (HF) method with a 6-31G(d) basis set. Further geometry refinements and the calculation of zero point energies and vibration frequencies were performed using the density functional theory B3LYP method with the expanded 6-311+G(d) basis set. Finally, single point energies were calculated from the optimized B3LYP/6-311+G(d) geometries at the

B3LYP/6-311+G(3df,2p) level. Calculations for molecules in the singlet and non-singlet states were carried out with and without spin restriction, respectively.

Enthalpies of formation were calculated following the approach of Curtiss and Pople, *et al.*¹⁴ and are compared with experimental data where available from the literature. While this approach is considered theoretical, the calculated values depend on experimental data for the enthalpies of formation of isolated atoms and the elemental corrections to enthalpy for the standard states of the elements. Enthalpy of formation at 0 K [$\Delta H_{f, Si_w C_x O_y H_z}^0(0K)$] is given by Eq. (4-1).^{12, 14} The values for atomic enthalpies of formation, $\Delta H_{f, at}^0$, for gaseous Si, C, O, and H are taken from the JANAF tables (Si=106.52; C=169.98; O=58.98; H=51.63 kcal/mol).²⁴ The atomization energy of each molecule, $\Delta H_{at, Si_w C_x O_y H_z}^0$, is the stoichiometric summation of the atomic B3LYP/6-311+G(3df,2p) single point energies corrected for the scaled zero-point energies calculated at the B3LYP/6-311+G(d) level where vibrational frequency calculations were performed. The zero-point energies and vibrational frequencies were scaled by a factor of 0.96.

$$\begin{aligned} \Delta H_{f, Si_w C_x O_y H_z}^0(0K) &= \sum \Delta H_{f, at}^0 - \Delta H_{at, Si_w C_x O_y H_z}^0 \\ &= \left\{ w\Delta H_{f, Si}^0 + x\Delta H_{f, C}^0 + y\Delta H_{f, O}^0 + z\Delta H_{f, H}^0 \right\} \\ &\quad - \left\{ w[E(Si)] + x[E(C)] + y[E(O)] + z[E(H)] \right. \\ &\quad \left. - [E(Si_w C_x O_y H_z)] + 0.96 * ZPE(Si_w C_x O_y H_z) \right\}. \end{aligned} \quad (4-1)$$

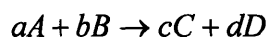
Standard enthalpies of formation were then calculated by Eq. (4-2).^{12, 14} Elemental corrections, $\sum \Delta H_{corr, st}^0$, for Si, C, O, and H are based on the standard states of the elements and are taken from the JANAF tables (Si_{ref}=0.77, C_{ref}=0.25,

$O_{2,ref}/2=1.04$, $H_{2,ref}/2=1.01$ kcal/mol).²⁴ The thermal correction to enthalpy, $\Delta H_{corr,Si_wC_xO_yH_z}^0$, includes the PV term, the classical approximations for translational ($3/2 RT$) and rotational ($3/2 RT$ for nonlinear species and RT for linear species) contributions to enthalpy, as well as the harmonic approximation for vibrational contributions to enthalpy. Eq. (4-3) shows the method for calculating $\Delta H_{corr,Si_wC_xO_yH_z}^0$ for each $Si_wC_xO_yH_z$ molecule.¹²

$$\begin{aligned}\Delta H_{f,Si_wC_xO_yH_z}^0(298K) &= \Delta H_{f,Si_wC_xO_yH_z}^0(0K) + \Delta H_{corr,Si_wC_xO_yH_z}^0 - \sum \Delta H_{corr,st}^0 \\ &= \Delta H_{f,Si_wC_xO_yH_z}^0(0K) + \Delta H_{corr,Si_wC_xO_yH_z}^0 - \left\{ w[H_{Si}^0(298K) \right. \\ &\quad \left. - H_{Si}^0(0K)] + x[H_C^0(298K) - H_C^0(0K)] + y[H_O^0(298K) \right. \\ &\quad \left. - H_O^0(0K)] + z[H_H^0(298K) - H_H^0(0K)] \right\},\end{aligned}\quad (4-2)$$

$$\begin{aligned}\Delta H_{corr,Si_wC_xO_yH_z}^0 &= PV + \Delta U_{trans}^0 + \Delta U_{rot}^0 + \Delta U_{vib}^0 \\ &= RT + \frac{3}{2}RT + \left(\frac{3}{2}RT \quad \text{or} \quad RT \right) + R \sum_i \frac{0.96\nu_i h}{k} \left[\exp\left(\frac{0.96\nu_i h}{kT} \right) - 1 \right]^{-1}.\end{aligned}\quad (4-3)$$

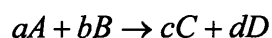
After calculating the enthalpies of formation for the species of interest, enthalpies of reaction at 298 K for the simple monomer fragmentation reactions (bond dissociation energies, BDE) as well as the reactions of methyl- and methoxymethylsilanes with atomic oxygen, $O(^3P_2)$, and hydrogen, $H(^2S_{1/2})$, are calculated by the stoichiometric sum of the species enthalpies of formation as given in Eq. (4-4).



$$\Delta H_{rxn}^0(298K) = c\Delta H_C^0(298K) + d\Delta H_D^0(298K) - a\Delta H_A^0(298K) - b\Delta H_B^0(298K).\quad (4-4)$$

Total Gibbs free energies were calculated at 298 K from the absolute enthalpies and scaled entropies at 298 K by Eq. (4-5).²¹ Gibbs free energies of reaction were calculated based on the stoichiometric sum of total Gibbs energies of the species, given in generic form by Eq. (4-6).

$$G_{Si_w C_x O_y H_z}^0(298K) = H_{Si_w C_x O_y H_z}^0(298K) - 298.15 * (1.0015) S_{Si_w C_x O_y H_z}^0(298K). \quad (4-5)$$



$$\Delta G_{rxn}^0(298K) = cG_C^0(298K) + dG_D^0(298K) - aG_A^0(298K) - bG_B^0(298K). \quad (4-6)$$

4.3 RESULTS AND DISCUSSION

4.3.1 ENTHALPIES OF FORMATION

Total energies and zero-point energies in Hartree are given in Table 4-1 along with the total atomization energy, ΣD_0 , thermal corrections to the enthalpy and standard enthalpies of formation at 0 K, and 298 K in kcal/mol. Experimental enthalpies of formation at 298 K, where available in the literature^{14, 24-31}, along with the corresponding deviations of the theoretical values are also given in Table 4-1. The average absolute deviation is 3.89 kcal/mol which compares well with the 3.11 kcal/mol reported for species in the expanded G2 test set.¹⁴ When considering only the species which overlap between the two studies the average absolute error is reduced to 1.74 kcal/mol. The average absolute deviation for the 12 species with reported literature values³² of ΣD_0 is 1.22 kcal/mol. The average absolute deviation for the 13 species with reported literature values^{14, 24, 26} for enthalpies of formation at 0 K is 1.60 kcal/mol.

In general there is very good agreement (less than 3 kcal/mol difference) with the literature enthalpies of formation; however there are a few notable exceptions. Examining the series of methylsilanes from silane to tetramethylsilane, the enthalpic exchange value of methyl for hydrogen is calculated as -12.25 kcal/mol as opposed to the reported substitution value of -16.0 kcal/mol.³⁰ This leads to the errors change by approximately 3.75 kcal/mol with the addition of each methyl group which is mostly due to the under-prediction for the enthalpy of formation of $\cdot\text{CH}_3$ by 2.74 kcal/mol. It should also be noted that there is a large range of reported enthalpies of formation for the family of methylsilanes summarized by Doncaster *et al.* they are given in kcal/mol as -4.0 to -11.8, -15.3 to -29.8, -28.0 to -44.5, and -42.2 to -58.7 for methylsilane, dimethylsilane, trimethylsilane and tetramethylsilane respectively.³³⁻⁴⁰ The corresponding values calculated in this study all fall toward the high end of the reported experimental ranges and are -5.88, -18.15, -30.50, and -42.38 kcal/mol. The largest errors are associated with those compared to the theoretical and estimated enthalpies of formations calculated using the BAC-MP2 method with the applied empirical correction of Ho *et al.*²⁷ As noted by Ho *et al.* there is a dearth of literature heats of formation for $\text{Si}_w\text{C}_x\text{O}_y\text{H}_z$ species, so the values presented by Ho *et al.* and those presented here represent a range of values for ab initio predictions with and without empirical corrections. Fortunately, any systematic accumulation of errors in the DFT methods should not interfere with obtaining accurate enthalpies of reaction for simple reactions of the $\text{Si}_w\text{C}_x\text{O}_y\text{H}_z$ class of molecules examined in this work.

Table 4-1. Total energies and un-scaled zero-point energies, in Hartree, with thermal corrections to enthalpy, sum of atomization energies and enthalpies of formation (both theory and experimental with deviations), in kcal/mol.

Si _w C _x O _y H _z Species	E ^a	ZPE ^b	ΔH ^o _{corr} ^c	Σ D ₀ ^d	ΔH ^o _f (0K) ^e	ΔH ^o _f (298K) Theory ^f	ΔH ^o _f (298K) Expt. ^f	Δ ^g
Si(3P ₀)	-289.3945	0.0000	1.4812	0.0	106.52	107.23	107.55 ^h	-0.32
C(3P ₀)	-37.8575	0.0000	1.4812	0.0	169.98	171.21	171.29 ^h	-0.08
O(3P ₂)	-75.0909	0.0000	1.4812	0.0	58.98	59.43	59.55 ^h	-0.13
H(2S _{1/2})	-0.5022	0.0000	1.4812	0.0	51.63	52.10	52.10 ^h	0.00
(H ₃ CO) ₄ Si	-750.3997	0.1704	8.2273	1896.5	-254.49	-264.33	-218.8 ⁱ	17.47
(H ₃ CO) ₃ SiCH ₃	-675.1288	0.1652	8.9290	1786.7	-203.70	-211.80		
(H ₃ CO) ₂ Si(CH ₃) ₂	-599.8431	0.1586	7.6984	1668.4	-144.41	-152.70		
(H ₃ CO)Si(CH ₃) ₃	-524.5665	0.1532	7.3576	1555.1	-90.08	-97.68		
(H ₃ CO) ₃ Si·	-635.1243	0.1275	7.6314	1407.4	-149.30	-155.41	-161.3 ^{l,q}	5.89 ^q
(H ₃ CO) ₃ Si ⁺	-634.8978	0.1290	7.8147	1264.3	-6.24	-12.17		
(H ₃ CO) ₂ Si·CH ₃	-559.8462	0.1214	6.9001	1293.6	-94.51	-100.31		
(H ₃ CO) ₂ Si ⁺ CH ₃	-559.6286	0.1229	7.0504	1156.2	42.96	37.31		
(H ₃ CO)Si·(CH ₃) ₂	-484.5632	0.1151	5.6376	1176.9	-36.79	-42.82		
(H ₃ CO)Si ⁺ (CH ₃) ₂	-484.3437	0.1158	5.4629	1038.7	101.41	95.21		
Si·(CH ₃) ₃	-409.2905	0.1097	5.3626	1066.1	15.07	9.81	4.1 ± 1.7 ^k	5.74
Si ⁺ (CH ₃) ₃	-409.0604	0.1093	5.0610	921.9	159.23	153.66		
(H ₃ CO) ₃ SiO·	-710.4009	0.1308	7.8050	1521.9	-204.86	-211.84	-217.7 ^{l,q}	5.86 ^q
(H ₃ CO) ₂ SiO·(CH ₃)	-635.1160	0.1244	7.1605	1404.1	-145.96	-152.54		
(H ₃ CO)SiO·(CH ₃) ₂	-559.8462	0.1188	6.8578	1295.2	-96.09	-101.94		
(CH ₃) ₃ SiO·	-484.5652	0.1127	6.1165	1179.6	-39.43	-44.98	-48.5 ^{l,q}	3.52 ^q
(H ₃ CO) ₃ SiH	-635.7839	0.1370	7.6528	1500.5	-190.75	-197.86	-208.2 ^{l,q}	10.34 ^q
(H ₃ CO) ₂ SiH(CH ₃)	-560.5031	0.1308	6.9100	1385.1	-134.33	-141.14		
(H ₃ CO)SiH(CH ₃) ₂	-485.2231	0.1247	6.1457	1270.1	-78.28	-84.82		
(H ₃ CO) ₂ SiH ₂	-521.1528	0.1015	5.3853	1096.1	-118.63	-124.68		
(H ₃ CO)SiH ₂ (CH ₃)	-445.8776	0.0960	5.0048	983.8	-65.29	-70.69		
(H ₃ CO) ₃ SiOH	-711.1019	0.1432	8.3867	1639.3	-270.55	-277.95	-293.3 ^{l,q}	15.35 ^q
(H ₃ CO) ₂ SiOH(CH ₃)	-635.8205	0.1369	7.7247	1523.5	-213.75	-220.78		
(H ₃ CO)SiOH(CH ₃) ₂	-560.5381	0.1305	7.1148	1407.2	-156.43	-163.04		
(CH ₃) ₃ SiOH	-485.2577	0.1246	6.3573	1291.8	-100.08	-106.40	-119.4 ⁱ	13.00
·CH ₃	-39.8578	0.0296	2.5290	292.0	32.84	32.08	34.8 ^h	-2.74
+CH ₃	-39.8555	0.0279	2.3827	291.7	33.22	32.31	33.2 ± 1.9 ^l	-0.89
H ₃ CO·	-115.0993	0.0363	2.5164	382.5	1.37	-0.44	4.1 ± 0.9 ^{m,p}	-4.54
H ₃ CO·	-115.1531	0.0349	2.4270	417.2	-33.29	-35.19	-33.2 ± 2.4 ^l	-1.99
H·	-0.5099	0.0000	1.4812	4.8	46.80	47.27		
O·	-75.1499	0.0000	1.4812	37.0	21.99	22.44	24.3 ^h	-1.91
·OH	-75.7656	0.0083	2.0737	103.2	7.39	7.42	9.4 ± 0.1 ^m	-1.98
·OH	-75.8301	0.0083	2.0737	143.8	-33.16	-33.14		
CH ₄	-40.5368	0.0448	2.3966	393.9	-17.36	-19.26	-17.9 ^h	-1.36
H ₂ CO	-114.5494	0.0266	2.3974	358.4	-26.18	-27.10	-26.0 ± 0.1 ^m	-1.10

SiH ₄	-291.9185	0.0312	2.5359	304.6	8.43	6.15	8.2 ^a	-2.05
CH ₃ SiH ₃	-331.2611	0.0611	3.2818	588.4	-2.07	-5.88	-6.9 ± 0.9 ^a	1.05
(CH ₃) ₂ SiH ₂	-370.6039	0.0902	4.2847	872.6	-13.07	-18.15	-22.7 ± 0.9 ^a	4.56
(CH ₃) ₃ SiH	-409.9465	0.1190	5.3814	1157.0	-24.24	-30.50	-39.0 ± 0.9 ^a	8.46
Si(CH ₃) ₄	-449.2890	0.1474	6.5880	1441.5	-35.50	-42.83	-55.7 ± 0.8 ^a	12.91
Si·H ₃	-291.2647	0.0212	2.4998	215.5	45.90	44.60	48.5 ± 1.5 ^l	-3.90
Si ⁺ H ₃	-290.9650	0.0221	2.4845	26.9	234.53	233.21	237.1 ^l	-3.89
CH ₃ Si·H ₂	-330.6066	0.0513	3.2310	498.7	36.00	33.15		
CH ₃ Si ⁺ H ₂	-330.3346	0.0514	3.4075	327.9	206.73	204.06		
(CH ₃) ₂ Si·H	-369.9485	0.0807	4.2275	782.2	25.68	21.56		
(CH ₃) ₂ Si ⁺ H	-369.6998	0.0804	4.4589	626.3	181.60	177.70		
Si·(CH ₃) ₂ (¹ A ₁)	-369.3313	0.0718	4.1666	715.4	40.92	37.74	33.0 ^{o,p}	4.74
Si·(CH ₃) ₂ (³ B ₁)	-369.2900	0.0731	4.1317	688.7	67.60	64.39		
HSi·CH ₃ (¹ A ₁)	-329.9871	0.0420	3.0777	430.6	52.41	50.42	49.2 ^{o,p}	1.22
HSi·CH ₃ (³ B ₁)	-329.9506	0.0425	3.1977	407.4	75.67	73.80		
Si·H ₂ (¹ A ₁)	-290.6430	0.0111	2.3961	146.6	63.21	62.82	65.2 ± 0.7 ^{m,p}	-2.38
Si·H ₂ (³ B ₁)	-290.6105	0.0116	2.4159	125.8	83.95	83.57	86.2 ± 1.0 ^m	-2.63

|Δ|_{av} = 3.89

^a Total Energy at 0 K and 1 atm at the B3LYP/6-311+(3df,2p)//B3LYP/6-311+G(d) level, in Hartrees.

^b Un-scaled zero-point energy calculated at the B3LYP/6-311+G(d)//B3LYP/6-311+G(d) level, in Hartrees.

^c Thermal correction to enthalpy to 298.15 K and 1 atm, including PV term (RT), 3/2 RT for translational energy, 3/2 RT or RT for rotational energy, and utilizing the scaled 0.96 B3LYP/6-311+G(d) frequencies in the harmonic approximation for vibrational energy, in kcal/mol from Eq. (4-3).

^d Sum of the atomization energies, in kcal/mol.

^e Enthalpy of formation at 0 K and 1 atm, in kcal/mol, from Eq. (4-1).

^f Standard Enthalpy of formation at 298K and 1 atm, in kcal/mol, theoretical value from Eq. (4-2).

^g Deviation of theory from experimental values from the literature, where available.

^h Reference 20.

ⁱ Reference 27.

^j Reference 23; ^k Based on the theoretical values of Reference 23.

^k Reference 21.

^l Reference 24.

^m Reference 9.

ⁿ Reference 22.

^o Reference 26.

^p Reference 25.

Figure 4-1 shows the family plot for a family of methoxymethylsilanes, (CH₃)_nSi(OCH₃)_{4-n}, for n from 0 to 4, and (CH₃)_nSiOH(OCH₃)_{3-n}, (CH₃)_nSiH(OCH₃)_{3-n}, (CH₃)_nSiH₂(OCH₃)_{2-n}, (CH₃)_nSiO·(OCH₃)_{3-n}, and (CH₃)_nSi·(OCH₃)_{3-n} for n from 0 to 3. Each series yields a methyl for methoxy substitution energy of 55.4 ± 1.3 kcal/mol. The average hydroxyl (OH) for methoxy, hydrogen for methoxy, methyl for hydrogen, and hydrogen for hydroxyl substitution energies are given as -10.4 ± 3.2, 68.1 ± 1.6, -14.3 ± 2.1, and 78.5 ± 2.6 kcal/mol, respectively.

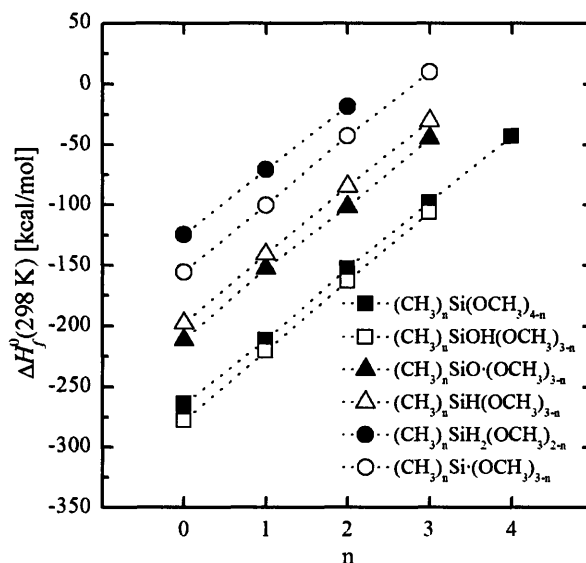


Figure 4-1. Family plot for methoxymethylsilanes – a. (CH₃)_nSi(OCH₃)_{4-n}, b. (CH₃)_nSiOH(OCH₃)_{3-n}, c. (CH₃)_nSiH(OCH₃)_{3-n}, d. (CH₃)_nSiH₂(OCH₃)_{2-n}, e. (CH₃)_nSiO(OCH₃)_{3-n}, and f. (CH₃)_nSi(OCH₃)_{3-n}.

Figure 4-2 shows a family plot for methylsilanes, methylsilyl radicals, and methylsilylene diradicals, (CH₃)_nSiH_{4-n}, (CH₃)_nSi·H_{3-n}, (CH₃)_nSi·H_{2-n} (¹A₁), and (CH₃)_nSi·H_{2-n} (³B₁) for n from 0 to 4, 3, 2 and 2, respectively. The calculated average methyl for hydrogen substitution energies are -12.25 ± 0.24, -11.60 ± 0.15, -12.54 ± 0.14, and -9.59 ± 0.18 kcal/mol for methylsilanes and the corresponding silyl radicals, singlet silylene diradicals and the less stable triplet silylene diradicals, respectively.

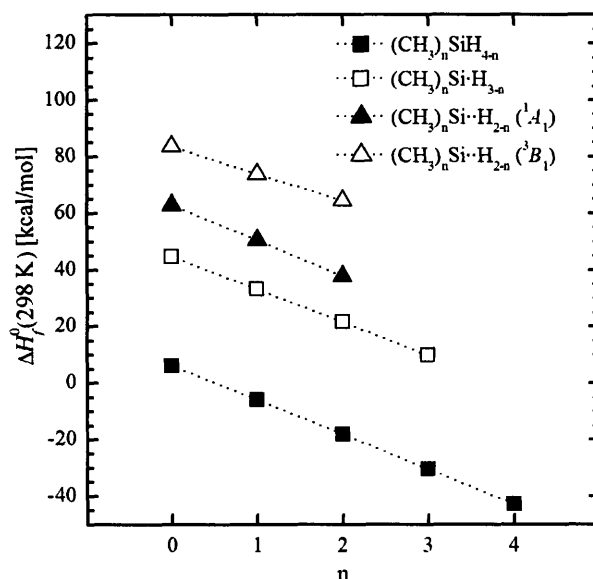


Figure 4-2. Family plot for methylsilanes – a. $(\text{CH}_3)_n\text{SiH}_{4-n}$, b. $(\text{CH}_3)_n\text{Si}\cdot\text{H}_{3-n}$, c. $(\text{CH}_3)_n\text{Si}\cdot\text{H}_{2-n}$ (1A_1), and d. $(\text{CH}_3)_n\text{Si}\cdot\text{H}_{2-n}$ (3B_1).

4.3.2 REACTION ENTHALPIES AND BOND DISSOCIATION ENERGIES

Table 4-2 summarizes the bond dissociation energies (BDEs) in enthalpy and Gibbs free energy of reaction at 298 K and 1 atm, $\Delta G^0_{rxn}(298\text{ K})$, for methylsilanes and methylsilyl radicals. Experimental values are reported when available.^{26, 41} Of particular interest for this work is the comparison of Si–H *v.* Si–C BDEs for the methylsilanes. The difference in BDEs of the Si–H and Si–C bond is also given in Table 4-2. The calculated Si–H bond strength increases by approximately 0.6 kcal/mol with each additional methyl substitution, agreeing well with the literature.⁴¹ A similar trend is seen with the Si–C bond strength increasing by approximately 0.9 kcal/mol per additional methyl. These trends are evident in Figure 4-3 which plots the BDEs of methylsilanes and methylsilyl radicals as a function of methyl substitution. Of the greatest significance to understanding the chemistry during a CVD process is the difference in bond strengths. The Si–H bond is an average of 8.4 kcal/mol stronger than the Si–C bond in methylsilanes and an

average of 7.5 kcal/mol stronger in the corresponding methylsilyl radicals. This relationship is true as well same for ΔG°_{rxn} (298 K) with the entropic contribution to the energy of the reaction ranging from 2.08 to 3.56 kcal/mol and increasing with methylation. The calculated difference in bond strengths indicates that the Si–C bond will break before the Si–H bond corresponding with a mass spectrometry study of trimethylsilane.⁴² This order of bond strengths is undesirable for CVD of low dielectric constant materials where retention of carbon content lowers the dielectric constant.

Table 4-2. Bond dissociation energies for methylsilanes and methylsilyl radicals.

Species	Si–H Bond Dissociation Energy				Si–C Bond Dissociation Energy				$D_{298}(\text{Si–H})$ – $D_{298}(\text{Si–C})^d$
	ΔG°_{rxn} (298 K) Theory ^a	ΔH°_{rxn} (298 K) Theory ^b	ΔH°_{rxn} (298 K) Expt. ^b	Δ^c	ΔG°_{rxn} (298 K) Theory ^a	ΔH°_{rxn} (298 K) Theory ^b	ΔH°_{rxn} (298 K) Expt. ^b	Δ^c	
SiH ₄	80.85	90.55	91.1 ± 1.4 ^e	-0.55					
CH ₃ SiH ₃	82.05	91.14	92.1 ± 1.2 ^e	-0.92	70.82	82.56			8.58
(CH ₃) ₂ SiH ₂	82.85	91.81	92.8 ± 1.2 ^e	-0.96	71.67	83.38			8.43
(CH ₃) ₃ SiH	84.35	92.41	94.7 ± 1.4 ^e	-2.28	72.52	84.14			8.27
Si(CH ₃) ₄					72.14	84.72	89.6 ± 2.2 ^f	-4.91	
Si·H ₃	63.46	70.32							
CH ₃ Si·H ₂	61.93	69.37			52.23	61.74			7.62
(CH ₃) ₂ Si·H	60.75	68.29			50.75	60.94			7.35
Si·(CH ₃) ₃					48.92	60.01	57.4 ± 2.9 ^f	2.65	
				$ \Delta _{av} = 1.18$				$ \Delta _{av} = 3.78$	

^a Gibbs free energy of reaction at 298 K and 1 atm, in kcal/mol, from Eq. (4-6).

^b Bond dissociation energy in enthalpy of reaction at 298 K and 1 atm, in kcal/mol, from Eq. (4-4).

^c Deviation of theory from experimental values from the literature, where available.

^d Difference in bond dissociation energy in enthalpy at 298 K and 1 atm of the Si–H and Si–C bonds, in kcal/mol.

^e Reference 37.

^f Reference 22.

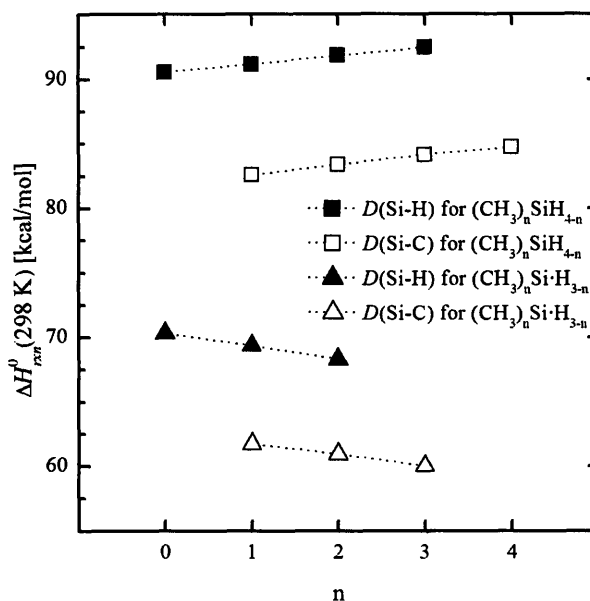


Figure 4-3. BDEs for methylsilanes and methylsilyl radicals as a function of methyl substitution (n).

Table 4-3 summarizes the bond dissociation energies (BDEs) in enthalpy and Gibbs free energy of reaction at 298 K and 1 atm, $\Delta G^{\circ}_{rxn}(298\text{ K})$, for methoxymethylsilanes. Similar to the focus on BDEs of methylsilanes, the comparison of Si–C *v.* Si–O *v.* O–C BDEs for the methoxymethylsilanes is of the greatest significance for understanding monomer fragmentation patterns in CVD. The difference in BDEs for the series of bonds is also presented in Table 4-3. The Si–O bond is stronger than the Si–C bond by 22.5 ± 2.5 kcal/mol. The Si–C bond is marginally stronger than the O–C bond in methoxytrimethylsilane and dimethoxydimethylsilane by 2.16 and 1.62 kcal/mol, respectively, but is 2.87 kcal/mol weaker than the O–C bond in trimethoxymethylsilane. Relationships between bond strengths for methoxymethylsilanes, particularly the nuances comparing the Si–C and O–C bonds, are depicted clearly in Figure 4-4. The same observations can be made considering the $\Delta G^{\circ}_{rxn}(298\text{ K})$ with entropic effects

contributing anywhere from -3.0 to 1.2 additional kcal/mol to the differences in bond strengths. The motivation for choosing methoxymethylsilanes as a CVD precursor for low dielectric constant thin films is to take advantage of the built in structure of Si-O and Si-C bonds. With the bond strengths of the Si-C and O-C bonds being so similar, it would be difficult control the desired reaction pathways and unlikely to retain a large percentage of methyl content in a CVD process from methoxymethylsilane precursors.

Table 4-3. Bond dissociation energies for methoxymethylsilanes.

Species	Si-C Bond Strength		Si-O Bond Strength		O-C Bond Strength		$D(\text{Si-C}) - D(\text{Si-O})^c$	$D(\text{Si-C}) - D(\text{O-C})^d$	$D(\text{Si-O}) - D(\text{O-C})^e$
	ΔG_{rxn}^0 (298 K)	ΔH_{rxn}^0 (298 K)	ΔG_{rxn}^0 (298 K)	ΔH_{rxn}^0 (298 K)	ΔG_{rxn}^0 (298 K)	ΔH_{rxn}^0 (298 K)			
	Theory ^a	Theory ^b	Theory ^a	Theory ^b	Theory ^a	Theory ^b			
$(\text{H}_3\text{CO})_4\text{Si}$			92.69	108.48	71.77	84.57			23.90
$(\text{H}_3\text{CO})_3\text{SiCH}_3$	77.00	88.47	98.91	111.05	81.56	91.34	-22.58	-2.87	19.71
$(\text{H}_3\text{CO})_2\text{Si}(\text{CH}_3)_2$	71.73	84.47	97.49	109.44	70.91	82.84	-24.97	1.62	26.59
$(\text{H}_3\text{CO})\text{Si}(\text{CH}_3)_3$	76.42	86.93	95.34	107.04	73.64	84.77	-20.11	2.16	22.27

^a Gibbs free energy of reaction at 298 K and 1 atm, in kcal/mol, from Eq. (4-6).

^b Bond dissociation energy in enthalpy of reaction at 298 K and 1 atm, in kcal/mol, from Eq. (4-4).

^c Difference in bond dissociation energy in enthalpy at 298 K and 1 atm of the Si-C and Si-O bonds, in kcal/mol.

^d Difference in bond dissociation energy in enthalpy at 298 K and 1 atm of the Si-C and O-C bonds, in kcal/mol.

^e Difference in bond dissociation energy in enthalpy at 298 K and 1 atm of the Si-O and O-C bonds, in kcal/mol.

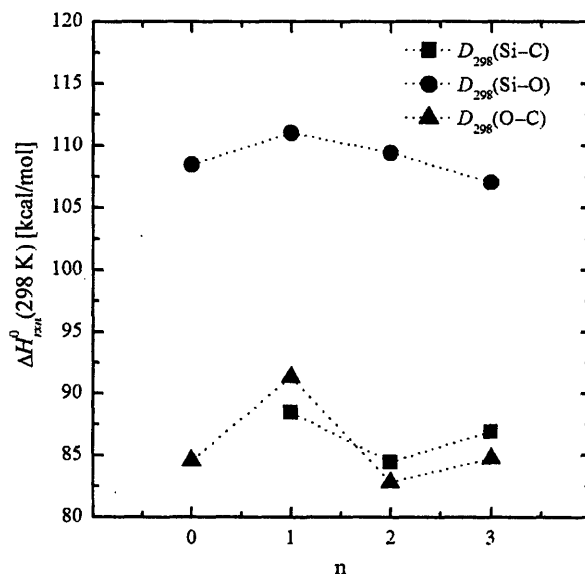


Figure 4-4. BDEs for the Si-C, Si-O, and O-C bonds for methoxymethylsilanes as a function of increasing methyl content (n).

The thermochemistry of the primary reactions of methylsilanes with oxygen atom, $O(^3P_2)$, and methoxymethylsilanes with $O(^3P_2)$ and hydrogen atom, $H(^2S_{1/2})$, are examined and summarized in Table 4-4. The calculated energy splitting between singlet and triplet states, ΔE_{ST} or divalent state stabilization energy, of the silylenes is also reported in Table 4-4 along with the few experimental enthalpies of reaction available from the literature^{30, 43}. The average absolute deviation from experimental values is 1.86 kcal/mol.

All reactions of methylsilanes with O atom studied are found to be exothermic. Hydrogen abstraction from methylsilanes from oxygen atom to yield an OH radical and a methylsilyl radical is a low barrier reaction.^{9, 44} Horrie *et al.* determined kinetic parameters for the reactions of silane, methylsilane, dimethylsilane, and trimethylsilane with oxygen and concluded that only the primary reaction is OH abstraction.⁴⁴ While this work considers the favored reactions determined by thermodynamics, the conclusions for methylsilanes are consistent with the observation in literature. For reactions of methylsilanes with oxygen atom, hydrogen abstraction ($\cdot OH$ formation) is favored over methyl abstraction ($\cdot OCH_3$ formation) by 3.74 ± 0.15 kcal/mol. This is significant for controlling the CVD process. The fragmentation of the monomer methylsilanes indicates loss of methyl rather than hydrogen; however, with the addition of oxygen atom to the CVD process, hydrogen abstraction is favored retaining the methyl functionality of the monomer species. The calculated silylene splitting energies agree well with the literature.³⁰ The singlet silylene species are more stable than their triplet counterparts by 20.8, 23.4, and 26.7 kcal/mol for silylene,

methylsilylene, and dimethylsilylene, respectively. The good agreement with the few available literature values for these reactions along with the good agreement with the enthalpies of formation gives credibility to this method. While there is no indication to the degree of precision of the calculated enthalpies of reaction, the thermodynamic comparison of reactions can be reasonably accepted.

Studied reactions of methoxymethylsilanes with O atom are also found to be exothermic. The results for the reactions of methoxymethylsilanes with oxygen are no different than the bond dissociation energies when determining the favored reaction pathway. Abstraction of a methyl from a methoxy group is favored for trimethoxymethylsilane + O atom, but abstraction of a methyl from silicon is favored for dimethoxydimethyl- or methoxytrimethylsilane + O atom. Considering that both are methyl abstraction reactions, barrier energies for the reactions may be similar with the expectation that they scale with steric effects caused by substitution patterns (i.e. the barrier energy for methyl abstraction for silicon is expected to be lower with increased methylation of the silicon center). This again makes for difficult control over reaction pathways in a CVD process in which Si-C bond retention is desired. Included at the bottom of Table 4-4 are reactions of the methylsilanes and methoxymethylsilanes with O atom to yield all neutral species including formaldehyde (H_2CO). These reactions are all very exothermic, but the energy barrier is expected to be much higher than for simple abstraction mechanisms due to the requirement of a four center complex for proton transfer and should therefore be considered less likely than the abstraction reactions.

Table 4-4. Gibbs free energy of reaction and enthalpy of reaction at 298 K and 1 atm for a series of reactions of methylsilanes with oxygen and methoxymethylsilanes with oxygen and with hydrogen.

Reactants	Products	ΔG°_{rxn} (298 K) Theory ^a	ΔH°_{rxn} (298 K) Theory ^b	ΔH°_{rxn} (298 K) Expt. ^b	Δ^c
<i>Methylsilanes + O(3P₂)</i>					
Si(CH ₃) ₄ + O·	→ ·Si(CH ₃) ₃ + ·OCH ₃	-11.96	-7.23		
(CH ₃) ₃ SiH + O·	→ ·Si(CH ₃) ₃ + ·OH	-13.42	-11.70		
	→ ·SiH(CH ₃) ₂ + ·OCH ₃	-11.58	-7.81		
(CH ₃) ₂ SiH ₂ + O·	→ ·SiH(CH ₃) ₂ + ·OH	-14.92	-12.30		
	→ ·SiH ₂ (CH ₃) + ·OCH ₃	-12.43	-8.57		
(CH ₃)SiH ₃ + O·	→ ·SiH ₂ (CH ₃) + ·OH	-15.72	-12.98		
	→ ·SiH ₃ + ·OCH ₃	-13.27	-9.39		
SiH ₄ + O·	→ ·SiH ₃ + ·OH	-16.92	-13.56	-11.09 ± 1.5 ^d	-2.47
<i>Silylene splitting</i>					
Si··H ₂ (3B ₁)	→ Si··H ₂ (1A ₁)	-20.21	-20.75	-19.4 ± 2.2 ^e	-1.35
(CH ₃)Si··H (3B ₁)	→ (CH ₃)Si··H (1A ₁)	-22.19	-23.39		
Si··(CH ₃) ₂ (3B ₁)	→ Si··(CH ₃) ₂ (1A ₁)	-25.99	-26.65	-28.4 ± 3.9 ^e	1.75
<i>Methoxymethylsilanes + O(3P₂)</i>					
Si(OCH ₃) ₄ + O·	→ (H ₃ CO) ₃ SiO· + ·OCH ₃	-12.33	-7.37		
(H ₃ CO) ₃ SiCH ₃ + O·	→ (H ₃ CO) ₃ Si· + ·OCH ₃	-7.10	-3.48		
	→ (H ₃ CO) ₂ SiO·(CH ₃) + ·OCH ₃	-2.54	-0.61		
(H ₃ CO) ₂ Si(CH ₃) ₂ + O·	→ (H ₃ CO) ₂ Si·(CH ₃) + ·OCH ₃	-12.37	-7.48		
	→ (H ₃ CO)SiO·(CH ₃) ₂ + ·OCH ₃	-13.18	-9.11		
(H ₃ CO)Si(CH ₃) ₃ + O·	→ (H ₃ CO)Si·(CH ₃) ₂ + ·OCH ₃	-7.68	-5.02		
	→ (CH ₃) ₃ SiO· + ·OCH ₃	-10.45	-7.18		
<i>Methoxymethylsilanes + H(2S_{1/2})</i>					
Si(OCH ₃) ₄ + H·	→ (H ₃ CO) ₃ SiO· + CH ₄	-22.86	-18.86		
	→ (H ₃ CO) ₃ SiOH + ·CH ₃	-38.94	-33.64		
(H ₃ CO) ₃ SiCH ₃ + H·	→ (H ₃ CO) ₂ SiO·(CH ₃) + CH ₄	-13.07	-12.10		
	→ (H ₃ CO) ₂ SiOH(CH ₃) + ·CH ₃	-31.03	-29.00		
	→ (H ₃ CO) ₃ Si· + CH ₄	-17.63	-14.97		
	→ (H ₃ CO) ₃ SiH + ·CH ₃	-8.92	-6.08		
(H ₃ CO) ₂ Si(CH ₃) ₂ + H·	→ (H ₃ CO)SiO·(CH ₃) ₂ + CH ₄	-23.72	-20.60		
	→ (H ₃ CO)SiOH(CH ₃) ₂ + ·CH ₃	-34.07	-30.36		
	→ (H ₃ CO) ₂ Si·(CH ₃) + CH ₄	-22.91	-18.97		
	→ (H ₃ CO) ₂ SiH(CH ₃) + ·CH ₃	-12.47	-8.46		
(H ₃ CO)Si(CH ₃) ₃ + H·	→ (CH ₃) ₃ SiO· + CH ₄	-20.99	-18.67		
	→ (CH ₃) ₃ SiOH + ·CH ₃	-31.63	-28.75		
	→ (H ₃ CO)Si·(CH ₃) ₂ + CH ₄	-18.22	-16.51		
	→ (H ₃ CO)SiH(CH ₃) ₂ + ·CH ₃	-10.19	-7.16		
<i>Reactions with neutral products including H₂CO</i>					
Si(CH ₃) ₄ + O·	→ (CH ₃) ₃ SiH + H ₂ CO	-78.11	-74.20		
(CH ₃) ₃ SiH + O·	→ (CH ₃) ₂ SiH ₂ + H ₂ CO	-76.23	-74.18		
(CH ₃) ₂ SiH ₂ + O·	→ (CH ₃)SiH ₃ + H ₂ CO	-76.28	-74.26		
(CH ₃)SiH ₃ + O·	→ SiH ₄ + H ₂ CO	-75.93	-74.49		

$\text{Si}(\text{OCH}_3)_4 + \text{O}\cdot \rightarrow (\text{H}_3\text{CO})_3\text{SiOH} + \text{H}_2\text{CO}$	-104.84	-100.15
$(\text{H}_3\text{CO})_3\text{SiCH}_3 + \text{O}\cdot \rightarrow (\text{H}_3\text{CO})_2\text{SiOH}(\text{CH}_3) + \text{H}_2\text{CO}$	-96.93	-95.51
$(\text{H}_3\text{CO})_2\text{Si}(\text{CH}_3)_2 + \text{O}\cdot \rightarrow (\text{H}_3\text{CO})\text{SiOH}(\text{CH}_3)_2 + \text{H}_2\text{CO}$	-99.97	-96.86
$(\text{H}_3\text{CO})\text{Si}(\text{CH}_3)_3 + \text{O}\cdot \rightarrow (\text{CH}_3)_3\text{SiOH} + \text{H}_2\text{CO}$	-97.53	-95.25
$\text{Si}(\text{OCH}_3)_4 \rightarrow (\text{H}_3\text{CO})_3\text{SiH} + \text{H}_2\text{CO}$	24.96	39.38
$(\text{H}_3\text{CO})_3\text{SiCH}_3 \rightarrow (\text{H}_3\text{CO})_2\text{SiH}(\text{CH}_3) + \text{H}_2\text{CO}$	32.91	43.57
$(\text{H}_3\text{CO})_2\text{Si}(\text{CH}_3)_2 \rightarrow (\text{H}_3\text{CO})\text{SiH}(\text{CH}_3)_2 + \text{H}_2\text{CO}$	29.08	40.79
$(\text{H}_3\text{CO})\text{Si}(\text{CH}_3)_3 \rightarrow (\text{CH}_3)_3\text{SiH} + \text{H}_2\text{CO}$	29.19	40.08

$|\Delta|_{\text{av}} = 1.86$

^a Gibbs free energy of reaction at 298 K and 1 atm, in kcal/mol, from Eq. (4-6).

^b Enthalpy of reaction at 298 K and 1 atm, in kcal/mol, from Eq. (4-4).

^c Deviation of theory from experimental values from the literature, where available.

^d Enthalpy of reaction at 0 K, Reference 39.

^e Reference 26.

Investigating reactions of the methoxymethylsilanes with H atom leads to a thermodynamically diverse set of reactions. Again all reactions studied are exothermic. In general, the favored products in order of thermodynamic favorability are (1) methyl radical and methoxymethylsilanol, (2) methane and methoxymethylsiloxyl radical, (3) methane and methoxymethylsilyl radical, and (4) methyl radical and protonated methoxymethylsilane. The products are favored relative to (4) methyl radical and protonated methoxymethylsilane by (1) ~ 22.1 kcal/mol, (2) ~ 11.8 kcal/mol (excluding trimethoxymethylsilane), and (3) ~ 9.6 kcal/mol, respectively. The expectation is for trimethoxymethylsilane where the order of the favored products is set (1) silanol formation, (3) silyl radical formation, (2) siloxyl radical formation by only 6.0 kcal/mol relative to ~11.8 kcal/mol for other methoxymethylsilanes, followed by (4) formation of the protonated methoxymethylsilane. By controlling the reaction pathways of methoxymethylsilanes to promote silanol formation, greater control over the chemical composition of thin films deposited by CVD is possible. Silanol species are highly reactive via condensation reactions in which two silanol groups react to create a Si–O–Si bridge and liberate H₂O.^{45, 46}

4.4 CONCLUSIONS

The B3LYP hybrid functional has been applied to compute the thermochemistry of methyl- and methoxymethylsilanes and investigate bond strengths and primary reactions with atomic oxygen and hydrogen. Total energies were calculated at the B3LYP/6-311+G(3df,3p) level using B3LYP/6-311+G(d) optimized geometries. Thermal corrections to the energy included the scaled (0.96) zero-point energies and enthalpic corrections to 298 K which consists of the classical rotational, translational, and PV terms along with the vibrational contributions calculated making use of the scaled (0.96) vibrational frequencies calculated at the B3LYP/6-311+G(d) level. The average absolute deviation of computed enthalpies of formation was 3.89 kcal/mol, and the average absolute deviation of computed enthalpies of reaction at 298 K was 1.86 kcal/mol.

Bond strengths and reactions of methyl- and methoxymethylsilanes with O atom and H atom are examined in the context of understanding the initial reaction in the CVD process. The Si-H bond was calculated to be 8.4 kcal/mol stronger than the Si-C bond in methylsilanes and to increase by 0.6 kcal/mol with increased methylation. Methylsilanes react with O atom to preferentially produce hydroxyl radical and methylsilyl radical allowing for retention of the Si-C bond which is not favored in the regime considering only methylsilane fragmentation. Thermodynamic control over the reaction pathways of methoxymethylsilanes is possible only when considering the reaction with H atom. Formation of methoxymethylsilanols is favored in the reaction scheme with H atom. Silanol groups react readily with other

silanol groups creating Si–O–Si bridges and liberating water. This leads to a conceivable strategy to control the Si–O bond network and retained methyl content in a CVD thin film by controlling the molecular ratio of the corresponding methoxymethylsilane precursors and creating an H atom rich environment. Density functional theory is a useful tool in understanding and subsequently controlling the initial chemistry in the CVD process.

REFERENCES

1. B. Narayanan, R. Kumar, and P. D. Foo, *Microelectron. J.*, **33**, 971 (2002).
2. Q. G. Wu and K. K. Gleason, *J. Vac. Sci. Technol. A*, **21**, 388 (2003).
3. A. Grill, *J. Appl. Phys.*, **93**, 1785 (2003).
4. A. Grill and V. Patel, *Appl. Phys. Lett.*, **79**, 803 (2001).
5. D. D. Burkey and K. K. Gleason, *J. Appl. Phys.*, **93**, 5143 (2003).
6. D. D. Burkey and K. K. Gleason, *J. Electrochem. Soc.*, **151**, F105 (2004).
7. A. Grill and D. A. Neumayer, *J. Appl. Phys.*, **94**, 6697 (2003).
8. H. G. P. Lewis, T. B. Casserly, and K. K. Gleason, *J. Electrochem. Soc.*, **148**, F212 (2001).
9. Q. Z. Zhang, S. K. Wang, J. H. Zhou, and Y. H. Gu, *J. Phys. Chem. A*, **106**, 115 (2002).
10. Q. Zhang, S. Wang, C. Liu, J. Zhang, M. Ru, and Y. Gu, *Huaxue Wuli Xuebao*, **13**, 528 (2000).
11. Q. Z. Zhang, Y. S. Gu, and S. K. Wang, *J. Chem. Phys.*, **118**, 633 (2003).
12. K. K. S. Lau, K. K. Gleason, and B. L. Trout, *J. Chem. Phys.*, **113**, 4103 (2000).
13. T. B. Casserly and K. K. Gleason, *J. Phys. Chem. B*, submitted (2005).
14. L. A. Curtiss, K. Raghavachari, P. C. Redfern, and J. A. Pople, *J. Chem. Phys.*, **106**, 1063 (1997).
15. B. Miehlich, A. Savin, H. Stoll, and H. Preuss, *Chem. Phys. Lett.*, **157**, 200 (1989).
16. A. D. Becke, *Phys. Rev. A*, **38**, 3098 (1988).
17. C. T. Lee, W. T. Yang, and R. G. Parr, *Phys. Rev. B*, **37**, 785 (1988).
18. S. H. Vosko, L. Wilk, and M. Nusair, *Can. J. Phys.*, **58**, 1200 (1980).
19. L. A. Curtiss, K. Raghavachari, P. C. Redfern, and J. A. Pople, *Chem. Phys. Lett.*, **270**, 419 (1997).
20. G. Rauhut and P. Pulay, *J. Phys. Chem.*, **99**, 3093 (1995).
21. A. P. Scott and L. Radom, *J. Phys. Chem.*, **100**, 16502 (1996).
22. M. W. Wong, *Chem. Phys. Lett.*, **256**, 391 (1996).
23. M. J. Frisch, G. W. Trucks, H. B. Schlegel, G. E. Scuseria, M. A. Robb, J. R. Cheeseman, V. G. Zakrzewski, J. A. Montgomery, R. E. Stratmann, J. C. Burant, S. Dapprich, J. M. Millam, A. D. Daniels, K. N. Kudin, M. C. Strain, O. Farkas, J. Tomasi, V. Barone, M. Cossi, R. Cammi, B. Mennucci, C. Pomelli, C. Adamo, S. Clifford, J. Ochterski, G. A. Petersson, P. Y. Ayala, Q. Cui, K. Morokuma, D. K. Malick, A. D. Rabuck, K. Raghavachari, J. B. Foresman, J. Cioslowski, J. V. Ortiz, B. B. Stefanov, G. Liu, A. Liashenko, P. Piskorz, I. Komaromi, R. Gomperts, R. L. Martin, D. J. Fox, T. A. Keith, M. A. Al-Laham, C. Y. Peng, A. Nanayakkara, C. Gonzalez, M. Challacombe, P. M. W. Gill, B. G. Johnson, W. Chen, M. W. Wong, J. L. Andres, M. Head-Gordon, E. S. Replogle, and J. A. Pople, Gaussian Inc., Pittsburgh, PA, 1998.
24. *NIST-JANAF Thermochemical Tables*, 4th ed., AIP-ACS, Woodbury, NY, (1998).
25. L. Y. Ding and P. Marshall, *J. Am. Chem. Soc.*, **114**, 5754 (1992).
26. A. M. Doncaster and R. Walsh, *Journal Of The Chemical Society-Faraday Transactions II*, **82**, 707 (1986).
27. P. Ho and C. F. Melius, *J. Phys. Chem.*, **99**, 2166 (1995).
28. S. G. Lias, J. E. Bartmess, J. F. Liebman, J. L. Holmes, R. D. Levin, and W. G. Mallard, *J. Phys. Chem. Ref. Data*, **17**, 1 (1988).
29. G. Pilcher, M. L. P. Leita, M. Y. Yang, and R. Walsh, *J. Chem. Soc.-Faraday Trans.*, **87**, 841 (1991).
30. R. Walsh, *Organometallics*, **8**, 1973 (1989).
31. R. Walsh, *In: The Chemistry of Organic Silicon Compounds*, p. 371, Wiley, New York, (1989).
32. L. A. Curtiss, K. Raghavachari, G. W. Trucks, and J. A. Pople, *J. Chem. Phys.*, **94**, 7221 (1991).
33. T. N. Bell, K. A. Perkins, and P. G. Perkins, *Journal Of The Chemical Society-Faraday Transactions I*, **77**, 1779 (1981).
34. M. J. S. Dewar, D. H. Lo, and C. A. Ramsden, *J. Am. Chem. Soc.*, **97**, 1311 (1975).
35. A. M. Mosin and Y. K. Shaurov, *Russ. J. Phys. Chem.*, **46**, 1054 (1972).
36. H. E. Oneal and M. A. Ring, *J. Organomet. Chem.*, **213**, 419 (1981).
37. J. B. Pedley and B. S. Iseard, *CATCH Table for Silicon Compounds*, University of Sussex, (1972).

38. P. Potzinger and F. W. Lampe, *J. Phys. Chem.*, **74**, 587 (1970).
39. D. Quane, *J. Phys. Chem.*, **75**, 2480 (1971).
40. W. V. Steele, *J. Chem. Thermodyn.*, **15**, 595 (1983).
41. L. Y. Ding and P. Marshall, *J. Chem. Soc.-Faraday Trans.*, **89**, 419 (1993).
42. C. Q. Jiao, A. Garscadden, and P. D. Haaland, *Int. J. Mass Spectrom.*, **184**, 83 (1999).
43. L. Y. Ding and P. Marshall, *J. Chem. Phys.*, **98**, 8545 (1993).
44. O. Horie, R. Taege, B. Reimann, N. L. Arthur, and P. Potzinger, *J. Phys. Chem.*, **95**, 4393 (1991).
45. B. C. Bunker, D. R. Tallant, T. J. Headley, G. L. Turner, and R. J. Kirkpatrick, *Phys. Chem. Glasses*, **29**, 106 (1988).
46. A. J. Moulson and J. P. Roberts, *Transactions of the Faraday Society*, **57**, 1208 (1961).

CHAPTER FIVE

CHEMICAL VAPOR DEPOSITION OF ORGANOSILICON THIN FILMS FROM METHOXYMETHYLSILANES

T. B. Casserly, and K. K. Gleason, *J. Electrochem. Soc.*, submitted (2005).

ABSTRACT

Plasma enhanced chemical vapor deposition was used to deposit organosilicon thin films from methoxytrimethylsilane, dimethoxydimethylsilane, and trimethoxymethylsilane which were analyzed via FTIR, spectroscopic ellipsometry, and electrical measurements. Oxidative environments are sufficient for creating OSG thin films; however, reactions of methoxymethylsilanes with oxygen are not selective leading to loss of methyl functionality. Reducing chemistry is selective, with hydrogen atoms reacting preferentially with the methoxy methyl creating silanol or siloxane radicals which form networking bonds through condensation reactions without sacrificing the 'built-in' alkyl content of the precursor. Low- k OSG thin films from methoxymethylsilanes and hydrogen were deposited via a low power PECVD process resulting in material dielectric constants ranging from 2.84 to 3.18.

ACKNOWLEDGEMENTS: The authors thank Novellus and the Semiconductor Research Corporation for fellowship funding and the NSF/SRC Engineering Research Center for Environmental Benign Semiconductor Manufacturing for funding support.

5.1 INTRODUCTION

Plasma enhanced chemical vapor deposition (PECVD) of methoxymethylsilanes has been investigated to deposit fully oxygenated silicon oxide for use as a dielectric material,¹⁻³ as transparent hard water resistant optical coatings,^{4, 5} and depositions with some alkyl retention as a coating to control access to HY zeolite catalysts.⁶ As critical dimensions in integrated circuits continue to get smaller and smaller, there need for mechanically robust low dielectric constant thin films becomes greater and greater. Many CVD organosilicate glasses (OSGs) have been proposed for use as a low dielectric constant material, however, widespread integration into the manufacturing process has been limited due to issues concerning the mechanical properties of the films.⁷

Previous work has correlated the mechanical properties of thin films to their chemical composition.⁸⁻¹² Specifically, the impact of the concentration of different silicon-oxygen bonding environments to the hardness and modulus of the materials was studied. There are four typical bonding environments in OSG thin films which are referred to as M, D, T and Q groups. A mono-substituted M group consists of silicon bonded to three methyl (or alkyl) groups and is chain terminating group. The di-substituted moiety, or D group, is a chain building linear $(R)_2SiO_2$ unit. The tri-substituted T group contains three oxygen atoms and one methyl (or alkyl group) and is a branching or network forming group. The quad-substituted moiety is called a Q group which forms highly networked structures such as SiO_2 . While a film consisting of only Q groups is mechanically robust, its dielectric constant is ~ 4.0 . Introduction of alkyl groups into the silicon dioxide matrix lowers the dielectric

constant by introducing bonds with a low polarizability and via the loosening of the oxide lattice created by the incorporated alkyl groups. Theory predicts that a structure composed of entirely T groups is lower limit to provide sufficient mechanical strength, but a film of mostly T groups, the number of M and D groups must be offset by Q groups in order to maintain good mechanical hardness and modulus.^{9, 13, 14}

This work examines the structure of films deposited under continuous wave (CW) PECVD from methoxytrimethylsilane (MO₃MS), dimethoxydimethylsilane (2MO₂MS), and trimethoxymethylsilane (3MOMS). Depositions are performed under mild plasma conditions in an attempt to control the reaction chemistry while still creating robust OSG thin films. The experiments are designed based on predictions from molecular simulation of fragmentation patterns and elementary reactions of this family of methoxymethylsilanes. Additional advantages of the mild plasma conditions may include extendibility to future generations of porous OSG thin films which require mild plasma conditions for deposition of porogen materials.

5.2 RESULTS AND DISCUSSION

5.2.1. FOURIER TRANSFORM INFRARED (FTIR) SPECTROSCOPY

Figure 5-1 shows the FTIR spectra of films deposited from MO₃MS, 2MO₂MS, and 3MOMS. Table 5-1 summarizes common assignments from the literature.^{9, 15-19} As can be expected from the precursor structure, the film deposited from MO₃MS contains the most CH₃ stretching (3000 – 2800 cm⁻¹) and rocking (840 – 920 cm⁻¹) and the least intense Si–O–Si modes (1250 – 980 cm⁻¹).

Accordingly, the film from 3MOMS contains the least CH₃ stretching and rocking and the most intense Si–O–Si band with the intensities for these modes somewhere in between for the film from 2MO2MS.

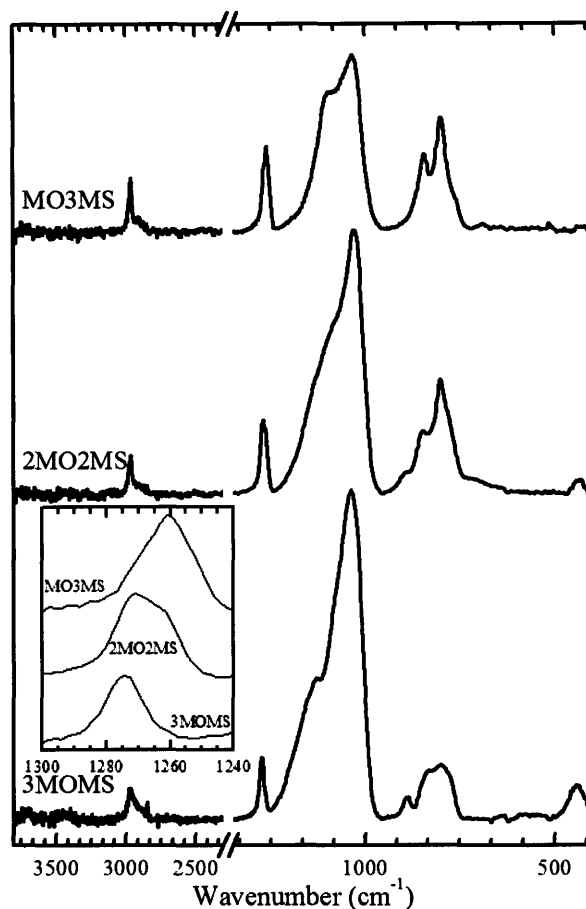


Figure 5-1. FTIR spectra of PECVD thin films deposited from MO₃MS, 2MO₂MS, and 3MOMS with inset focused on M, D, T region from 1300–1240 cm⁻¹.

The inset in Figure 5-1 provides a close look at the location of the peak assigned to Si–CH₃ stretching. This stretching mode is shifted according to the extent of oxygen substitution on the silicon. The mono-substituted M group absorbance is centered near 1255 cm⁻¹. The di-substituted moiety, or D group, is a chain building linear (CH₃)₂SiO₂ unit and absorbs near 1265 cm⁻¹. The tri-substituted branching T group absorbs near 1275 cm⁻¹. The quad-substituted moiety

is called a Q group which forms highly networked structures such as SiO₂ and does not absorb in this region as there are no silicon carbon bonds. It is important to note that while the Si-CH₃ moieties are expected to have the same relative intensities the number of Si-CH₃ bonds per group must be taken into account (e.g. – two peaks of equal intensity centered at 1275 cm⁻¹ and 1255 cm⁻¹, respectively, indicates three times the number of T groups as M groups). Examining the inset in Figure 5-1 reveals a mixture of M and D groups for the film from MO₃MS, D and T groups for the film from 2MO₂MS, and seemingly exclusively T groups for the film from 3MOMS. These observations are further supported by the shape of the Si-O-Si stretching mode. As the methoxy substitution of the precursor increases, the peak at 1040 cm⁻¹ corresponding to long chain or long range order Si-O-Si bonding increases in intensity while the shoulder at 1090 corresponding to long chains terminated by methyl or hydroxyl decreases. Also, the emergence of peaks at 1135 cm⁻¹ and 1190 cm⁻¹ indicate incorporation of short chain branching or ‘cage’ moieties analogous to those found in silsesquioxane.¹⁹ These structures indicate a greater presence of T groups. The dielectric constants after a 1 hour anneal at 400°C of the films deposited from MO₃MS, 2MO₂MS, and 3MOMS, were 2.78, 2.85, and 3.20, respectively.

Table 5-1. FTIR peak assignments for OSG thin films from the literature.^{9, 15-19}

Wavenumber [cm ⁻¹]	Relative intensity	Assignment	Reference
3200-3700	broad	$\nu(\text{O-H})$	a
3000-2800	medium	$\nu_s(\text{CH}_3) + \nu_a(\text{CH}_3)$ $+ \nu_s(\text{CH}_2) + \nu_a(\text{CH}_2)$	a
~1255	medium	$\nu(\text{Si-C})$ in M group	b
~1265	medium	$\nu(\text{Si-C})$ in D group	b
~1275	medium	$\nu(\text{Si-C})$ in T group	b
~1250-980	strong	$\nu(\text{Si-O-Si})$, siloxane	a,b,c, c,d
1190	medium	$\nu(\text{Si-O-Si})$, branching short chain or 'cage' with CH_3 or OH term + $\gamma(\text{Si-O-C})$	c,e
1135	medium	$\nu(\text{Si-O-Si})$, branching short chain, 'cage', linear disorder	c,e
1090	shoulder	$\nu(\text{Si-O-Si})$, long chain with CH_3 or OH term	c,d
1040	very strong	$\nu(\text{Si-O-Si})$, long chain	a,b,c,f
920	medium	associated with Si-OH	a,b,c,d
880	weak	$\delta(\text{Si-O-Si})$ associated with non bridging Si_2O_3	d
878	medium	$\gamma(\text{CH}_3)$ in $\text{Si}(\text{CH}_3)_2$ + $\delta(\text{Si-O-Si})$	d,f
839-845	medium	$\gamma(\text{CH}_3)$ in $\text{Si}(\text{CH}_3)_3$	d,f
804-806	medium	$\gamma(\text{CH}_3)$ in $\text{Si}(\text{CH}_3)_2$ + $\nu_a(\text{Si-C}) + \delta(\text{Si-O-Si})$	d,f
460-440	weak	$\gamma(\text{Si-O-Si})$	d

Vibrational modes: ν_a \equiv asymmetrical stretching, ν_s \equiv symmetrical stretching, ν \equiv stretching, δ_a \equiv asymmetrical bending, δ_s \equiv symmetrical bending, γ \equiv rocking, ^a Reference 17, ^b Reference 9, ^c Reference 19, ^d Reference 15, ^e Reference 18, ^f Reference 16.

For each methoxymethylsilane investigated, depositions were performed under three conditions: from the monomer alone, from an oxidizing environment with the addition of oxygen, and from a reducing environment with the addition of hydrogen. Figure 5-2 shows the Si-O-Si and Si-C bonding regions of the FTIR spectra from films deposited from 2MO2MS, 2MO2MS with hydrogen, and the as deposit and post anneal spectra for the film from 2MO2MS with oxygen. Taking the film deposited from 2MO2MS as a baseline, the addition of hydrogen alters the shape of the main Si-O-Si peak, increasing the shoulder at higher wavenumbers

indicating a higher degree of disorder in the Si–O–Si network¹⁸ and slightly decreases the overall methyl content of the film. The addition of oxygen to 2MO₂MS drastically reduces the CH₃ stretch in the 3000 – 2800 cm⁻¹ range to the extent that the signal is barely perceived above the noise (not pictured) and significantly increases the intensity of the Si–O–Si band shifting it from 1030 cm⁻¹ to 1058 cm⁻¹. The peak near 1270 cm⁻¹ is shifted to 1279 cm⁻¹ indicating that all D groups are converted to T groups or Q groups. This is evidence that oxygen does not have a strict preference for reacting with the methoxy group versus the methyl group. Further evidence is the presence of silanol groups present in the film deposited with oxygen as seen by the absorbance at 920 cm⁻¹ and by the presence of a broad envelope from ~3700 – 3200 cm⁻¹ from OH stretching (not pictured). Any silanol formed in the gas phase of the reactor is likely to react with another silanol or methoxy creating a siloxane linkage and would not be present in the film. The silanol present is likely a result of unsaturated siloxane radicals reacting with water vapor upon exposure to atmosphere. Upon annealing at 400°C for 1 hour, proximal silanol groups undergo condensation reactions forming siloxane bridges and liberating water.^{9,20,21} There is no spectroscopic evidence of silanol groups remaining in the film after the annealing step, nor is there any silanol present in films not deposited from methoxymethylsilanes with oxygen. The dielectric constants for the annealed films from 2MO₂MS, 2MO₂MS + H₂, and 2MO₂MS + O₂ are 2.85, 3.01, and 3.93, respectively.

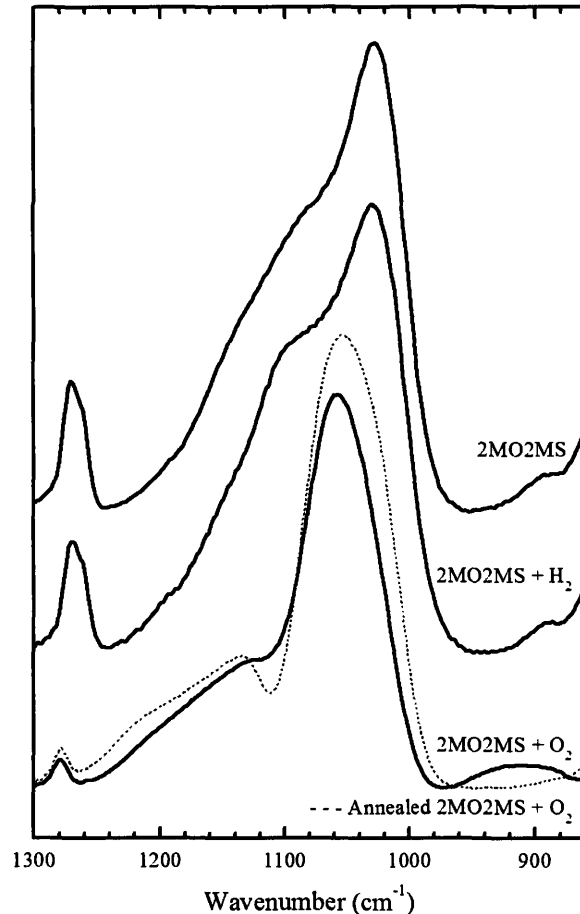


Figure 5-2. FTIR spectra of PECVD thin films from 2MO₂MS, 2MO₂MS + H₂, and 2MO₂MS + O₂ with an additional (---) spectrum of the 2MO₂MS + O₂ film after anneal.

Similar changes are seen in the FTIR of films from MO₃MS. Compared to films deposited from MO₃MS, those deposited in a hydrogen rich reducing environment showed considerable changes in the siloxane network. The peaks representing M, D, and T groups are centered at 1260 cm⁻¹ for the film from MO₃MS, but with addition of hydrogen, the intensity of the peak at 1260 cm⁻¹ decreases with the appearance of a clear shoulder at 1270 cm⁻¹ indicating that many of the M and MO^{CH₃} (M-like moiety, (CH₃)₂(CH₃O)SiO, which would absorb between a M and D group or around ~1260 cm⁻¹) groups are converted to D and D^{CH₃} groups

(analogous to M^{OCH_3} and absorbing at $\sim 1270 \text{ cm}^{-1}$). This likely occurs through the conversion of methoxy groups to silanol groups which then react forming Si–O–Si bonds. The broad siloxane stretching region also shows a decrease in the peak at 1090 cm^{-1} coupled with an increase in the peak at 1135 cm^{-1} indicating a more branched random network containing short siloxane segments with methyl terminal groups. The film deposited from MO_3MS and oxygen is similar in structure to films deposited from other methoxymethylsilanes with oxygen. The film contained Si–OH bonding which was removed upon annealing through condensation reactions. The intensity of the Si–O–Si peak at 1030 cm^{-1} increases significantly and shifts to 1055 cm^{-1} , much closer to the 1070 cm^{-1} reported for silicon dioxide.¹⁵ The composition of the Si–CH₃ bonding indicates only T groups are present and the CH₃ stretching at $3000 - 2800 \text{ cm}^{-1}$ is not clearly observable. The dielectric constants for films deposited from MO_3MS , $\text{MO}_3\text{MS} + \text{H}_2$, and $\text{MO}_3\text{MS} + \text{O}_2$ were measured to be 2.78, 2.84, and 4.07, respectively.

Films deposited from 3MOMS had a much more intense Si–O–Si absorption band as compared to films deposited with from the other methoxymethylsilanes without oxygen. The film deposited from 3MOMS and hydrogen had a slightly more intense Si–O–Si band and shifted the peak at 1273 cm^{-1} representing T and D^{OCH_3} groups to 1275 cm^{-1} by converting more D^{OCH_3} groups to T or T^{OCH_3} groups through gas phase conversion of methoxy to silanol groups which undergo condensation reactions extending the siloxane network. Films deposited from 3MOMS and oxygen show an increased Si–O–Si band and the peak at 1273 cm^{-1} in the film from 3MOMS alone is shifted to 1279 cm^{-1} indicating only T groups are present. Silanol groups are present in the as deposited films and removed after annealing and the CH₃

stretching at $3000 - 2800 \text{ cm}^{-1}$ is not clearly observable. The dielectric constants for films deposited from 3MOMS, 3MOMS + H_2 , and 3MOMS + O_2 were measured to be 3.20, 3.18, and 4.29 respectively.

These spectroscopic results paired with the knowledge that T groups are required for to increase hardness and modulus,^{8-10, 13, 14} led to further study of the 3MOMS system. Figure 5-3 shows the effect of the ratio of 3MOMS and hydrogen gas flows to the reactor. Increasing the ratio of 3MOMS to H_2 from 1:1.5 to 1:4 increases the intensity of the Si–O–Si band and shifts its center from 1036 cm^{-1} to 1039 cm^{-1} . The absorbance corresponding to T and D^{OCH_3} is shifted to a higher frequency by 1 wavenumber corresponding to increased conversion of available methoxy moieties to siloxane linkages through silanol condensation chemistry. Doubling the gas flow ratio to 1:8, 3MOMS: H_2 , further increases the intensity of the Si–O–Si band and shifts its center to 1042 cm^{-1} . The Si– CH_3 stretching region shows only evidence of T groups indicating complete consumption of methoxy groups. The dielectric constants for the films deposited from 3MOMS and hydrogen with gas feed ratios of 1:1.5, 1:4, and 1:8 were measured to be 3.53, 3.18 and 3.43, respectively.

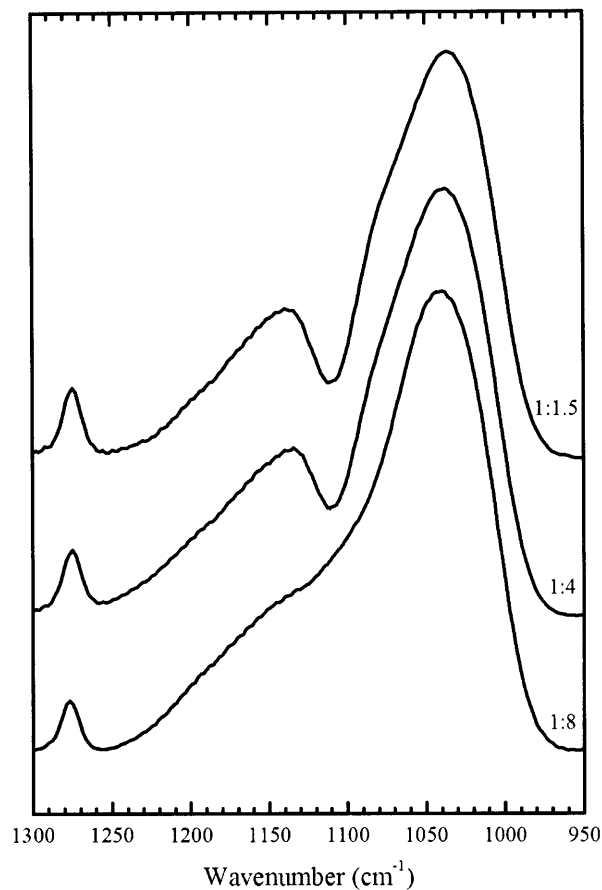


Figure 5-3. FTIR spectra of PECVD films deposited from 3MOMS and hydrogen with 3MOMS:H₂ gas flow ratios of 1:1.5, 1:4 and 1:8.

The effect of plasma power was also investigated. Figure 5-4 shows the FTIR spectra of a series of films from 3MOMS, 3MOMS + H₂, and 3MOMS + O₂, deposited using plasma powers of 20W, 40W and 100W. For all cases, increasing the plasma power had the effect of increasing the intensity of the Si – O – Si band and shifting it to a higher wavenumber. The content of T groups decreased with power, with these moieties being converted to Q groups, silyl radicals, or silicon-silicon bonds. There was significant silanol formation for the films deposited at 20W and 40W with oxygen and slight silanol incorporation for the films deposited at 100W from 3MOMS only and at 40W and 100W 3MOMS with hydrogen. Upon annealing the

silanol groups react to form siloxane bridges liberating water. The dielectric constants for the films from 3MOMS at 20W, 40W, and 100W were measured to be 3.20, 3.53, and 4.54, respectively. The dielectric constants for the films from 3MOMS and hydrogen deposited with 20W, 40W, and 100W plasma power were measured to be 3.18, 4.15, and 4.92, respectively. Finally, the films deposited from 3MOMS and oxygen at plasma powers of 20W, 40W, and 100W had measured dielectric constants of 4.29, 5.02, and 4.57 respectively.

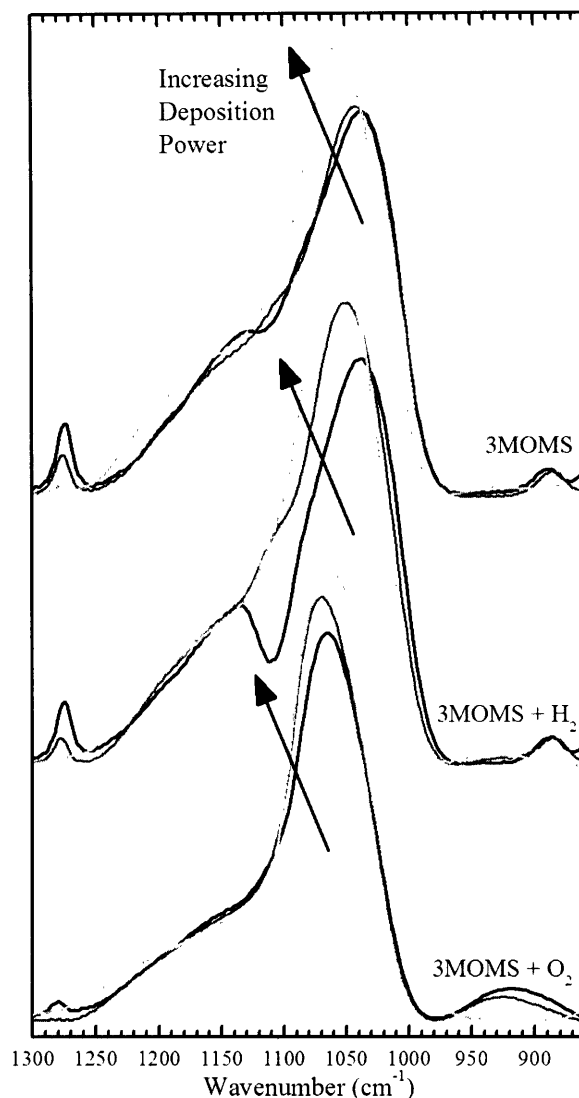


Figure 5-4. FTIR spectra of films deposited from 3MOMS, 3MOMS + H₂, and 3MOMS + O₂ at plasma powers of 20W (black lines), 40W (medium gray lines), and 100W (light gray lines).

5.2.2. OPTICAL AND ELECTRICAL CHARACTERIZATION

The optical properties of the thin films deposited in this study were determined via spectroscopic ellipsometry. The minimum dielectric constant for a material is the square of the index of refraction at a wavelength of 633 nm (n_{633}). This approximation is most useful for insulating materials contained the smallest induced dipoles and considers only electronic polarization.^{22, 23} Figure 5-5 plots the

dielectric constant, k , as a function of the index of refraction for the as deposited films that did not contain hydroxyl groups and the annealed films. The films containing hydroxyl bonding were omitted from this family plot as the OH bond is very easily polarized having a dramatic effect on the dielectric constant. The dielectric constant measured after annealing was lower in every case. Annealing allows for the healing of unsaturated radical sites in the film which increase the dielectric constant of the material.

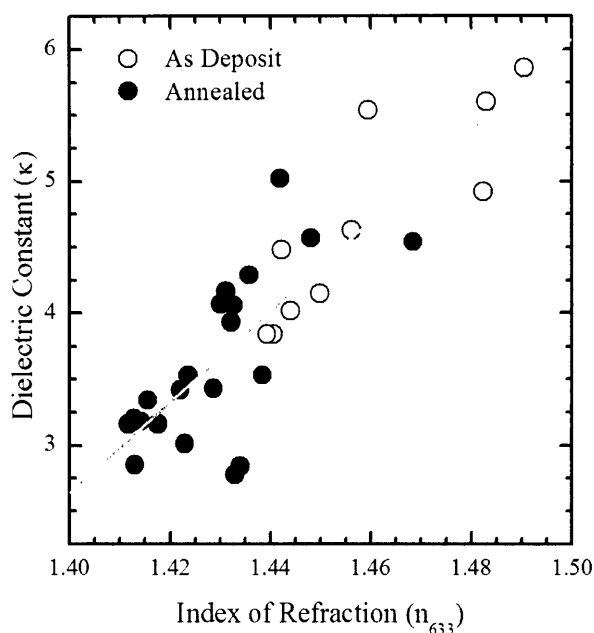


Figure 5-5. Dielectric constant of PECVD films from methoxymethylsilanes, with hydrogen, and with oxygen for the as deposited samples and after annealing as a function of the index of refraction at a wavelength of 633 nm.

Silicon dioxide has a dielectric constant of 4.0, so it is expected that the highest dielectric constant observed would be near 4.0. However, many films deposited with oxygen or at high power had dielectric constants above 4.0 after annealing. For films deposited with oxygen this is likely due to silicon-silicon bonding which significantly increases the dielectric constant. The oxygen reacts

without prejudice with both the methyl and methoxy groups. When a methyl is removed via reaction with atomic oxygen in the plasma a silyl radical is formed which can react with other silyl radicals to form a silicon-silicon bond. The FTIR indicates the absence of any bonding other than silicon and oxygen. The dielectric measurements indicate that the silicon is not fully oxidized providing a silicon to oxygen atomic ratio of less than 1:2 or that elimination of OH bonding was not complete. These films all had significant hydroxyl bonding before the annealing step and while FTIR of the annealed films did not clearly show any OH bonding, even a slight amount significantly increases the measured dielectric constant. The only other films with a dielectric constant after anneal above 4.0 were the 40W and 100W films from 3MOMS deposited with hydrogen with values of 4.15 and 4.92, respectively, and the film from 3MOMS deposited at 100W with a dielectric constant of 4.54. All three films showed a small amount of OH bonding in the as deposit film that was not detected via FTIR after annealing. The films were deposited under much harsher plasma conditions greater precursor fragmentation and exposing the film to more intense UV radiation and ion bombardment, all of which can contribute to a silicon to oxygen ratio of less than 1:2. The only sample with even slight alkyl group retention was the 40W 3MOMS film deposited with hydrogen which accordingly had the lowest dielectric constant of the three. All other dielectric constants fall in the range between 2.78 and 3.53.

5.2.3. INTERPRETING THE RESULTS IN LIGHT OF DFT SIMULATIONS

Recent density functional theory (DFT) simulations concerning the thermochemistry of methoxymethylsilanes lead to the design of these experiments.²⁴

Calculated bond dissociation energies indicated that methoxymethylsilane fragmentation can not be easily controlled as there is less than a 3 kcal/mol difference in the bond strengths of the SiO-CH₃ bond and the Si-CH₃ bond. Reactions with oxygen atom favor abstraction of the methoxy methyl for MO₃MS and 2MO₂MS, but abstraction of the methyl from the silicon atom for 3MOMS. Even so, the largest difference in reaction enthalpies is again only 3 kcal/mol. DFT predicted that thermodynamic control over the reaction pathways of methoxymethylsilanes is possible only when considering the reaction with H atom. Formation of methoxymethylsilanols is favored in the reaction scheme with H atom. Silanol groups react readily with other silanol groups creating Si-O-Si bridges and liberating water. This leads to a conceivable strategy to control the Si-O bond network and retained methyl content in a CVD thin film by controlling the molecular ratio of the corresponding methoxymethylsilane precursors and creating an H atom rich environment.

The FTIR results confirm the predicted chemistry. Depositions with oxygen shows little selectivity for retention of the methyl groups, while depositions with hydrogen (as long it is not in great excess) show preferential reactions with the methoxy methyl allowing for network siloxane bond formation through silanol condensation reactions utilizing only the oxygen native to the precursor. Depositions from the methoxymethylsilanes with no addition species are limited by the similar bond dissociation energies of the Si-C and O-C bonds. Not all oxygen native to the precursor is converted to siloxane units and some degree of crosslinking is evident via cleavage of the Si-C bond decreasing the amount of retained alkyl groups and thus not achieving the lowest possible dielectric constant.

5.3 CONCLUSIONS

Low power plasma excitation is sufficient for depositing low dielectric constant thin films from methoxymethylsilanes. Spectroscopic evidence of films containing only T and Q groups indicates that mechanically robust OSGs are attainable utilizing modest power conditions. The low deposition power is an important restraint for extendibility of PECVD OSGs to future generations of porous low-k films requiring use of a carbon polymer porogen. Porogen materials often require mild processing conditions to retain proper functionality and physical properties to act as an efficient porogen.

The chemistry of PECVD of methoxymethylsilanes correlates well with DFT predictions of the thermochemistry of the same system emphasizing the impact of research in CVD precursor selection via ab initio studies. Oxidative environments are sufficient for creating OSG thin films from methoxymethylsilanes, however, reactions of methoxymethylsilanes with oxygen are not selective leading to loss of methyl functionality incorporated into the precursor to aid in lowering the dielectric constant of the resulting material. Reducing chemistry is apparently selective, with hydrogen atoms reacting preferentially with the methoxy methyl and creating silanol or siloxane radicals which form networking bonds through condensation reactions without sacrificing the 'built-in' alkyl content of the precursor. The index of refraction of the resulting material is a good indicator of its dielectric properties allowing for rapid screening of chemistries. Low-k OSG thin films from

methoxymethylsilanes and hydrogen were deposited via a low power PECVD process resulting in material dielectric constants ranging from 2.84 to 3.18.

For films believed to have the best mechanical properties, the lowest dielectric constant achieved was 3.16. Good mechanical properties are derived from a film structure composed entirely of T and Q groups. To achieve this end while still obtaining a low dielectric constant, the precursor with 'built in' T group functionality, 3MOMS, was used in a reducing environment. The thermochemistry driving the reduction chemistry of methoxymethylsilanes favors the conversion of methoxy groups into silanol groups which react readily to create network forming siloxane bonds. In order to take advantage of this selective chemistry, the plasma power must remain modest. Doubling the plasma power increased the dielectric constant from 3.16 to 4.15, indicating a loss in selectivity of the reducing chemistry.

5.4 EXPERIMENTAL

Organosilicon thin films are deposited from methoxytrimethylsilane, dimethoxydimethylsilane, and trimethoxymethylsilane via plasma enhanced chemical vapor deposition in a custom built vacuum chamber described in detail elsewhere.²⁵ Plasma was generated utilizing a 13.56 MHz RF source and matching network. The reactor utilizes a parallel plate capacitively-coupled system with an upper powered electrode which also acts as a showerhead for distributed gas delivery and a grounded lower electrode. The substrate temperature was controlled using backside silicon oil cooling. Reactor pressure was controlled via a butterfly valve controlled by an MKS model 252A exhaust valve controller. The series of

depositions in this study were performed at a reactor pressure of 300 mtorr with plasma powers of 20W, 40W and 100W.

Methoxytrimethylsilane (99%, Aldrich), dimethoxydimethylsilane (99.5%, Aldrich) and trimethoxymethylsilane (98%, Aldrich) were used without purification and delivered via an MKS 1479A mass flow controller. Methoxymethylsilane flow rates were kept constant at 1 sccm. Oxygen and hydrogen flow rates were maintained at 4 sccm except when noted otherwise. Total flow to the reactor was kept a constant 20 sccm with the remainder of the gas flow attributed to Argon. All gases were delivered via MKS 1479A mass flow controllers. Deposition rate was monitored via *in-situ* laser interferometry.

Variable-angle spectroscopic ellipsometry (VASE) was used to measure thickness and optical properties making use of a J.A. Woolam M-2000 spectroscopic ellipsometer. Measurements were taken at 65°, 70° & 75° over 225 wavelengths. The resulting data was fit using the Cauchy-Urbach model.²⁶ FTIR spectra were collected utilizing a Nicolet Nexus 870 ESP spectrometer in normal transmission mode. All spectra are normalized to a sample thickness of 300 nm and are baseline corrected. Samples were annealed in a vacuum chamber with a nitrogen purge at 5 torr using a custom built substrate heater from Watlow. Electrical measurements to determine dielectric properties of the films were performed made using mercury probe from MDC. A frequency of 1MHz was utilized and a standard CVD oxide was used to determine the mercury contact area. The dielectric constant was calculated based on the saturation capacitance values measured, the film thickness determined by VASE, and the mercury spot size.

REFERENCES

1. C. Bayer, E. Bapin, and P. R. von Rohr, *Surf. Coat. Technol.*, **119**, 874 (1999).
2. A. Hozumi, N. Sugimoto, H. Sekoguchi, and O. Takai, *J. Mater. Sci. Lett.*, **16**, 860 (1997).
3. Y. Inoue and O. Takai, *Plasma Sources Sci. Technol.*, **5**, 339 (1996).
4. Y. Y. Wu, M. Bekke, Y. Inoue, H. Sugimura, H. Kitaguchi, C. S. Liu, and O. Takai, *Thin Solid Films*, **457**, 122 (2004).
5. Y. Y. Wu, H. Sugimura, Y. Inoue, and O. Takai, *Thin Solid Films*, **435**, 161 (2003).
6. J. H. Kim, Y. Ikoma, and M. Niwa, *Microporous Mesoporous Mat.*, **32**, 37 (1999).
7. L. Peters, in *Semiconductor International*, 2005.
8. D. D. Burkey and K. K. Gleason, *J. Appl. Phys.*, **93**, 5143 (2003).
9. D. D. Burkey and K. K. Gleason, *Journal Of The Electrochemical Society*, **151**, F105 (2004).
10. Q. G. Wu and K. K. Gleason, *J. Vac. Sci. Technol. A*, **21**, 388 (2003).
11. A. D. Ross and K. K. Gleason, *J. Vac. Sci. Technol. A*, submitted (2005).
12. A. D. Ross and K. K. Gleason, *J. Appl. Phys.*, submitted (2005).
13. J. C. Phillips, *J. Non-Cryst. Solids*, **34**, 153 (1979).
14. M. F. Thorpe, *J. Non-Cryst. Solids*, **57**, 355 (1983).
15. A. Hozumi, H. Sekoguchi, and O. Takai, *Journal Of The Electrochemical Society*, **144**, 2824 (1997).
16. H. G. P. Lewis, T. B. Casserly, and K. K. Gleason, *Journal Of The Electrochemical Society*, **148**, F212 (2001).
17. D. Lin-Vien, N. B. Colthup, W. G. Fateley, and J. G. Grasselli, Academic Press, San Diego, CA, 1991, 503.
18. J. R. Martinez, F. Ruiz, Y. V. Vorobiev, F. Perez-Robles, and J. Gonzalez-Hernandez, *J. Chem. Phys.*, **109**, 7511 (1998).
19. C. Y. Wang, Z. X. Shen, and J. Z. Zheng, *Appl. Spectrosc.*, **54**, 209 (2000).
20. B. C. Bunker, D. R. Tallant, T. J. Headley, G. L. Turner, and R. J. Kirkpatrick, *Phys. Chem. Glasses*, **29**, 106 (1988).
21. A. J. Moulson and J. P. Roberts, *Trans. Faraday Soc.*, **57**, 1208 (1961).
22. C. J. F. Böttcher, O. C. van Belle, P. Bordewijk, and A. Rip, *Theory of Electric Polarization*, 2nd ed., p. 2, Elsevier Scientific Pub. Co., New York, (1973).
23. J. H. Mulvey, *The Nature of Matter*, Oxford University Press, New York, (1981).
24. T. B. Casserly and K. K. Gleason, *Journal of the Electrochemical Society*, submitted (2005).
25. H. G. P. Lewis, D. J. Edell, and K. K. Gleason, *Chemistry Of Materials*, **12**, 3488 (2000).
26. H. G. Tomkins and W. A. McGahan, *Spectroscopic Ellipsometry and Reflectometry: A User's Guide*, p. 228, Wiley-Interscience, New York, (1999).

CHAPTER SIX

EFFECT OF SUBSTRATE TEMPERATURE ON THE PLASMA POLYMERIZATION OF POLY(METHYL METHACRYLATE)

T. B. Casserly, and K. K. Gleason, *Chemical Vapor Deposition*, submitted
(2005).

ABSTRACT

Low power plasma enhanced CVD polymerization of methylmethacrylate (MMA) can be achieved to deposit thin films of poly(methyl methacrylate) (PMMA) with minimal loss of functional groups as evidenced by FTIR, XPS, and Raman spectrometry. Retention of functional groups decreases with increased substrate temperature. From XPS data, the calculated percent loss of functional groups ranges from 0.9% to 43.4% changing as a function of deposition conditions. Raman spectrometry confirms the presence of C=C bonds in the polymer backbone as a result of scission of the ester group from MMA. The thermal properties of PECVD films from MMA can be tailored by varying the substrate temperature. Onset of thermal decomposition increases with increased substrate temperature by eliminating thermally labile peroxide linkages in the polymer backbone and by crosslinking that occurs at radical sites generated via scission of functional group bonds. The post-anneal thicknesses of the remaining polymer is on the order of 4 nm or less indicating that low power PECVD PMMA is viable candidate to act as a sacrificial material for air gap fabrication.

ACKNOWLEDGEMENTS: The authors thank Novellus and the Semiconductor Research Corporation for fellowship funding and the NSF/SRC Engineering Research Center for Environmental Benign Semiconductor Manufacturing for funding support.

6.1 INTRODUCTION

Thin films of poly(methyl methacrylate) (PMMA) are of interest for a variety of applications including organic vapor and moisture sensors,¹⁻⁴ electron-beam resists,⁵⁻⁸ photonic waveguides and optical fibers,^{9, 10} and as dielectric sacrificial layers in MEMS fabrication.¹¹ Thin films of PMMA have been created using spin-on,^{1, 12} laser assisted vapor deposition,¹³ and plasma enhanced (PE)CVD.^{3-7, 11, 14-18} Utilizing its clean and nearly complete thermal degradation and its properties as an e-beam resist, PMMA has the potential to be a directly patternable sacrificial material for fabrication of closed cavity air gap structures which have applications in photonics and in semiconductor devices as an ultra low-k dielectric.

This work examines the structure of films deposited under continuous wave (CW) and pulsed plasma (PP) enhanced CVD from methylmethacrylate (MMA) monomer at various processing conditions. The precise chemical structure of the resulting film affects the thermal properties and thus impacts the film's effectiveness for all the potential applications previously mentioned. A key parameter in deposition of plasma polymers is power input per mass, or W/FM.¹⁹ After initial optimization of PMMA deposition, a series of films with a constant W/FM of 4.8 J/g was deposited varying substrate temperature utilizing either CW or PP excitation. The effect of substrate temperature on the structure and thermal properties of PECVD films from MMA is studied.

6.2 RESULTS AND DISCUSSION

6.2.1 FOURIER TRANSFORM INFRARED (FTIR) SPECTROSCOPY TO DETERMINE OPTIMAL W/FM

Initial attempts to deposit PMMA resulted in thin films that more closely resembled highly crosslinked polycarboxylic acid. Figure 6-1 shows the FTIR spectra of thin films deposited from MMA at various process conditions and a PMMA standard from Alpha Aesar. A key parameter in deposition of plasma polymers is power input per mass, or W/FM, which for polymer thin films has a large effect on functional group retention.¹⁹ The PECVD films represented in Figure 6-1 were deposited at a with a substrate temperature of 50°C and have W/FM values of (2a) 168.3, (2b) 84.2, (2c) 67.3, and (2d) 4.8 J/g. The films deposited at higher W/FM show decreased intensity and broadening of the carbonyl peak near 1700 cm⁻¹ relative to standard PMMA as is seen in some previous PECVD PMMA.^{2, 3, 6, 15, 16} These films also show very broad O–H stretching centered near 3400 cm⁻¹ which combined with the broad carbonyl peak is more representative of polycarboxylic acid than PMMA. Conversion of the methoxy ester to carboxylic acid is possible via scission of the C-OCH₃ bond creating a radical site which can then react with water in the deposition chamber or upon exposure to air to form the –COOH moiety. As W/FM is decreased, retention of the carbonyl peak increases and finally with a W/FM of 4.8 J/g, the spectrum of the CVD film contains the same peaks as bulk PMMA although not the identical resolution or intensities and the O–H stretching peak is not observable above the background noise.



Figure 6-1. FTIR spectra of PECVD thin films from MMA with W/FM of (a) 168.3, (b) 84.2, (c) 67.3, and (d) 4.8 J/g along with a (e) PMMA standard.

Table 6-1 identifies the major peak assignments from the literature for PMMA.²⁰ Only the low W/FM sample contains only the characteristic C-H

stretching and bending, C=O stretching, and C–O bending of PMMA seen in the standard spectra. While it is clear that the methoxy functionality is present, the amount relative to bulk PMMA is clearly diminished as noted by the lessened intensity of the characteristic peaks at 1240 and 1270 cm^{-1} in the CVD films relative to that of the standard. Based upon the resolution and relative intensities of the FTIR spectra, the series of low power plasma polymerized PMMA films in this work retain a greater amount of α -methyl and ester functionality and greater homogeneity when compared to previous plasma films.^{3, 6, 15} Morita *et al.*, observe ‘merely blunt’ peaks of diminished intensity and note the presence of O–H bonding in one sample.⁶ Jeon *et al.* observe a significant decrease in C–C and C–O stretching near 1200 cm^{-1} and decreased intensity of the C=O stretching mode.¹⁵ Zhang *et al.* note ‘comparatively weak and broader’ characteristic peaks as compared to PMMA and significant decreased intensity of the C=O peak along with some broadening attributed to conversion of the ester to carboxylic acid.³

Table 6-1. FTIR assignments for PMMA from the literature²⁰

Wavenumber [cm ⁻¹]	Relative intensity	Assignment
2995	medium	$\nu_a(\text{CH}_3\text{-O}) + \nu_a(\text{CH}_2)$
2948	medium	$\nu_s(\text{CH}_3\text{-O}) + \nu_a(\alpha\text{-CH}_3)$ $+ \nu_s(\alpha\text{-CH}_3) + \nu_s(\text{CH}_2)$
2920	shoulder	} combination band associated with CH ₃ -O
2835	very weak	
1730	very strong	$\nu(\text{C=O})$
1483	medium	$\delta_a(\alpha\text{-CH}_3)$
1465	shoulder	$\delta_a(\text{CH}_3\text{-O})$
1452	strong	$\delta(\text{CH}_2)$
1438	strong	$\delta_s(\text{CH}_3\text{-O})$
1388	medium	$\delta_s(\alpha\text{-CH}_3)$
1370	weak shoulder	$\delta_s(\alpha\text{-CH}_3)$ (amorphous)
1270	strong	} $\nu_a(\text{C-C-O})$ coupled with $\nu(\text{C-O})$
1240	strong	
1190	very strong	} internal C-H deformation vibration coupled with skeletal stretching
1150	very strong	
1063	weak	intramolecular interaction
988	medium	$\nu_s(\text{C-O-C})$ coupled with $\gamma(\text{CH}_3\text{-O})$
967	medium	$\gamma(\alpha\text{-CH}_3)$
749	weak	$\gamma(\text{CH}_2)$ coupled with skeletal stretching

Vibrational modes: ν_a \equiv asymmetrical stretching, ν_s \equiv symmetrical stretching, ν \equiv stretching, δ_a \equiv asymmetrical bending, δ_s \equiv symmetrical bending, γ \equiv rocking

6.2.2 THERMAL PROPERTIES/DEGRADATION OF PMMA

The thermal properties of PMMA have been well studied.²¹⁻³⁶ Holland and Hay provide a thorough discussion of much of the previous work.³⁰ The thermal stability of a series of PECVD PMMA films deposited at various substrate temperatures with a constant W/FM of 4.8 J/g was examined by annealing the films under nitrogen in a metal crucible. The temperature during the anneal was ramped at a rate of 10°C/min to 150°C, held for 30 minutes, ramped at 10°C/min to 240°C,

held for 30 minutes, and finally ramped to 410°C and held for 60 minutes before being cooled to room temperature. Laser interferometry was utilized to monitor thickness loss. Variable angle spectroscopic ellipsometry was utilized to determine as deposited and post-anneal film thicknesses. The onset of thermal decomposition is determined by the initial oscillation of the laser signal from interferometry.³⁷

Table 6-2. Summary of onset of thermal decomposition and % residue for PECVD films deposited at various substrate temperatures with a constant W/FM of 4.8 J/g.

Sample Label	Substrate Temperature (°C)	Plasma Excitation	Onset of thermal decomposition (°C)	Residue (%)
CW1	50	10W continuous	85	0.8
CW2	75	10W continuous	95	2.7
CW3	100	10W continuous	85	1.5
CW4	130	10W continuous	110	3.7
PP1	50	100W peak power PP 10 ms on, 90 ms off	115	1.2
PP2	75	100W peak power PP 10 ms on, 90 ms off	120	1.8*
PP3	100	100W peak power PP 10 ms on, 90 ms off	185	4.7
PP4	130	100W peak power PP 10 ms on, 90 ms off	220	5.2

*Nitrogen purge failed during high temperature portion of anneal

Table 6-2 summarizes deposition conditions results determining the onset of thermal decomposition and amount of residue calculated as a percentage of original thickness remaining after annealing. (*Note that the nitrogen purge failed during the 'hold at 410°C' annealing step for sample PP3.) The films are referred to as CW1 through CW4 and PP1 through PP4, with the CW and PP referring to the type of plasma excitation, and the numerals corresponding with the substrate temperatures of 50°C (1), 75°C (2), 100°C (3), and 130°C (4). Figure 6-2 shows the onset of

thermal decomposition increases with increased substrate temperature. For all cases with the exception of CW4 and PP4, the annealed samples are visually indistinguishable from bare silicon. Measured film residue also increases as a function of substrate temperature as shown in Figure 6-3 with one set of data omitted due to nitrogen purge failure. Cleanliness and completeness of decomposition for the PECVD films compares favorably with reported literature values of 3.0 – 5.8 percent char after thermogravimetric measurements of hydrogen terminated and 2,2-diphenyl hexyl group terminated PMMA.²⁹

The PECVD films do undergo classic two stage decomposition first observed by Grassie.²⁴ The exact mechanism has been debated in the literature with Manring favoring side group scission followed by chain scission and macro decomposition,^{32, 34} Kashiwagi favors the first stage of decomposition to be a result of weak head-to-head linkages in the polymer backbone,³¹ but Holland convincingly argues that the two stage decomposition of radically polymerized PMMA is due to thermally labile peroxide linkages formed when the polymerization takes place in the presence of air.³⁰ Incorporation of these peroxide linkages in PECVD thin films is possible as depositions are performed at moderate pressures, 1 torr, and there is the possibility to generate free oxygen radicals in the plasma. The inclusion of thermally labile peroxide linkages along with dangling radical sites will decrease the onset of thermal decomposition for the PECVD films below the reported onset of bulk PMMA of 170 – 230°C.³⁶ At elevated substrate temperatures, three factors increase the onset of thermal decomposition. First, lower deposition rates at higher substrate temperatures increases the time the growing film is exposed to UV radiation and ion bombardment which can lead to creation of radical sites via functional group loss.³⁸

Second, polymer chain mobility is increased allowing for a higher degree of crosslinking via the radical sites created. Finally, at very high substrate temperatures the peroxide linkages are not stable and do not remain in the PECVD polymer. Thus it is possible to control the onset of thermal decomposition by varying the substrate temperature and other deposition parameters of the CVD process.

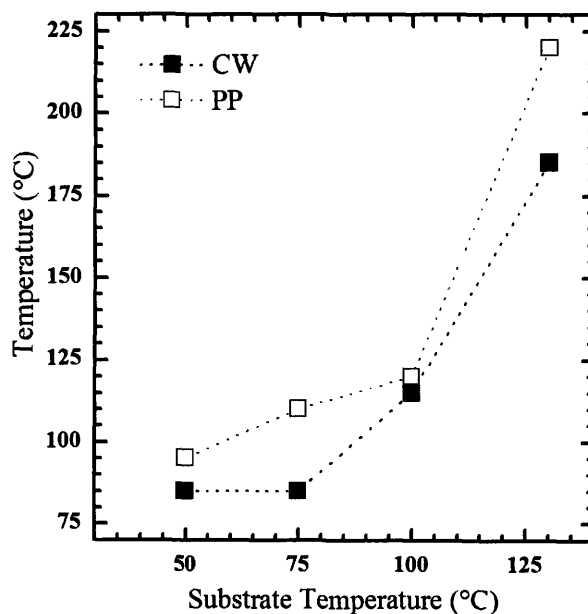


Figure 6-2. Onset of Thermal Decomposition as a function of substrate temperature for both CW and PP CVD PMMA films.

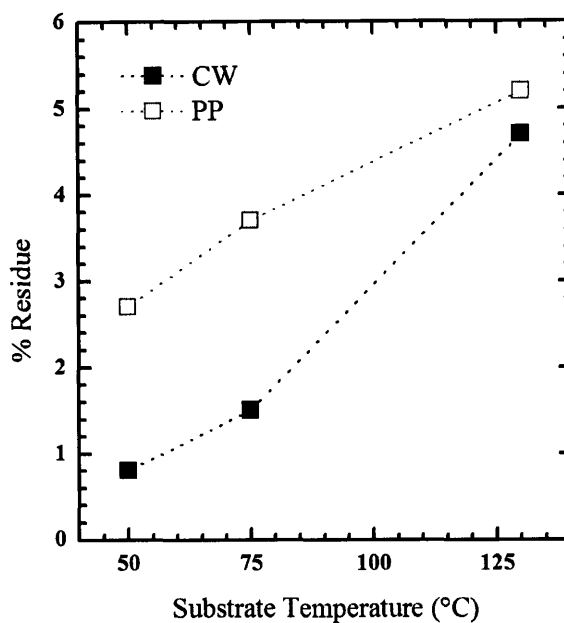


Figure 6-3. Percent residue remaining after anneal as a function of substrate temperature for both CW and PP CVD PMMA films.

The annealed substrates were analyzed using FTIR and x-ray photoelectron spectroscopy (XPS). There was insufficient residue to observe any peaks in the FTIR spectra apart from an increased thickness in the native oxide on the silicon wafer. XPS survey scans indicate the presence of Si 2p in the ~ 4 nm depth probed. The atomic concentration of Si 2p observed ranged from 0.12% for the PP4 sample to 11.33% for the CW1 sample. Carbon and oxygen are also observed in the XPS survey scans of every sample.

The onset of thermal decomposition and percent residue both increases as a function of substrate temperature for both the CW and PP series of films. At a constant substrate temperature, the PP films have a higher thermal stability than the CW films exhibiting a higher onset of decomposition and leaving a higher percentage of residue. The XPS, Raman, and FTIR spectroscopy are utilized

to determine changes in the chemical structure of the polymer which lead to the differences in thermal stability.

6.2.3 X-RAY PHOTOELECTRON SPECTROSCOPY (XPS)

Figure 6-4 shows high resolution C 1s and O 1s XPS scans of the Alpha Aesar PMMA standard and the CW1 PECVD film. Table 6-3 reports the binding energies and peak areas for the films in Figure 6-4 and reports the literature values for solution polymerization PMMA.³⁹ Figure 6-5 shows PMMA with the carbon and oxygen atoms labeled corresponding to the peaks assigned to them in the XPS high resolution scans. The C 1s scan of the CW1 film shows the four characteristic carbon moieties of the standard PMMA with an additional peak at 287.7 eV corresponding to a C=O or O–C–O bonding environment. The O 1s scan of the CW1 film shows the two characteristic oxygen moieties with an additional peak centered at 533.18 eV assigned to the same C=O or O–C–O moiety. The moiety is likely C=O and occurs in all the PECVD films as a result of scission of the C–OCH₃ bond. Removal of the ester methoxy is further supported by the greatly reduced area of Peak 2 in the O 1s high resolution scan, corresponding to the methoxy oxygen at 533.87 eV, relative to PMMA. In the C 1s spectrum of CW1, the increase relative to the standard PMMA of Peak 1, corresponding to polymer backbone carbons, also indicates of a loss of ester functionality. There are two mechanisms for loss of the ester methoxy.³⁸ One is via the scission of the C–OCH₃ bond creating a radical site on the carbonyl carbon available for crosslinking or initiation reactions. The other is removal of the entire ester group via scission of the C–COOCH₃ bond which decreases the concentration of both oxygen moieties and two of the four carbon moieties. Observance in the high

resolution C 1s and O 1s spectra of film CW1 of the Peaks 5 and 3, respectively, indicate that some degree of functional loss is due to scission of the C–OCH₃ bond. Close inspection of the high resolution C 1s spectrum of the CW1 film reveals that there is loss of the ester carbon, Peak 4, in addition to the amount converted to carbonyl carbon, Peak 5, through loss of the ester methoxy (i.e. - the sum of the areas corresponding to Peaks 4 and 5 in sample CW1 do not total the area of Peak 4 in the standard PMMA).

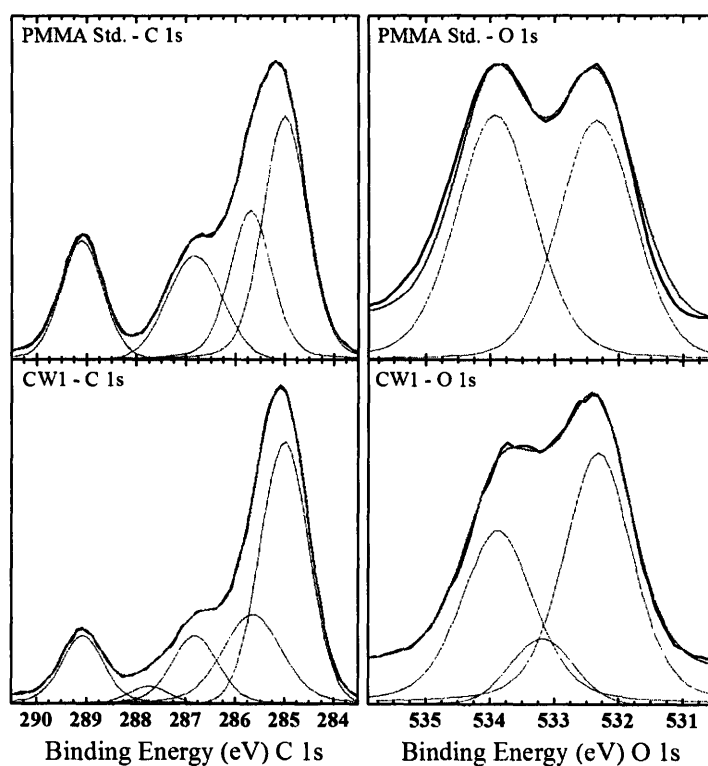


Figure 6-4. Fit XPS spectra, C 1s and O 1s for the PMMA standard and the PECVD film CW1.

Table 6-3. Comparison of XPS spectra fits from Figure 6-4 with reference data.

Core/Level	Peak	PECVD film CW1		Measured Standard		Reference ³⁹	
		Binding Energy (eV)	Area (%)	Binding Energy (eV)	Area (%)	Binding Energy (eV)	Area (%)
C 1s	1	285.00	50.3	285.00	39.3	285.00	42
	2	285.65	22.1	285.69	23.5	285.72	21
	3	286.81	13.1	286.83	19.6	286.79	21
	4	289.07	11.9	289.10	17.7	289.03	17
	5*	287.74	2.7			287.89	0
O 1s	1	532.31	51.1	532.35	48.1	532.21	51
	2	533.87	37.7	533.93	51.9	533.77	49
	3*	533.18	11.2			533.06	0

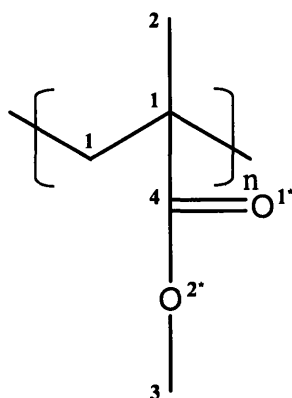
**Figure 6-5. PMMA with labeled carbon (1-4) and oxygen (1*-2*) moieties.**

Table 6-4 shows the elemental composition and C/O ratio for the series of CVD films as determined by XPS. For both the CW and PP films, there is a significant decrease in oxygen content for a substrate temperature of 130°C. This results in an increase of the C/O ratio relative to the theoretical value of 2.5 for pure PMMA. A range for the degree of functional group loss can be calculated from the C/O ratio by considering two extreme methods of functional group loss. Based upon the area of Peak 2, corresponding to the α -CH₃ moiety, in the high resolution C 1s scan of the CW1 sample we assume zero loss of the α -CH₃ functionality for these calculations. The upper bound for the range of functional loss is determined by

assuming all loss of oxygen occurs via scission of the C–OCH₃ bond resulting in one less carbon and one less oxygen atom per polymer unit. These polymer units have a C/O ratio of 4 rather than 2.5 allowing for the percentage of units undergoing scission of the C–OCH₃ bond to be calculated. The calculated upper bound ranges from 2.6% to 43.4% for the CW films and 5.2% to 35.2% for the PP films. However, as previously discussed, the C 1s scan shows evidence of loss in the ester carbon which can not be attributed solely to loss of the methoxy group. To calculate the lower bound for functional loss it is assumed that all loss of carbon and oxygen occurs via scission of the C–COOCH₃ bond resulting in two fewer carbon and oxygen atoms per polymer unit than PMMA. The calculated lower bound on functional group loss ranges from 0.9% to 13.5% for the CW films and from 1.8% to 11.2% for the PP films. For both cases, retention of the α -methyl functionality is assumed which has the effect of lowering the calculated limits if the assumption is not correct. For the PP films which are exposed to 100W peak power, some loss of the α -methyl can be expected indicating the upper bounds presented for the PP films are likely under predicted and may very well exceed the values for the CW films. The actual percent loss of functional groups likely lies between 2 and 10% for the films deposited at 50°C and between 20 and 50% for the films deposited at 130°C. Because the C/O ratio changes with constant W/FM and method of plasma excitation, it can be concluded that some degree of functional loss is due to the UV irradiation and ion bombardment of the deposited film. The deposition rates decreases as a function of substrate temperature (as discussed in Section 2.5) indicating that films deposited at a higher substrate temperature are exposed to the damaging plasma for a greater period of time to deposit films of similar thickness.

Table 6-4. Elemental analysis and C/O ratio from XPS scans along with calculated upper and lower bounds for functional group loss.

Sample	% C	% O	C/O ratio	Upper bound functional loss (%)	Lower bound functional loss (%)
CW1	71.7	28.3	2.54	2.6	0.9
CW2	73.8	26.2	2.82	21.0	7.0
CW3	73.1	26.9	2.72	14.5	5.0
CW4	75.9	24.1	3.15	43.4	13.5
PP1	73.1	26.9	2.71	14.2	4.8
PP2	72.1	27.9	2.58	5.2	1.8
PP3	72.5	27.5	2.64	9.2	3.2
PP4	75.2	24.8	3.03	35.2	11.2

6.2.4 RAMAN SPECTROSCOPY

Figure 6-6 shows the Raman spectra of the PECVD films PP4, CW4, PP1, CW1, and a PMMA standard. Assignments from the literature are reported in Table 6-5.^{10, 40} Comparing the Raman spectra confirms that the PECVD films are structurally similar to PMMA containing all the characteristic Raman modes. As in the FTIR, some of the Raman modes exhibit peak broadening or diminished intensity. Deriving detail from the CW4 and PP4 samples is particularly difficult as there was a large fluorescence background for these samples. As seen in Figure 6-6, present in the PECVD films but absent in the PMMA standard is the strong absorbance at 1645 cm^{-1} corresponding to R–C=C–R stretching.⁴⁰ This carbon-carbon double bond arises from the scission of the entire ester group (C–COOCH₃ bond) creating a double bond in the polymer backbone. This peak is even more prominent in the PP4 and CW4 films indicating a higher degree of ester loss compared to PP1 and CW1. It should be noted that the C=C bond is a very strong Raman absorber, indicating the relative intensity of the peak is much greater than the percentage of R–C=C–R in the film. Figure 6-6 also gives insight into the

difference between PP and CW plasma excitation. Comparing the intensities of the C=O peak at 1724 cm^{-1} and the $\alpha\text{-CH}_3$ peak at 1452 cm^{-1} for films deposited at the same substrate temperature, the CW films retain a greater deal of C=O and $\alpha\text{-CH}_3$ functionality. Loss of both of these functionalities leads to a loss of C–H stretching in the region c. 2900 cm^{-1} . Loss of C=O indicates a loss of the entire ester group, therefore losing the contributions of the ester methoxy to C–H stretching, while loss of the $\alpha\text{-CH}_3$ group is a direct loss of C–H stretching. Scission of the C– CH_3 bond of the $\alpha\text{-CH}_3$ is another pathway for C=C formation although XPS evidence suggests that the majority of the C=C bonding is a result of loss of the entire ester group.

As seen in the detailed Raman spectra in Figure 6-7, the peaks associated with the ester methoxy, namely the $\text{CH}_3\text{-O}$ rock and C–O–C stretch seen at 988 and 812 cm^{-1} respectively, are present but diminished in the CW1 and PP1 films indicating a degree of lost methoxy functionality. Confidently distinguishing these same peaks for the CW4 and PP4 is not possible due to the limitations faced in acquiring the spectra. Additionally, the increased intensity of the peak associated with skeletal stretching of the C–C bonds at 735 cm^{-1} is evidence of a degree of crosslinking in the PECVD sample not present in the PMMA standard.

Table 6-5. Raman assignments from the literature.^{10, 40}

Raman Wavenumber [cm ⁻¹]	Relative intensity	Assignment
2954	very strong	$\nu_s(\text{C-H})$ of $\text{CH}_3\text{-O}$ + $\nu_a(\text{CH}_2)$
2920	weak	combination band involving $\text{CH}_3\text{-O}$ and $\nu_s(\text{CH}_2)$
2864	medium	combination band involving $\text{CH}_3\text{-O}$
1724	medium	$\nu(\text{C=O})$
1645	strong	$\nu(\text{C=C})$ ⁴⁰
1452	strong	$\delta_a(\alpha\text{-CH}_3)$
1238	weak	$\nu(\text{C-O}) + \nu(\text{C-COO})$
988	strong	$\gamma(\text{CH}_3\text{-O})$
914	weak	$\nu(\text{CH}_2)$
878	very weak	$\nu(\text{CH}_2)$
812	strong	$\nu_s(\text{C-O-C})$
732	weak	$\nu(\text{C-C})$ skeletal mode
600	strong	$\nu(\text{C-COO}) + \nu_s(\text{C-C-O})$
537	weak	$\delta(\text{C-C-C})$

Vibrational modes: ν_a \equiv asymmetrical stretching, ν_s \equiv symmetrical stretching, ν \equiv stretching, δ_a \equiv asymmetrical bending, δ \equiv bending, γ \equiv rocking

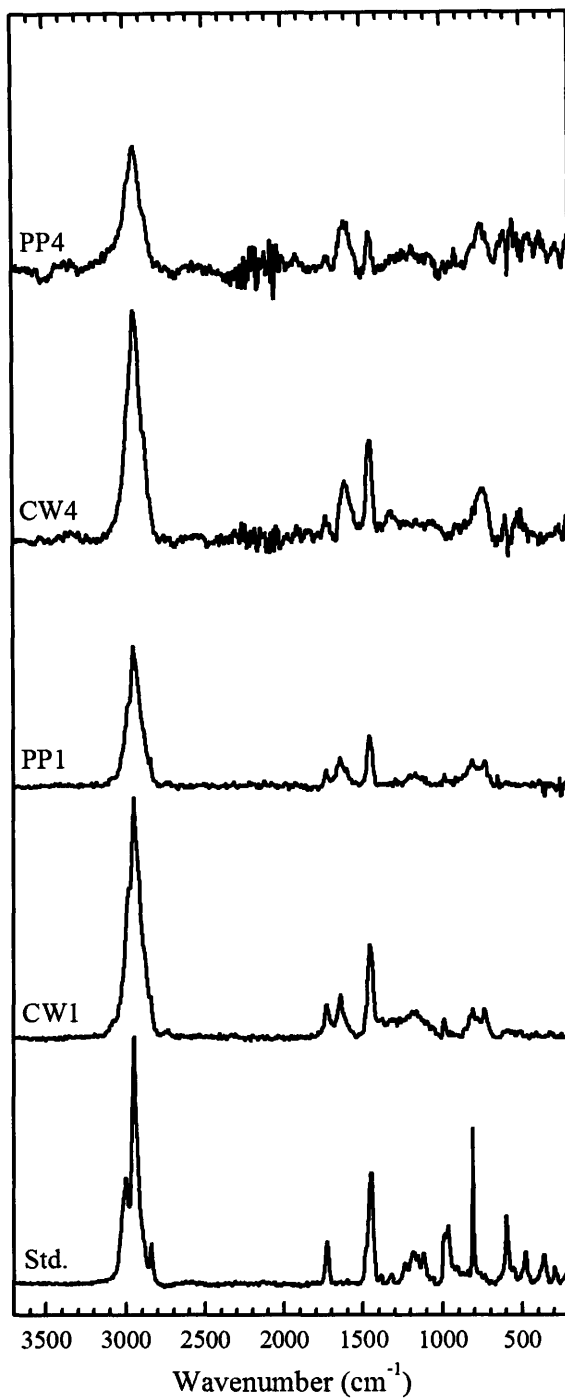


Figure 6-6. Raman spectra of films PP4, CW4, PP1, CW1, and a PMMA standard (Std.).

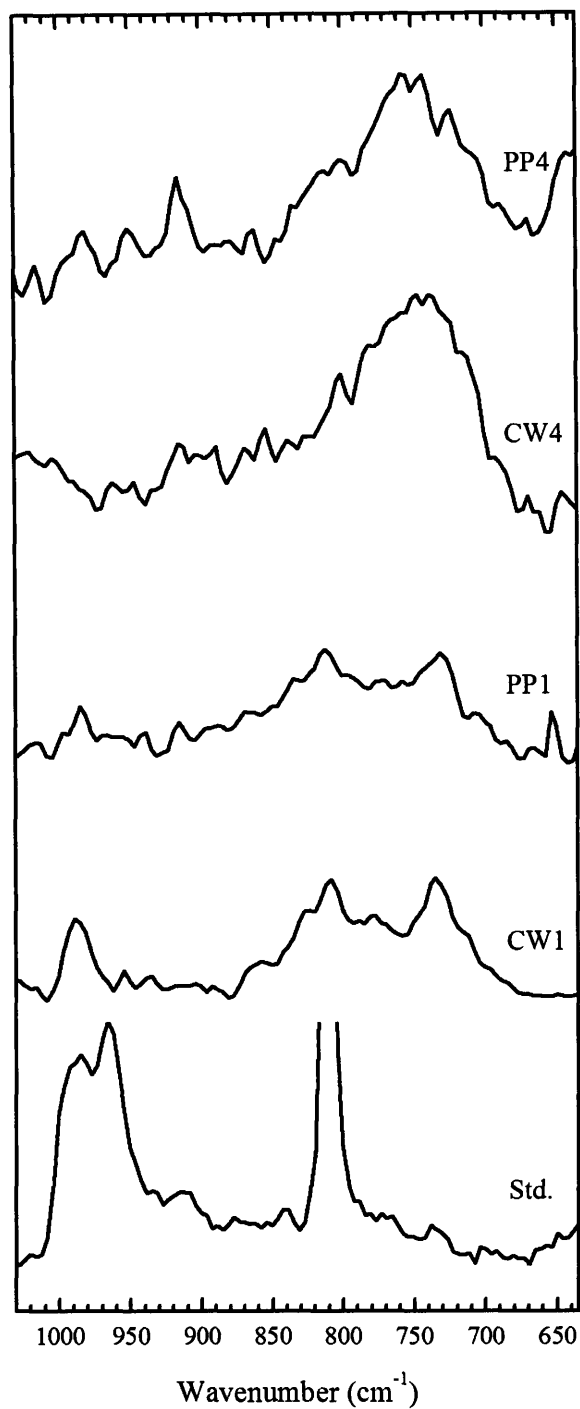


Figure 6-7. Detail of the Raman spectra of films PP4, CW4, PP1, CW1, and a PMMA standard at the methoxy and skeletal stretching region.

6.2.5 DEPOSITION KINETICS

Figure 6-8 shows an Arrhenius plot of the deposition rate as a function of the inverse of the substrate temperature. For both the CW and PP series, the deposition rate decreases as a function of increasing substrate temperature. The apparent negative activation energies indicate that both the CW and PP depositions are absorption limited. Thus, even while the rate constant for polymerization increases as a function of temperature, the surface concentration of adsorbed monomer decreases more quickly, leading to an overall decrease in deposition rate with increasing temperature. The apparent activation energy for depositions under CW excitation, -7.2 ± 0.4 kcal/mol, is approximately three times that for depositions under PP excitation, -2.4 ± 0.1 kcal/mol. Under CW excitation, radical species are continuously generated allowing for the initiation of new polymer chains as well as activate sites for additional polymerization on the surface while generation of reactive species during PP excitation occurs only 10% of the time (although likely to a greater degree per unit time). Another explanation for the lower deposition rate for the PP films is that the higher peak power does more damage to the deposited film, more readily breaking bonds that can liberate monomer or dimer species from the film. Also, a 100W plasma generates more powerful UV radiation than a 10W plasma and the C-COOCH₃ bond in PMMA is known to be sensitive to UV irradiation.³⁸ The faster growth under CW excitation would reduce the UV damage per thickness of film. This may account in part for the lower degree of residue left after annealing CW films as compared to PP films deposited at the same W/FM and substrate temperature (Figure 6-3).

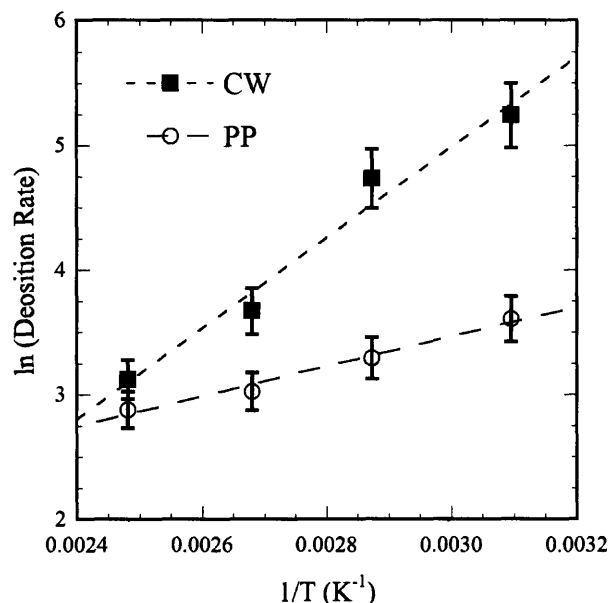


Figure 6-8. Arrhenius plot of deposition rate as a function of substrate temperature at constant $W/FM = 4.8 \text{ J/g}$ showing relative apparent energies 3:1 for CW:PP.

6.3 CONCLUSIONS

Low power plasma polymerization of MMA can be achieved to deposit thin films of PMMA with minimal loss of functional groups as evidenced by FTIR, XPS, and Raman spectrometry. As has been found with other systems,⁴¹ the retention of functional groups decreases with increased substrate temperature. Based on XPS data, the percent loss of functional groups is as small as 0.9% to 2.6% for the CW₁ film and as large as 13.5% to 43.4% for the PP₄ film. Raman spectrometry indicates the presence of C=C bonds in the polymer backbone as a result of scission of the ester group from MMA. As the substrate temperature increases, the loss of functional groups is a result of increased exposure to ion bombardment and UV radiation created by the plasma excitation.

The thermal properties of PECVD films from MMA can be tailored by varying the substrate temperature. Onset of thermal decomposition increases with increased substrate temperature by eliminating thermally labile peroxide linkages in the polymer backbone and by crosslinking that occurs at radical sites generated via scission of functional group bonds. The post-anneal thicknesses of the remaining polymer is on the order of 4 nm or less indicating that low power PECVD PMMA is a viable candidate to act as a sacrificial material for air gap fabrication.

6.4 EXPERIMENTAL

Thin films of poly(methyl methacrylate) (PMMA) are deposited via plasma enhanced chemical vapor deposition in a custom built vacuum chamber described in detail elsewhere.⁴² Plasma was generated utilizing a 13.56 MHz RF source and matching network. The reactor utilizes a parallel plate capacitively-coupled system with an upper powered electrode which also acts as a showerhead for distributed gas delivery and a grounded lower electrode. The substrate temperature was controlled with a custom stage heater from Watlow. The heater was grounded to the bottom electrode. Reactor pressure was controlled via a butterfly valve controlled by an MKS model 252A exhaust valve controller. The series of depositions in this study were performed at a reactor pressure of 1 torr. For continuous wave (CW) experiments, the plasma input power was set to 10W. For pulsed plasma (PP) experiments, the peak power was set at 100W and square wave pulse generator was used to modulate the plasma corresponding to 10 ms on times and 90 ms sec off times for a 10% duty cycle. Initially, various pressures and plasma excitation

schemes were examined. The spectra of CVD films in Figure 6-1 correspond to processing conditions of (2a) pressure of 300 mtorr, gas flow of 8 sccm MMA, pulsed plasma excitation of 400W with 10 ms on, 90 ms off or 10% duty cycle, equivalent to W/FM of 168.3 J/g, (2b) 300 mtorr, 8 sccm MMA, 200W with 10 ms on, 90 ms off or 10% duty cycle, 84.2 J/g, (2c) 600 mtorr, 10 sccm MMA, 400W with 10 ms on, 190 ms off or 5% duty cycle, 67.3 J/g, (2d) 1.00 torr, 20 sccm MMA and 20 sccm Argon, continuous wave plasma excitation of 10W equivalent to a W/FM of 4.8 J/g. The effect of substrate temperature was examined by depositing a series of CW and PP films with a constant W/FM of 4.8 J/g at four different substrate temperatures. These samples are referred to as CW1 through CW4 and PP1 through PP4, with the CW and PP referring to the type of plasma excitation, and the numerals corresponding with the substrate temperatures of 50°C (1), 75°C (2), 100°C (3), and 130°C (4).

MMA (99.0%, Aldrich) was used without purification and delivered via an MKS 1152C mass flow controller. Argon was delivered via an MKS 1479A mass flow controller. Flow rates were varied initially, but maintained at 20 sccm for MMA and 20 sccm Argon for the series of depositions at various substrate temperatures. Deposition rate was monitored via *in-situ* laser interferometry.

Variable-angle spectroscopic ellipsometry (VASE) was used to measure thickness and optical properties making use of a J.A. Woolam M-2000 spectroscopic ellipsometer. Measurements were taken at 65°, 70° & 75° over 225 wavelengths. The resulting data was fit using the Cauchy-Urbach model.⁴³ FTIR spectra were collected utilizing a Nicolet Nexus 870 ESP spectrometer in normal transmission mode. XPS spectra were collected using a Kratos Axis Ultra spectrometer. Raman

spectra were collected using the FT Raman accessory for the Nicolet Nexus 870 ESP using a Raman laser power of 1.5W. Samples were prepared for Raman spectroscopy by scraping the polymer film from the wafer and placing it in an NMR tube for analysis. Thermal properties were studied using the interferometry for thermal stability (ITS) system described elsewhere.³⁷

REFERENCES

1. R. Capan, A. K. Ray, A. K. Hassan, and T. Tanrisever, *J. Phys. D-Appl. Phys.*, **36**, 1115 (2003).
2. S. P. Russell and D. H. Weinkauff, *Polymer*, **42**, 2827 (2001).
3. C. Zhang, J. Wyatt, and D. H. Weinkauff, *Polymer*, **45**, 7665 (2004).
4. A. R. K. Ralston, J. A. Tobin, S. S. Bajikar, and D. D. Denton, *Sens. Actuator B-Chem.*, **22**, 139 (1994).
5. M. Yamada, J. Tamano, K. Yoneda, S. Morita, and S. Hattori, *Jpn. J. Appl. Phys. Part 1 - Regul. Pap. Short Notes Rev. Pap.*, **21**, 768 (1982).
6. S. Morita, J. Tamano, S. Hattori, and M. Ieda, *J. Appl. Phys.*, **51**, 3938 (1980).
7. L. Martinu and H. Biederman, *Vacuum*, **33**, 253 (1983).
8. L. M. Gavens, B. J. Wu, D. W. Hess, A. T. Bell, and D. S. Soong, *J. Vac. Sci. Technol. B*, **1**, 481 (1983).
9. Y. Zhao, F. Wang, Z. C. Cui, J. Zheng, H. M. Zhang, D. M. Zhang, S. Y. Liu, and M. B. Yi, *Microelectron. J.*, **35**, 605 (2004).
10. X. S. Xu, H. Ming, Q. J. Zhang, and Y. S. Zhang, *J. Opt. A-Pure Appl. Opt.*, **4**, 237 (2002).
11. W. H. Teh, C. T. Liang, M. Graham, and C. G. Smith, *J. Microelectromech. Syst.*, **12**, 641 (2003).
12. C. B. Walsh and E. I. Franses, *Thin Solid Films*, **429**, 71 (2003).
13. D. B. Chrisey, A. Pique, R. A. McGill, J. S. Horwitz, B. R. Ringeisen, D. M. Bubb, and P. K. Wu, *Chem. Rev.*, **103**, 553 (2003).
14. J. A. Tobin and D. D. Denton, *Applied Physics Letters*, **60**, 2595 (1992).
15. H. S. Jeon, J. Wyatt, D. Harper-Nixon, and D. H. Weinkauff, *J. Polym. Sci. Pt. B-Polym. Phys.*, **42**, 2522 (2004).
16. Y. V. Pan, E. Z. Barrios, and D. D. Denton, *Journal of Polymer Science Part a-Polymer Chemistry*, **36**, 587 (1998).
17. G. F. Li, J. A. Tobin, and D. D. Denton, *Applied Physics Letters*, **64**, 560 (1994).
18. Y. Kashiwagi, Y. Einaga, and H. Fujita, *Polym. J.*, **12**, 271 (1980).
19. H. Yasuda and C. R. Wang, *Journal of Polymer Science Part a-Polymer Chemistry*, **23**, 87 (1985).
20. H. Nagai, *J. Appl. Polym. Sci.*, **7**, 1697 (1963).
21. S. M. Dakka, *J. Therm. Anal. Calorim.*, **74**, 729 (2003).
22. S. M. Dakka, *J. Therm. Anal. Calorim.*, **73**, 17 (2003).
23. S. M. Dakka, *J. Therm. Anal. Calorim.*, **75**, 765 (2004).
24. N. Grassie and H. W. Melville, *Faraday Soc. Discuss.*, **2**, 378 (1947).
25. N. Grassie and H. W. Melville, *Proc. R. Soc.*, **199**, 14 (1949).
26. N. Grassie and H. W. Melville, *Proc. R. Soc.*, **199**, 1 (1949).
27. N. Grassie and H. W. Melville, *Proc. R. Soc.*, **199**, 24 (1949).
28. N. Grassie and H. W. Melville, *Proc. R. Soc.*, **199**, 36 (1949).
29. B. J. Holland and J. N. Hay, *Polymer*, **42**, 4825 (2001).
30. B. J. Holland and J. N. Hay, *Polym. Degrad. Stabil.*, **77**, 435 (2002).
31. T. Kashiwagi, A. Inaba, J. E. Brown, K. Hatada, T. Kitayama, and E. Masuda, *Macromolecules*, **19**, 2160 (1986).
32. L. E. Manring, *Macromolecules*, **21**, 528 (1988).
33. L. E. Manring, *Macromolecules*, **22**, 2673 (1989).
34. L. E. Manring, *Macromolecules*, **24**, 3304 (1991).
35. L. E. Manring, D. Y. Sogah, and G. M. Cohen, *Macromolecules*, **22**, 4652 (1989).
36. J. D. Peterson, S. Vyazovkin, and C. A. Wight, *J. Phys. Chem. B*, **103**, 8087 (1999).
37. B. Cruden, K. Chu, K. K. Gleason, and H. Sawin, *J. Electrochem. Soc.*, **146**, 4590 (1999).
38. J. F. Rabek, *Polymer Photodegradation: Mechanisms and Experimental Methods*, Chapman & Hall: London, England, (1995).
39. G. Beamson and D. Briggs, Wiley, Chichester, West Sussex, England, 1992, 295 p.
40. D. Lin-Vien, N. B. Colthup, W. G. Fateley, and J. G. Grasselli, Academic Press, San Diego, CA, 1991, 503.

41. G. P. Lopez, A. Chilkoti, D. Briggs, and B. D. Ratner, *Journal Of Polymer Science Part A-Polymer Chemistry*, **30**, 2427 (1992).
42. H. G. P. Lewis, D. J. Edell, and K. K. Gleason, *Chemistry Of Materials*, **12**, 3488 (2000).
43. H. G. Tomkins and W. A. McGahan, *Spectroscopic Ellipsometry and Reflectometry: A User's Guide*, p. 228, Wiley-Interscience, New York, (1999).

CHAPTER SEVEN

CONCLUSIONS AND FUTURE DIRECTIONS

7.1 CONCLUSIONS

This thesis presents potential low dielectric constant solutions to address the future needs of the semiconductor industry. Dense organosilicon thin films have been deposited via HFCVD and PECVD resulting in films with dielectric constants as low as 2.78. A plasma polymerized sacrificial material has been presented to enable extendibility of low-k for future generations, initially through the development of porous low-k organosilicon thin films and forward to an air gap scheme for ultra low-k utilizing the CVD organosilicon film as a bridge layer.

This thesis applied the power of computation quantum mechanics to understanding the structure of CVD materials and to aid in the design of CVD experiments through predicting the initial chemical reaction of the CVD system.

7.1.1 CVD MATERIALS

Organosilicon thin films with dielectric and biopassivation applications were deposited from cyclic siloxane precursors via HFCVD. The impact of filament temperature on material composition was studied via FTIR, VASE, Raman, and ^{29}Si NMR. The OSG materials showed good insulating properties, excellent thermal stability, resistance to water uptake and a high degree of flexibility. While these are all desirable properties for biopassivation coatings, the films were not sufficiently hard for low-k applications; nor, frankly, was the semiconductor industry very receptive to the novel HFCVD process directing future work to the PECVD system.

Plasma enhanced chemical vapor deposition was used to deposit organosilicon thin films from methoxytrimethylsilane, dimethoxydimethylsilane,

and trimethoxymethylsilane. In a reducing environment, hydrogen atoms react preferentially with the methoxy methyl creating silanols or siloxane radicals which form networking bonds through condensation reactions without sacrificing the 'built-in' alkyl content of the precursor. Low-k OSG thin films from methoxymethylsilanes and hydrogen were deposited via a low power PECVD process resulting in material dielectric constants ranging from 2.84 to 3.18. These materials contain spectroscopic evidence of T and Q groups which indicates good mechanical properties. The films were deposited using low power plasma excitation providing a means to extend the material usage to future generations. While dense OSGs, are the immediate future of the low-k in the semiconductor industry, future generations will require the introduction of air into the dielectric either through the incorporation of pores in a dense OSG matrix or via an air gap strategy.

PMMA is a promising sacrificial material. Low power plasma enhanced CVD polymerization of methylmethacrylate (MMA) can be achieved to deposit thin films of poly(methyl methacrylate) (PMMA) with minimal loss of functional groups as evidenced by FTIR, XPS, and Raman spectrometry. The solubility, onset of thermal decomposition, and post-anneal residual thickness of PECVD films from MMA can be tailored by varying the substrate temperature. The post-anneal thicknesses of the remaining polymer char is on the order of 4 nm or less indicating that low power PECVD PMMA is viable candidate to act as a sacrificial material for porous low-k or for ultra low-k air gap fabrication.

7.1.2 COMPUTATIONAL QUANTUM MECHANICS

Density functional theory was utilized in a novel way to aid in the characterization of organosilicon CVD materials in order to fully discover the material structure and deepen the understanding of the process-structure-property relationship. Density functional theory at the B3LYP/6-311++G(*d,p*) level was applied to calculate the ^{29}Si NMR chemical shifts of a variety of organosiloxane moieties including structures believed to occur in OSG thin films deposited using HFCVD from cyclic siloxanes. Retention of the cyclic siloxane structure is confirmed and the chemical shift at -15 ppm is identified as a cross-linking Si-Si bond between two strained D groups and has not previously been reported. DFT is a powerful tool which can be used to interpret unidentified peaks in observed spectra and can identify bonding environments not previously known. A full understanding of the final film structure allows for a clear picture of the CVD chemistry to be presented. DFT can also be used to study the initial CVD chemistry directly.

The thermochemistry including enthalpies of formation and enthalpies of reaction at 298 K for a set of methyl- and methoxymethylsilane precursors was calculated using B3LYP density functional theory. Bond strengths and reactions with O atom and H atom are examined in the context of understanding the initial reactions in chemical vapor deposition. The Si-H bond was calculated to be 8.4 kcal/mol stronger than the Si-C bond in methylsilanes and to increase by 0.6 kcal/mol with increased methylation; however, the thermochemistry of methylsilane reactions with O atom favors scission of the Si-H bond to produce hydroxyl and methylsilyl radicals. Thermodynamic control over the reaction pathways of methoxymethylsilanes is possible only when considering the reaction with H atom

for which methoxymethylsilanol formation is favored. This illuminates a conceivable strategy to control the Si–O–Si bonding network while retaining methyl functionality in a CVD thin film by controlling the ratio of methoxy functionality and free hydrogen in the reactor. Density functional theory is a powerful tool applied to understanding and subsequently controlling the initial chemistry of the CVD process.

7.2 FUTURE DIRECTIONS

It is my hope that this thesis is not considered complete. No thesis that contains new ideas is ever really complete. I hope that the advances presented herein provide the tools and inspiration for further advancement of low dielectric constant materials and promote the use of computational quantum mechanics to understand and develop the CVD process.

The materials presented in this thesis were designed to provide an evolutionary pathway for low-k materials. The PECVD process for deposition of a dense OSG from trimethoxymethylsilane was developed using low power plasma excitation to enable control over reaction pathways in the CVD process and to provide a means for robust OSG deposition using processing conditions which overlap with sacrificial PMMA deposition. Co-deposition of this pair of materials should be investigated to determine the suitability for creation of a porous OSG.

The PECVD PMMA presented in this work has been used along with a dense CVD oxide to create initial air gap structures on the order of 2 mm wide. Using traditional lithography, air gaps on the order of 1 to 2 microns wide were fabricated,

however attempts to create two level structures were unsuccessful. PMMA has known electron beam sensitivity and has been used as an e-beam resist. A logical progression of this thesis would be the optimization of the PECVD PMMA as a directly patternable sacrificial material for air gap fabrication at the nano scale utilizing e-beam lithography.

The use of density functional theory as a screening process for CVD precursors has been shown to be a powerful tool. There is great value to be found through the expansion of computational experiments including the use of transition state theory to calculate reaction activation energies. Series of precursors can be examined without approaching a lab bench.

It is my hope that this thesis lays a foundation for the evolutionary path of low-k materials from dense OSG to an air as dielectric scheme.